Title
Integrated Microfluidic Molecular Diagnostics for Point-of-Care

Author
Yeh, Erh-Chia

Publication Date
2015

Peer reviewed|Thesis/dissertation

Integrated Microfluidic Molecular Diagnostics for Point-of-Care

by

Erh-Chia Yeh

A dissertation submitted in partial satisfaction of the

requirements for the degree of

Joint Doctor of Philosophy

with University of California, San Francisco

in

Bioengineering

in the

Graduate Division

of the

University of California, Berkeley

Committee in charge:

Professor Luke P Lee, Chair

Professor Randall Lee

Professor Ming C Wu

Spring 2015

Abstract

Integrated Microfluidic Molecular Diagnostics for Point-of-Care

By

Erh-Chia Yeh

Joint Doctor of Philosophy in Bioengineering with

University of California, San Francisco

University of California, Berkeley

Professor Luke P. Lee, Chair

Ideal point-of-care medical diagnostic devices are low cost assays capable of performing quantitative on-site rapid testing with high sensitivity and minimal manual steps.

Current mainstream assays have several key limitations. Take, for instance, the common lateral flow assay—e.g. the pregnancy dipstick test. Such assays produce rapid results at low cost; however, they are mostly qualitative tests yielding only positive/negative results rather than quantitative figures. Other standard immunosorbant assays such as ELISA yield quantitative results but require several hours and extensive manual operation. At the other end of the spectrum, nucleic acid amplification techniques such as quantitative real-time PCR can deliver much higher sensitivity and selectivity. Unfortunately, these require costly equipment and several sample preparation steps.

In this thesis, an integrated low-cost microfluidic chip and peripheral technologies for quantitative molecular diagnostics is described. These technical advances are designed to address the prevailing dilemmas described above.

Researchers have developed and integrated several key components with microfluidic lab-on-chip miniaturization technology. In line with cutting-edge technology, a novel reagent patterning method, termed “digital micro-patterning”, was developed. A very simple method, it can be adopted at low-resource laboratory settings with mainstream equipment. Digital micro-patterning is unique in the sense that it can digitally pattern and concentrate reagents into highly defined micro-patterns. As a proof of concept, it was possible to pattern isothermal amplification reagents in hundreds of microwells and run amplification reactions in these wells.

Next, a next-generation passive microfluidic pumping technology, termed the “vacuum battery system”, has been developed. This system allows for precise passive microfluidic pumping without external pumps, controls, or power sources for up to several hours. It does not require opaque fibers as in capillary systems (e.g. lateral flow assays), thus rendering this pumping method very attractive for optical detection platforms. The vacuum battery system is also significantly more robust compared to

previous degas pumping techniques. Due to its portability, excellent optical properties, low cost, and the ability for complete integration with microfluidics, this platform technology opens exciting new opportunities to create a nouveau generation of standalone microfluidic chips readily operable in field settings.

Additionally, a microfluidic sample preparation technology termed “digital plasma separation” has been developed. This technology uses parallel micro-cliff-like structures and gravity sedimentation to simultaneously separate plasma and compartmentalize samples into hundreds of micro-wells within minutes. Such sample preparation method enables isothermal digital nucleic acid amplification in one step.

As a proof of concept, these technologies were integrated into a single microfluidic chip, termed the Integrated Molecular Diagnostics Chip (iMDx). This chip is capable of performing one-step quantitative nucleic acid detection directly from human whole blood samples ($10\sim10^5$ copies/ μl in 30 minutes). One low-cost disposable chip (~ $10) is designed to integrate and automate sample preparation, quantitative isothermal digital nucleic acid detection, and next generation autonomous microfluidic pumping. This portable integrated chip can acquire template concentration data similar to bench top real-time PCR machines. As the latter can cost three or more orders ($30~80k), this chip opens exciting opportunities for rapid point-of-care diagnostics in resource-low settings.

Finally, in summarizing these cutting-edge methods, a blueprint for next-generation technical development plans is laid out. The key areas of focus are downstream microfluidic integration for advanced functionality such as protein and nucleic acid multiplexed detection on a single chip, telemedicine, mass production, and clinical studies in field settings.

Ultimately, the implication of the research in this dissertation is that these platform technologies can be adopted into future medical diagnostic devices to enable rapid on-site quantitative molecular level detection at significantly lower costs. Both the system-level design rationale and component technologies developed herein provide promising building blocks for future point-of-care diagnostic assays.

For my loving parents, Shyi-Dong Yeh and Bihhua Chen,

who supported and encouraged me throughout graduate school,

and my brother, Karl Yeh,

who always inspires me to reach new heights,

and to God,

who sustained me with providence and strength,

for His Glory.

Table of Contents

List of Technical Abbreviations

Acronym	Term
CLIA	clinical laboratory improvement amendments
CMOS	complementary metal–oxide–semiconductor
CRISPR	clustered regularly interspaced short palindromic repeat
DPS	digital plasma separation
DNA	deoxyribonucleic acid
ELISA	enzyme-linked immunosorbent assay
FET	field-effect transistor
GNP	gold nanoparticle
HIV	human immunodeficiency virus
iMDx	integrated molecular diagnostics system
LAMP	loop-mediated amplification
LED	light-emitting diode
LOD	limit of detection
MgOAc	magnesium acetate
MRSA	Methicillin resistant Staphylococcus aureus
PCR	polymerase chain reaction
PDMS	polydimethylsiloxane
POC	point-of-care
RBC	red blood cell
RNA	ribonucleic acid
RRE	RNA Restriction Enzymes
RPA	recombinase polymerase amplification
SIMBAS	self-powered integrated microfluidic blood analysis system
SNP	silver nanoparticle
TIR	total internal reflection
UVO	ultra violet light ozone

Acknowledgements

As I wrap up my thesis and look back at these years at grad school, I would like to give special thanks first of all, to my advisor, Professor Luke P. Lee, for his guidance and training. I was challenged and humbled by Prof. Lee's strict training and high standards, but now I can see that it was for me; he had greater vision to mold me into a new level than what I could have ever imagined. I would like to especially thank him for his patience and effort with me because I was a strong-willed person. His training has taught me to how pursue excellence, communicate scientifically, write grants, work diligently, and not to fear any circumstances. I will always remember at one particular difficult time in my life, he encouraged me by telling me "There is nothing to fear if one fears God". I am extremely thankful for his support and nurturing during these years.

In addition, I would like to thank Prof. Dorian Liepmann, Prof. Song Li, Prof. Randall Lee, and Prof. Ming Wu for serving on my qualifications committee. Also, I would also like to thank Prof. Liepmann, Prof. Tim Hamill, Prof. Randall Lee, Prof. Charles Chiu, and Prof. Ming Wu for serving on my dissertation committee. I have received lots of excellent suggestions from these professors. I would like to thank Prof. Liepmann particularly for his timely academic and career advice during my studies.

I would like to thank all members of the BIOPOETs group, for their constant support, debates, mentorship, and friendship. I would like to especially thank Dr. Chi-Cheng Fu, Dr. Pan Qiong, Dr. Annie Wu, and Dr. Hansang Cho for their care and encouragement all these years. In particular, I thank Chi-Cheng for all the great memories we had together.

Also, I would like to thank Dr. Paul Lum at the Bionanotechnology center for advice and technical help. In addition I thank the department, and especially Ms. Rebecca Pauling and Ms. Kristin Olson for advice. I would also like to thank the undergrads, Lucy Hu, Rohan Thakur, and Jeffrey Feng, for providing technical assistance.

I am indebted to the Bill & Melinda Gates Foundation, Siebel Scholarship, Ministry of Education in Taiwan, Dr. James Soong Fellowship, SHARP, BioChip, DARPA, the Bioengineering department, and my family for supporting me financially.

I also thank all my friends in the International Graduate Student Ministry for your prayers, your endless encouragement to me during difficult times, and most of all, for bringing the gospel to me.

To my parents Shyi-Dong and Bih-Hua, and my brother Karl, I would not have been able to do this without your unconditional love. I cannot express how lucky I am to have this family. I also thank Kate Feng, for her endless meals, encouragement, support, prayers, and love.

Finally, I give thanks to God for being my provider, giving me strength, and showering me with love. Blessed be your name.

Chapter 1. Introduction to Integrated Molecular Diagnostic Systems

Current standard quantitative molecular diagnostic tests, such as quantitative nucleic acid detection, are often done in centralized laboratories with costly bench top equipment. This kind of testing is challenging for resource-poor rural areas, which often lack infrastructure, funding, and trained personnel. Unfortunately, areas hardest hit with pandemic diseases are often developing countries with the least medical resources. For example, **Figure 1** shows that the highest prevalence of HIV occurs in developing countries, with more than 60% of infections taking place in sub-Saharan Africa, where less medical infrastructure is available.

Point-of-care diagnostic devices can be brought to the field for on-site testing. They are typically low-cost, portable and can be operated with few simple steps. Point-of-care diagnostic devices are designed to alleviate the need for patients to travel to centralized hospitals. They are designed to be brought to the patients instead. Current common examples of widespread commercially available point-of-care devices include the pregnancy test and glucose testing meters. However, these systems are limited in several ways. Pregnancy tests are not quantitative and glucose meters have sensitivities too poor (~mg/mL) to adopt for protein detection. There is a need to develop low-cost assays that can quantitatively detect nucleic acid molecules down to the molecular level for next-generation diagnostic systems.

In this dissertation, some of the developed integrated microfluidic components and

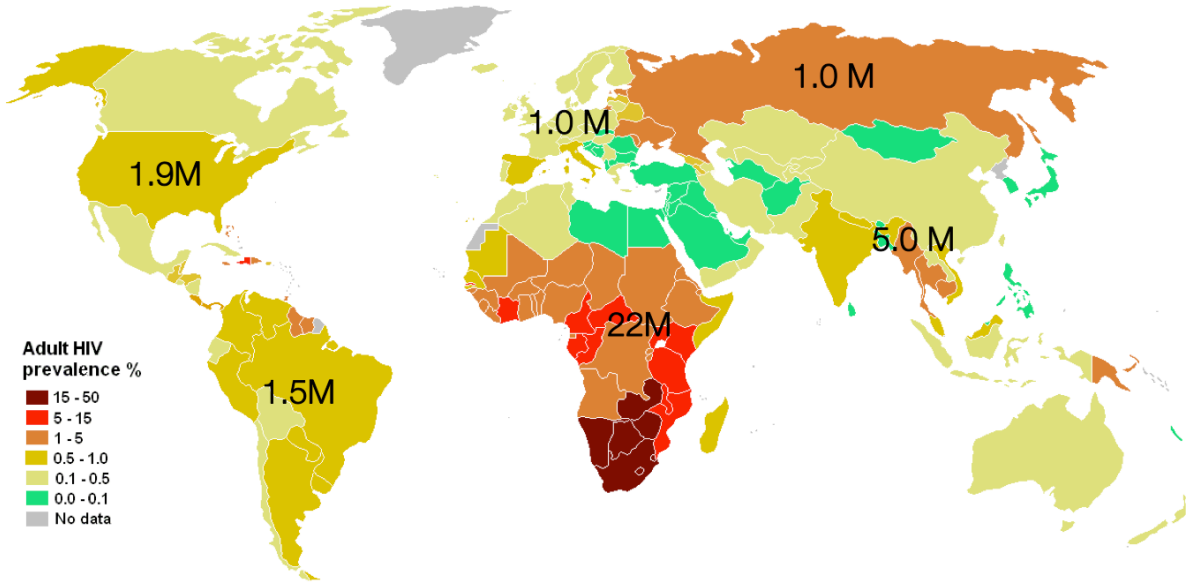

Figure 1 HIV prevalence is highest in developing countries, however these countries often have less medical resource such as trained personal, centralized labs, and income per capita. Numbers denote the number to infected patients in each continent in millions. (ref: UNAIDS)

systems that provide a comprehensive solution for quantitative molecular detection are presented. It is important to consider system integration early on, otherwise during later integration stages of assay development one may realize that intrinsic limitations pose major difficulties from incompatibilities among system components. With this in mind, it is crucial to first thoroughly review current state-of-art technologies in order to identify strength and weaknesses in each approach. Then will it be possible to build compatible systems that can be seamlessly integrated together.

The goal of chapter 1 of this dissertation is to give a comprehensive review and comparison of current state-of-art technologies relevant to the design of next generation point-of-care diagnostic devices. In this chapter, the majority of references stem from publications published after 2010. This was done in order to highlight the most recent advances in this field. Older references are sometimes added when they are of particular importance. In Chapter 1, first the key requirements necessary for next generation point-of-care diagnostic platforms is discussed. Then, individual components of each step of assay design will be presented

In later chapters of this dissertation, research results from the development of the Integrated Molecular Diagnostic Chip (iMDx) will be presented. Specific advances in microfluidic sample preparation, and next generation power-free passive microfluidic pumping will be discussed. A prototype of the iMDx chip that can perform quantitative nucleic acid detection directly from human blood samples in 30 minutes is shown. On-chip micro-patterning of reagents will also be detailed. Finally, conclusions and vision for future research and development plans is laid out.

1.1 Key requirements for next generation point-of-care diagnostic platforms

Current standards for antigen and nucleic acid detection

The current common standards for assays and their respective strengths and weaknesses are shown in **Figure 2**. Lateral flow assays[1] generally use antibodies to capture antigens in a fibrous wicking pad, and then latex beads or gold nanoparticles are used as signal enhancers for naked eye readout. The pregnancy dipstick test or HIV oral swab test are common examples of commercially available qualitative lateral flow assay tests. Nucleic acid hybridization assays[2–7] have also been developed for amplification result end-point detection with lateral flow assays. These assays can be done in 10~20 minutes. Though rapid and economical, these kinds of assays are typically not quantitative. Only a yes/no answer is given for readout. However, lateral flow assays are widely used in the field because of their simplicity.

Enzyme linked immunosorbant assays (ELISA) have a similar antibody-antigen

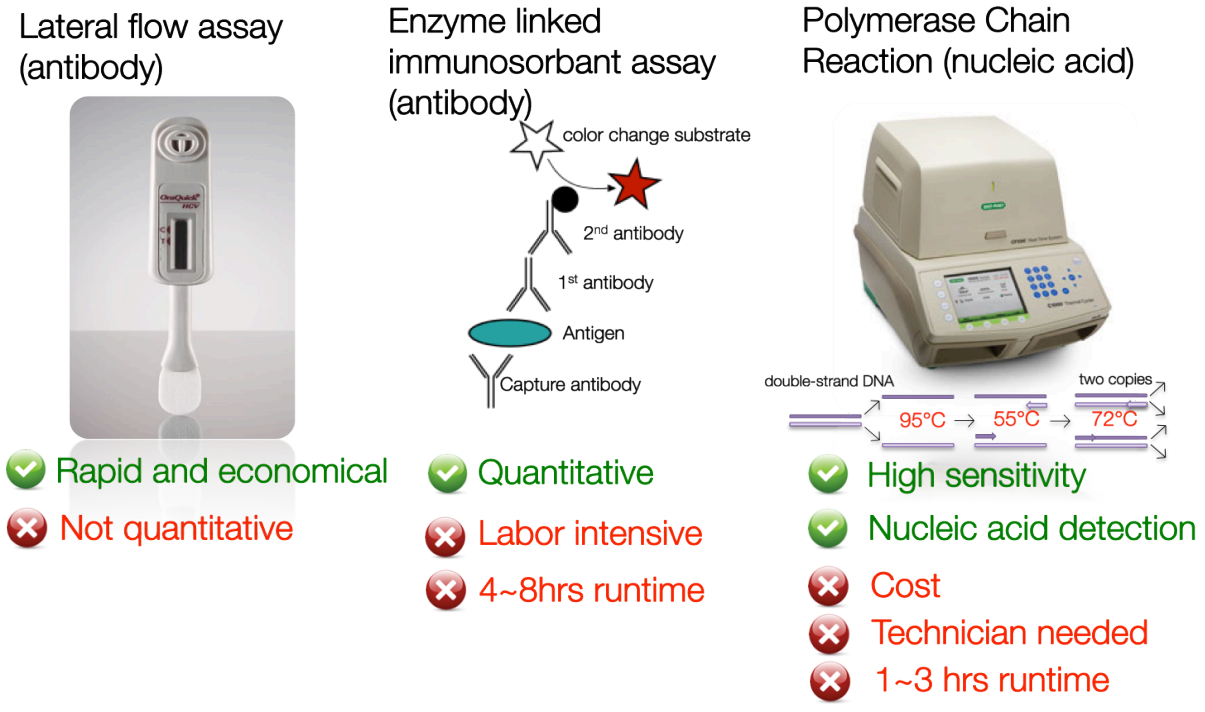

Figure 2 Examples of common diagnostic assay standards. (ref: pictures from Oraquick, Wikipedia (Jeffrey M. Vinocur), and Bio-Rad)

ligand binding process, however ELISA's are prepared on clear polystyrene or polycarbonate plates, and ELISA uses enzymes such as horse radish peroxidase or alkaline phosphatase to amplify the readout signal by causing a colour change in the substrate. Due to the clear optics and enzymatic signal enhancement, ELISA assays

are quantitative. However because ELISA needs multiple washes, several hours of assay time, and special plate reading machines, ELISA assays are difficult to perform in the field.

The current standard for nucleic acid detection is based on Polymerase Chain Reaction (PCR). This is commonly done on quantitative PCR machines. PCR is the most sensitive molecular assay, it is possible to detect down to one molecule per reaction. However, the main disadvantages are the high cost, the need of technical expertise, and long assay time. The high cost is because quantitative PCR machines need a heat cycling apparatus, computer, and a fluorescent detection shuttle that scans the microplate wells every few seconds. These machines can easily cost up to $40~80k, and they are usually bulky bench top machines that are not portable. In addition, they require external power sources, which are often taken for granted in developed countries, but may not be available or stable in rural areas of the world. Also, sample preparation is needed for PCR assays as nucleic acid needs to be purified from complex samples in order to avoid inhibition of the polymerase enzymes in PCR. Sample preparation is manually intensive and also as well as the setup of PCR too. These limitations render PCR testing to be performed predominately at centralized lab facilities. However, this may be a hindrance for those who have to travel far from rural villages to be tested. Finally, the total assay time is typically 1~3 hours so patients would often have to wait for results until the clinic contacts them later, which can be several days. This may cause additional problems because contact may be difficult once the patient returns to distant rural villages.

Standards for the next generation of point-of-care devices

Table 1 Components of a Clinical Laboratory Improvement Amendments (CLIA) waiver application. (ref: FDA, CLIA waiver applications for manufacturers of in vivo devices, 0910-0598)

CLIA wavier required demonstrations
• Demonstrating the device to be simple to use. • Results of risk analysis including the identification of potential sources of error for your device. • Demonstrate insensitivity to variations of environmental and usage. • (1) Describe measures implemented to mitigate risk of errors, and (2) demonstrate ability of failure alert, fail-safe mechanisms, and other control measures to mitigate risk errors. • Demonstrate that the device has an insignificant risk of erroneous result in the hands of the intended user. • Proposed labeling with instructions for use consistent with a device that is “simple”.

With the limitations of current systems laid out in the last section, there is a need to define what would be ideal assays for next generation point-of-care devices. Guidelines from the Food and Drug Administration is shown in **Table 1,** and **Table 2**. These guidelines are examples of the desirable characteristics of future devices for point-of-care.

Table 2 Definition of "simple" for CLIA waived devices. (ref: FDA, CLIA waiver applications for manufacturers of in vivo devices, 0910-0598)

Simple tests should include these characteristics
• Is a fully automated instrument or a unitized or self-contained test. • Uses direct unprocessed specimens, such as capillary blood (fingerstick), venous whole blood, nasal swabs, throat swabs, or urine. • Needs only basic, non-technique-dependent specimen manipulation, including any for decontamination. • Needs only basic, non-technique-dependent reagent manipulation, such as "mix reagent A and reagent B." • Needs no operator intervention during the analysis steps. • Needs no technical or specialized training with respect to troubleshooting or interpretation of multiple or complex error codes. • Needs no electronic or mechanical maintenance beyond simple tasks, e.g., changing a battery or power cord. • Produces results that require no operator calibration, interpretation, or calculation. • Produces results that are easy to determine, such as 'positive' or 'negative,' a direct readout of numerical values, the clear presence or absence of a line, or obvious color gradations. • Provides instructions in the package insert for obtaining and shipping specimens for confirmation testing in cases where such testing is clinically advisable. • Has test performance comparable to a traceable reference method as demonstrated by studies in which intended operators perform the test. If a reference method is not available for a test you are proposing for waiver, please contact OIVD to discuss your proposed plan prior to submitting your application. • Contains a quick reference instruction sheet that is written at no higher than a 7th grade reading level.
Should not include these characteristics
• Sample manipulation is required to perform the assay. (For example, tests that use plasma or serum are not considered simple.) Sample manipulation includes processes such as centrifugation, complex mixing steps, or evaluation of the sample by the operator for conditions such as hemolysis or lipemia. • Measurement of an analyte could be affected by conditions such as sample turbidity or cell lysis.

Table 1 shows the necessary components for the application of the Clinical Laboratory Improvement Amendments (CLIA) waiver defined by the FDA. All testing on human specimens for diagnostic, prevention, and treatment in lab facilities in the United States are regulated by the CLIA regulations set by FDA. A device that has obtained the CLIA waiver certificate is a device simple and robust enough that there will be low risk of error. For example, FDA approved home tests automatically qualifies for a CLIA wavier. In simple terms, companies that develop point-of-care devices generally wish to obtain a CLIA wavier, so they can prove that their device is simple and robust for point-of-care applications. More information can be found on FDA's definition of "simple" in **Table 2**.

In summary, the CLIA guidelines are important to have in mind early on in the design phase of developing assays. The CLIA waiver guidelines should be the basic framework when one develops a diagnostic device.

Design considerations for point-of-care molecular diagnostic systems

One of the first design considerations is to decide whether the assay platform will be fibre/paper[8–15] based or microfluidic[16–19] based. Fibre/paper systems are those found in lateral flow assays. Microfluidic based systems usually use a transparent polymer or elastomer (e.g. PC, PS, COC, PDMS) to make the devices. A

Table 3 Comparison of platform technologies.

	Advantages	Disadvantages
Paper /fibre based	Lower cost Ease of disposal (burning) High surface area Equipment-free pumping Proven in field	Optically opaque Evaporation 2D geometry No liquid storage Not ideal for PCR, ELISA Quantification more difficult Harder integration with electronics Difficult to integrate with microfluidics
Microfluidic based	Optical clarity Higher sensitivity Microfluidic integration Low evaporation for PCR Higher consistency Easier integration with electronics Easier integration with mechanics Micro/nano scale fluidics Digital PCR, ELISA possible Liquid reagent storage	Higher cost Pumping system needed Disposal problems Lower surface area

comparison of the relative advantages and disadvantages of the two systems is shown in **Table 3**. Considering the strengths of each platform, paper systems seem to be best suited for protein, chemistry, and post amplification nucleic acid amplicon verification assays. However, it is difficult to run paper-based systems for PCR amplification because evaporation can be a problem at elevated temperatures. The opaqueness of paper/fibre is also a major drawback for more sensitive and quantitative optical detection. On the other hand, microfluidic based methods have a lot of potential applications in quantitative detection, in particular nucleic acid amplification assays. This is because microfluidic platforms can be made with highly transparent polymers, so various types of optical detection techniques can be used on microfluidic platforms. For example, fluorescence, bright field, phase contrast, dark field, spectroscopy, and absorption can be done with a clear substrate. For this dissertation work, focus has been emphasized on developing microfluidic-based components due to these reasons.

The next step of design is to have a whole picture in mind of what is necessary for a complete integrated system. **Figure 3** shows what technologies one would need to consider involved in each stage of the assay. It is important to set the outline early during the development, and ensure each individual component is fundamentally compatible with the entire system. This chapter will provide a detailed up-to-date review of the most recent developments of each of these components.

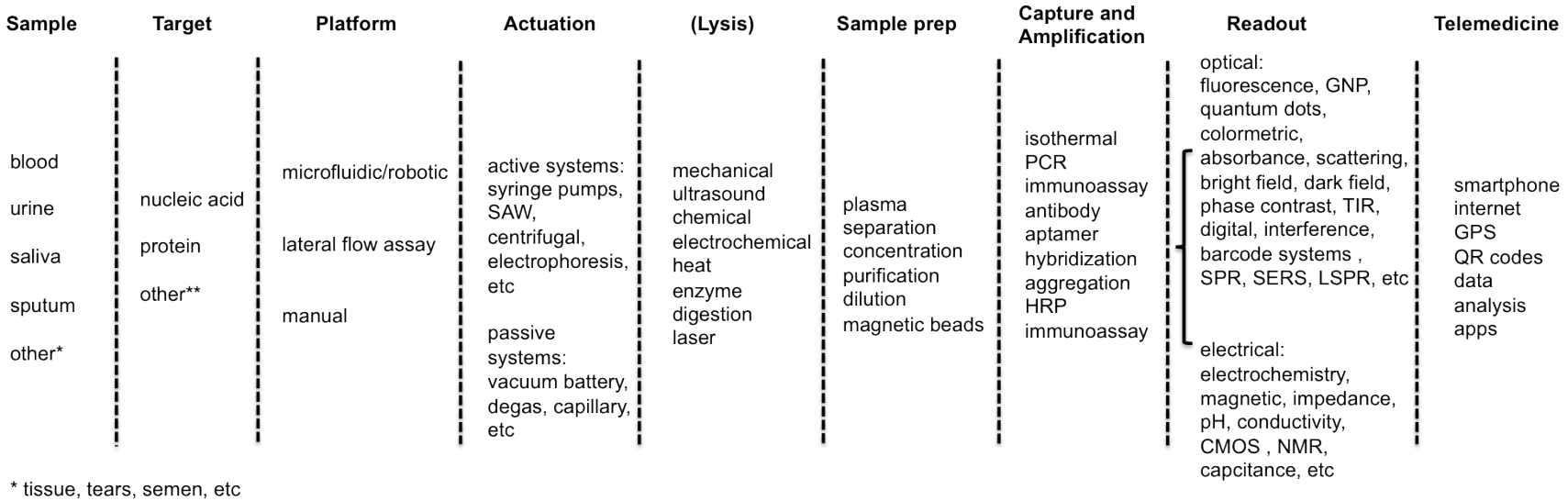

* tissue, tears, semen, etc

** other molecular targets such as glucose, ion concentration, etc

Figure 3 Design considerations for a complete integrated detection system.

1.2 Sample preparation with plasma separation

Table 4 A comparison of plasma separation methods.

	Comparison of plasma separation methods				
Mechanism	Centrifugation	Microfluidic size exclusion f iltration	Zweifach-Fung e ffect AM	Membrane s ize exclusion filtration	Microfluidic sedimentation
Example	Microfluidic ro tating disk	Microfluidic filters[2120]	Integrated barcode chip[2221]	www.amic.se	Digital Plasm a Separation
External P ower Requirements	Electrical or mechanical power source required	Controlled external pressure for flow propulsion is required.	Controlled external pressure for flow propulsion is required.	None	None
Manufacturing Precision	Low	High	Low	Low	Low
Cost	Medium	Medium	Low	Low	Low
Portability	Low	Low	Low	High	High
Separation Efficiency	90%	20%	50%	20%	>95 %
Clogging Prob lems	No	Yes	No	Yes	No

If the input sample is human whole blood, blood cell removal is often necessary for down stream analysis because the blood cells can interfere with assays. For example, hemoglobin in red blood cells is a major polymerase inhibitor because of hemoglobin's chelating nature. 0.1% of blood in a reaction mix can cause a PCR reaction to fail. Also blood cells can interfere with optical readout because they scatter light and can be opaque when concentration is high. **Table 4** is an example of several blood cell removal techniques commonly used. In addition, Kersaudy-Kerhoas[22] et al., has done an excellent review on blood separation methods. Methods using the Zweifach-fung[21] effect have a main microfluidic channel pumping at high speed, and small perpendicular side microfluidic channels pumping out of the side of the main channel; the blood cells are separated via inertial effects. The disadvantage of this type of separation is that precisely controlled external

pumps are required. In the later chapters of this dissertation, work on the digital plasma separation platform, which is a microfluidic sedimentation based method will be presented.

1.3 Next generation nucleic acid detection methods

Table 5 A comparison of nucleic acid detection methods.

Method	Advantages	Disadvantages
Real-time PCR	well established	higher equipment cost
	primers design straightforward	bulky machines
	no PCR reagent license issues	need power source
	quantitative	evaporation problems
		catastrophic bubble expansion
Ultrafast PCR	primers design straightforward	higher equipment cost
	no PCR reagent license issues	bulky machines
	rapid	need power source
	quantitative	evaporation problems
		catastrophic bubble expansion
Isothermal amplification	lower temperature	still patent protected
	possible without power source (heat packs)	primer design more complex
	less evaporation and bubble problems	less literature
	rapid	higher reagent cost
	power-free possible	certain types need more than 2 primers
	simpler equipment	
DNA microarrays	highly multiplexed	lower sensitivity
	broad detection	many washes and long assay time
	ideal for novel pathogen detection	need special scanner for readout
		lower signal intensity
Nucleic acid lateral flow assay	quick readout	not quantitative
	naked-eye readout	limited multiplexing
		often needs off-chip amplification

A comparison table of nucleic acid detection technologies is shown in **Table 5**. Currently, the most dominant form of quantitative nucleic acid analysis is via real-time PCR. Molecular level DNA/RNA template detection, template concentration identification, and melting curves are among the most commonly acquired data from real-time PCR. Another nucleic acid detection method- the DNA microarray[23–25], is also used widely for the analysis of gene expression applications. On the other hand, more recent technologies are such as nucleic acid lateral flow assays and isothermal amplification technologies. Both microarray and nucleic acid lateral flow assays is base on the principle of DNA hybridization. In essence, the nucleic acid lateral flow assay is very similar to antibody based lateral flow assays, except that the biomolecule capture mechanism is DNA hybridization instead of antibody-antigen binding reactions. More recent technologies are such as the ultrafast PCR[26–28] or isothermal amplification will be discussed in more detail in the following sections.

Isothermal amplification methods

Isothermal amplification[29–41] is one of the fastest growing technologies for applications in point-of-care settings. A comparison of isothermal amplification

Table 6 Comparison of isothermal amplification technologies. (ref: David Boyle et al., Point-of-care nucleic acid testing for infectious diseases, 2011).

Assay	Reaction temperature (°C)[a]	Reaction duration (min)[a]	Multiplex[b]	Rapid detection formats[c]	Target	Amplification product
Methods based on RNA transcription						
NASBA	41[d]	105	Y	RTF, NALF	RNA (DNA)	RNA, DNA
TMA	60[d]	140	Y	RTF	RNA (DNA)	RNA, DNA
SMART	41[d]	180	N/A	RTF	RNA, DNA	RNA
Methods based on DNA replication with enzymatic duplex melting/primer annealing						
HDA	65	75-90	Y	RTF, NALF	DNA[e]	DNA
RPA	30-42	20	Y	RTF, NALF	DNA[e]	DNA
Methods based on DNA-polymerase-mediated strand displacement from linear or circular targets						
LAMP	60-65[d]	60-90	N/A	RTF, NALF, RTT, TE	DNA[e]	DNA
CPA	65	60	N/A	RTF, NALF	DNA	DNA
SMART-AMP	60	45	N/A	RTF	DNA[e]	DNA
RCA	65	60	N/A	RTF	DNA[e]	DNA
RAM	63[d]	120-180	N/A	RTF	DNA[e]	DNA
Methods based on polymerase extension/strand displacement, plus a single strand cutting event						
SDA	37	120	Y	RTF, NALF	DNA[e]	DNA
NEAR	55	10	Y	RTF, NALF	DNA[e]	DNA
NEMA	65	30	N/A	NALF	DNA	DNA
ICA	60	60	N/A	RTF	DNA	DNA
EXPAR	55	10-20	Y	RTF, NALF	DNA	DNA
BAD AMP	40	40	N/A	RTF	DNA	DNA
PG-RCA	60	60-120	N/A	RTF	DNA	DNA

[a] Typical incubation temperature and reaction time, variability might exist.
[b] Capability to multiplex, defined as the ability to amplify simultaneously at least two different targets (or one target and an internal control): yes (Y) or data not available (N/A).
[c] Most commonly reported formats only. Other formats might exist, but are not included here.
[d] Initial incubation at a higher temperature is sometimes recommended.
[e] RNA can be the target if a reverse transcriptase step to generate cDNA is first included.Abbreviations: RTF, real-time fluorescence; NALF, nucleic acid lateral flow; RTT, real-time turbidity; TE, turbidity- related endpoint, including fluorescence and colorimetric enhancement.

technologies can be found in **Table 6**[4242]. Isothermal amplification is a new kind of nucleic acid amplification technology. Instead of using thermal cyclers to denature double stranded amplicons as in conventional PCR, isothermal amplification uses enzymatic activity to displace double stranded DNA, so no thermal cycling is required. This allows all amplifications to be carried at a constant temperature which is typically much lower than 95 °C, eliminating the need for costly thermal cycling equipment and allows for electricity-free heating alternative options. Various isothermal heating methods will be discussed in the next section. Also since reaction temperatures are lower, there are less evaporation problems and less chance of catastrophic air bubble expansion in microfluidic devices, making the design requirements easier for microfluidic chips. Another advantage of this kind of method is that reactions can often be extremely fast, for example, recombinase polymerase amplification[43] (RPA) can amplify in 5~20 minutes, and NEAR technology can amplify as fast as 10 minutes. Also there are many cases showing higher robustness in complex samples than PCR. For example, in later chapters of this dissertation, it is shown that RPA can amplify directly from human blood plasma whereas PCR is completely inhibited.

Nevertheless, there are several limitations with isothermal amplification. For one, primer design is not as straightforward as conventional PCR, for example, loop mediated amplification[44] (LAMP) uses up to six primers. Also, primer design algorithms may not be completely clear, and sometimes experimental optimization may be needed. Also, another potential limitation is that most of these isothermal techniques still have patent protection, and reagent costs may be higher than conventional PCR due to patent protection, though this problem will cease as patents expire in the next few years.

In recent years, RPA has started to see an explosion of research activity. RPA seems to be starting to replace the previous most popular LAMP technology. The reason for this adoption is because RPA is one of the fastest and robust isothermal technologies commercialized. Other types of isothermal amplification technologies often are not widely commercialized yet (except for LAMP, NASBA, and HDA). RPA also is very robust and can amplify directly from blood plasma, stool samples, leaf extract, and urine. Though the primers still need to be experimentally optimized, there are a plethora of target pathogen primers being developed these years. Also, for point-of-care devices, usually only a few primers are needed on one chip, so there is no need to redevelop primers for each disease. One can simply select primer sequences from literature for specific diseases, and integrate that on-chip. For these reasons, there have been several new commercial examples that use RPA as a detection platform. The most common current commercial platform is performing tube based amplification, then running the reaction mix through a nucleic acid lateral flow assay for a yes/no qualitative readout. With these merits, isothermal technologies similar to RPA would likely be the key to change future development of point-of-care diagnostics.

1.4 Microfluidic pumping methods

There are two main types of fluidic pumping- active and passive systems. **Table 7**[45] shows a list of examples of common active pumping techniques. **Table 8** shows a comparison of common passive pumping systems with the vacuum battery system that is presented in this dissertation; a more comprehensive report on the vacuum battery system will be discussed in the later chapters of this dissertation.

Active[46–54] pumping systems are systems that require external power and control sources. Active pumping includes surface acoustic waves, piezoelectric actuation, pneumatic valves, syringe pumps, and electroosmotic pumping, etc. In general, they have a higher degree of control and precision than passive systems. However, the high cost of active systems and the requirement for external pumps, pneumatic systems, power sources, control systems, makes active systems more difficult to adopt for low cost point-of-care diagnostic applications.

On the other hand, passive pumping systems are an attractive alternative for adoption in low cost point-of-care assays. One common example is fibre based capillary wicking; these are often seen in lateral flow assay tests such as the disposable pregnancy test. Paper based assays[8,55,56] also use wicking fibrous material for pumping. Though simple, these systems are opaque and can interfere with optical detection. A second common type of capillary pumping is using fluid wicking into plastic sheets gaps that are hydrophillically treated, this is often seen in glucose test strips. More recently, more complex logic functions have been developed with capillary microfluidic structures. For example, sequential flow[57] and programed circuits[58] utilizing triggers and valves have been developed. Though these new developments hold lots of promise for more complex liquid handling, there are a few challenges that are intrinsic with capillary systems. For example, the wicking surface needs to be hydrophilic, while most plastics are hydrophobic, so special surface treatments are needed to lower the surface energy. Also, since

Table 7 Common examples of microfluidic pumping. (ref: Pamela N. Nge, Chemical Reviews, 2013).

category	actuation mechanism	approach	advantages	disadvantages
passive	capillary (nonmechanical)	spontaneous fluid motion by capillary action	simple and straightforward; no additional fabrication steps	flow is not continuous over a long period of time; flow cannot be controlled easily
active	electroosmotic (nonmechanical)	electroosmotic force through interaction of applied electric field with electrical double layer	ease of manufacture; constant flow rate which can be manipulated by the applied voltage	adsorption can affect flow; only works with conductive solutions
	electrochemical (nonmechanical)	generation of gas bubbles, such as by electrolysis	ease of manufacture; small size; low power	gas bubbles and electrochemical byproducts can block conduction between the electrodes and hinder actuation
	pneumatic peristaltic (mechanical)	sequential actuation of a series of pneumatic microvalves with pressurized air	easily integrated; fast response time	requires external equipment to supply compressed air; pulsed fluid flow
	electrohydrodynamic (nonmechanical)	interaction between electrostatic forces and ions in nonconducting fluids	easily integrated; can pump a variety of liquids; requires low voltages	flow rate depends on material surface properties; typically low flow rates and pressures
	acoustic (mechanical)	force produced by the interaction of longitudinal waves with the surrounding fluid	does not generate byproducts that can contaminate sample	applied frequencies can denature biomolecules and lyse cells
	magnetohydrodynamic (nonmechanical)	Lorentz force produced when orthogonal electric and magnetic fields are applied to a conducting solution in a microchannel	ease of integration; continuous flow	possible electrolysis of water at the electrodes; bubble formation

Table 8 A comparison table of passive pumping technologies. Red highlights show disadvantages compared to the vacuum battery system.

	Active systems	Capillary Loading	Conventional degas flow	µSIP	Vacuum Battery System
Examples	syringe pumps, quake pumps	pregnancy test strips	SIMBAS[59] system	Microfluidic Solution Isolated Pumping[60]	this work
Mechanism	external power source	wicking by capillary action	degas through permeable materials	degas through membrane	void space stores vacuum and degas through lung like structures
Portability	difficult	yes	yes	yes	yes
Cost	high	low	low	low	low
Optical properties	NA	fibers are opaque or cause autofluorescence	transparent	transparent	transparent
Flow control	excellent	superior than degas	flow has fast exponential decay	depends on thumb pumping	5 times longer decay time constant than degas flow
Flow speed	nl~ml/min	µl~ml/min	~µl/min	~nl/min	10 times faster than degas, also faster than µSIP. (nl~µl/min)
Dead-end loading	no	no	yes	yes	yes
Loading volume	not limited	µl-ml	nl-µl	nl-µl	nl-ml
Operation time	not limited	secs~mins	mins	depends on thumb pumping	hours
Geometrical	NA	no deep height	none	none	none

constraints		channels			
Surface treatment	none	need to be hydrophillic	none	none	none
Equipment/ power free	no	yes	yes	need thumb pressing	none
Constructio n	complex with peripherals	simple	simple	extra valve structure and thumb pump layer needed.	Simple two layer fabrication

capillary force depends on geometry, deep channel designs are difficult to achieve in capillary pumping. Another problem is that capillary pumping does not remove trapped bubbles, which can become a problem if any heating steps such as thermal cycling in PCR are done, as these bubbles may expand and push out liquid in an uncontrollable manner.

An alternative kind of passive pumping is called degas pumping[61–76]. These degas pumping systems use PDMS degassing to create gentle vacuums to drive flow. However, degas loading is not consistent and decays very rapidly. This dissertation presents a unique system called the vacuum battery system, which uses large voids to store vacuum, and release the vacuum potential in a controlled manner. The main advantage of the vacuum battery system over conventional degas pumping is that the vacuum battery system has much better stability and consistency, loads faster, operates for longer time, and can be easily tuned. In addition, the vacuum battery system can also remove air bubbles, perform dead-end loading, and has excellent optical transparency. The vacuum battery system will be discussed in more detail in the following chapters of this dissertation. A patent application for the vacuum battery system has been submitted and is current under review.

1.5 Reagent patterning methods

For reagent patterning, several methods commonly used are shown in **Figure 4**[77]. The main considerations of patterning systems are the cost of the system and the volume size and footprint needed for each application. The reagent to be patterned also is a factor in determining which printing method to use. More detailed analysis of patterning methods will be discussed in Chapter 2 of this dissertation.

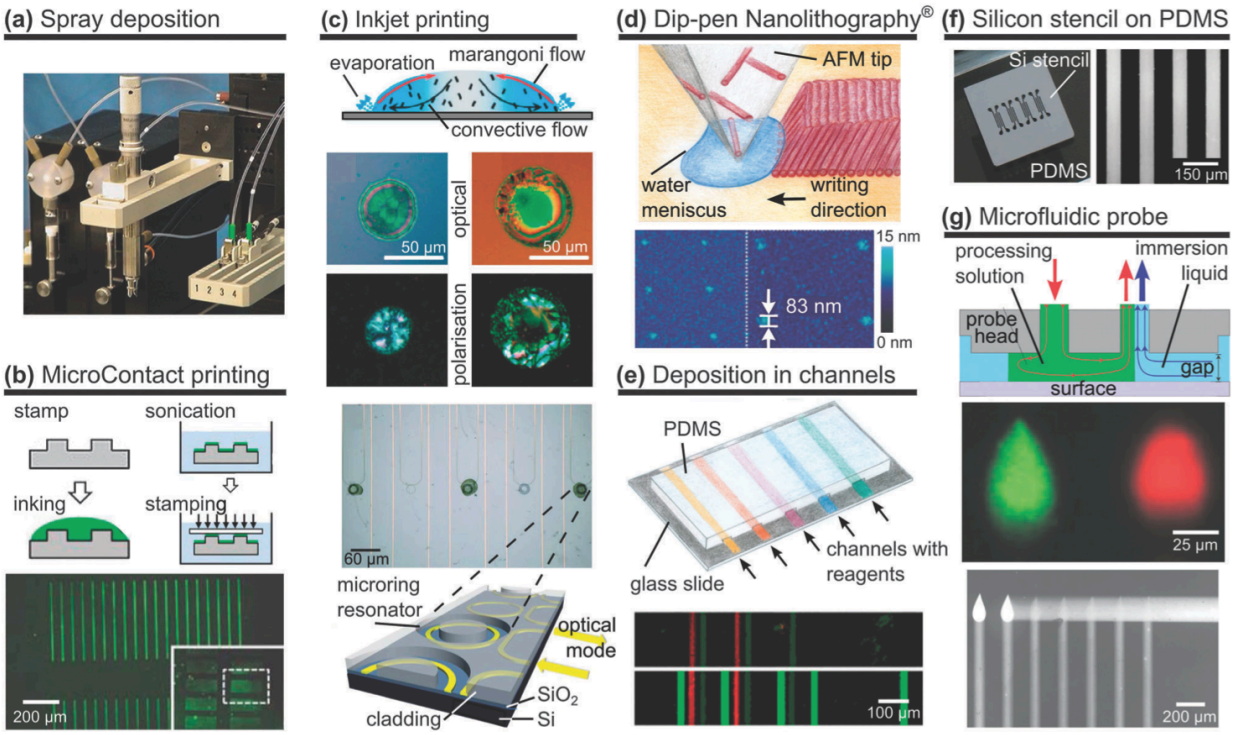

Figure 4 Reagent patterning methods. (a), electrospraying is often used to pattern lateral flow assays with little loss of enzyme activity. (b), contact printing has the advantage of nano-scale resolution printing, however surface energy have to modulated to be hydrophilic/hydrophobic. (c), inkjet printing is advantageous because there is no contact with the substrates, minimalizing substrate damage. It can also pattern a wide range of biological and substrates. It also is reprogrammable and can be used for mass production. Microarrays often use this kind of technology for printing DNA or proteins. (d), Dip-pen Nanolithography uses an AFM tip to transfer liquids via the meniscus at the tip to substrates. This kind of patterning can achieve resolution lower than 30nm, however throughput is low with this technology. (e), microfluidic channel patterning is simple and low cost, it is unique in the sense that multiple washes and reagents can be applied to the same surface in a precise way. One common example is patterning antibodies onto surfaces. (f), stencils can be used when individual islands of patterns are desired, as channel type patterning always require a continuous pattern from inlet to outlet. (g), the microfluidic probing method uses hydrodynamic focusing to focus reagents into a local region. A continuous flow processing solution run through a pre-wetted surface with immersion liquid, additional immersion liquid is applied to focus the processing solution. This method produces more uniform patterning, and avoids evaporation problems, but consumes more reagents than inkjet printing. (ref: Martina Hitzbleck et al. Chem. Soc. Rev., 2013.)

1.6 Digital amplification platforms

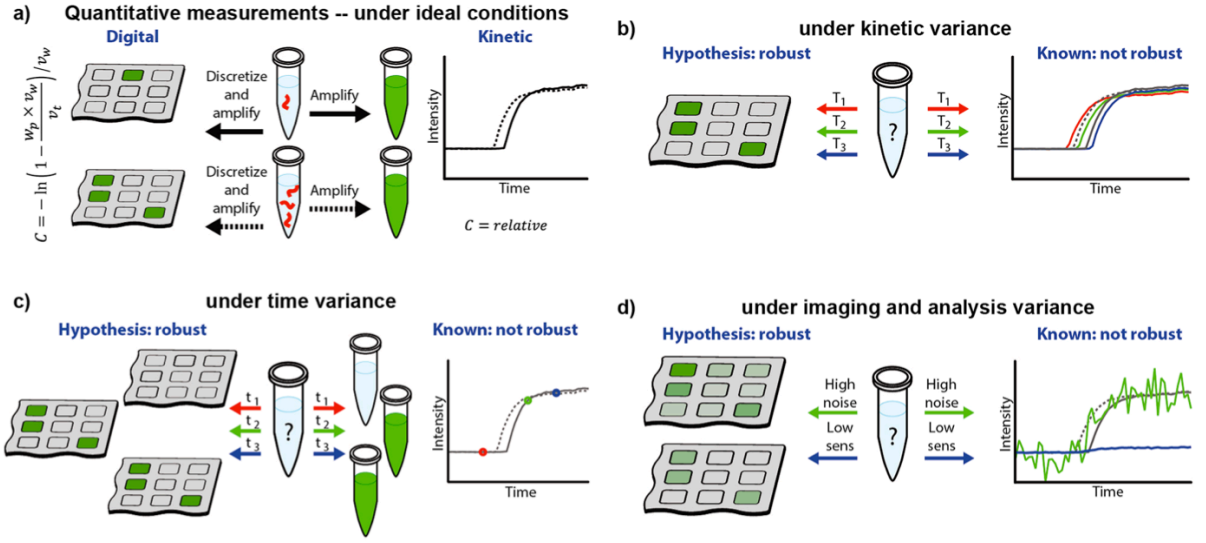

Figure 5 Concept of digital amplification and superior robustness than real-time PCR. (a) Digital amplification works by partitioning samples into small volumes and conducting end point detection. (b) and (c), since digital amplification is end-point detection, even though there are kinetic or time variances, the final number of positive wells will not vary. (d) imaging and analysis variance also has less effect on quantification results. (ref: David A. Selck, et al. Analytical chemistry, 2013.)

In recent years, there has been a new method of quantifying nucleic acid amplification called digital amplification[78]. This technology can deliver more sensitive and robust quantification under environmental variances compared to real-time PCR. The mechanism of digital amplification is shown in **Figure 5**[79]. The key concept of digital amplification is to partition one large sample into many nano-liter sized samples, and then run PCR reactions in each sub sample until endpoint saturation. As the samples are partitioned, each compartment becomes a mini-amplification reaction. Each compartment will have either zero or at least one target DNA/RNA. Those compartments that have target will amplify, and a final endpoint readout of the percentage of positively amplified wells (via fluorescence or colour change) is counted. This percentage can be correlated with the initial target concentration, similar to what the ct value in real-time PCR elucidates.

The key advantage of digital amplification is that it is robust against variations in kinetics, time, imaging, and analysis techniques, because quantification is end-point, not real-time, only the number of compartments that passes threshold are quantified. No real-time imagining equipment is needed. Additionally, it delivers much higher resolution than PCR systems. Also, the compartmentalization step lowers the sample interference from other sources, such as background non target DNA or amplification inhibitors, because compartmentalization is increases the target to background ratio.

Previously there have been examples[80] of digital amplification for SNP detection, copy variance detection, single cell population detection, single cell mRNA expression, rare variant detection, methylation-specific amplification, and gene expression analysis. There has also been point-of-care assays such as the SlipChip[81], degas LAMP[82], and Self-priming chip[83].

Recently there has also been interesting applications for the detection of other molecules than nucleic acids, such as single molecule ELISA[84] (**Figure 6**) and single molecule detection of bacteria[85] (**Figure 7**).

Common platforms of digital PCR can be found in **Table 18**[80]. There are two main categories, droplet based systems, and microfluidic chambers[86]. Droplet systems have the advantage of producing very large numbers of droplets for high sensitivity; while microfluidic chambers are easier to adopt for point-of-care settings, and can achieve larger compartment sizes for tuning the detection dynamic range. However, one thing to note is that most bench-top systems are still too costly for point-of-care applications, costing from $80k~$250k. Most systems need lots of peripherals such as pumps, control systems, electricity, and they also need considerable manual input. For the future, is essential to build systems that integrate all functions into one chip realizing lab-on-chip, rather than chip-in-lab setups.

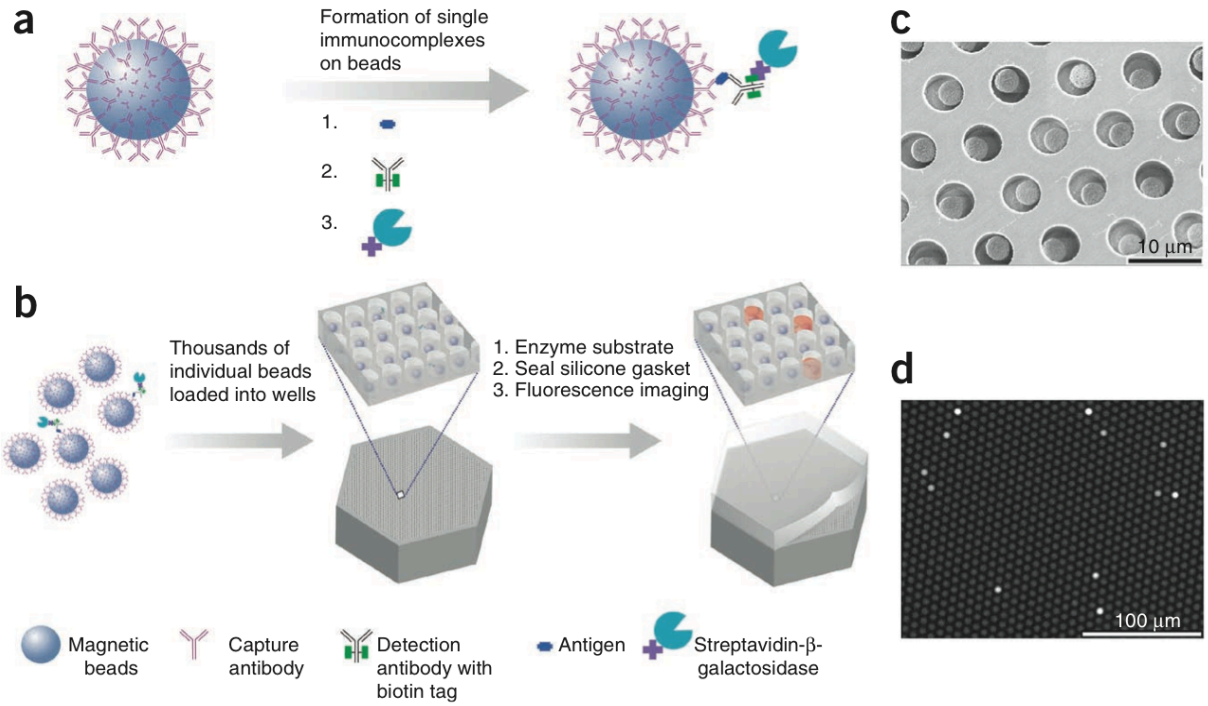

Figure 6 Single molecule digital ELISA. ~10^{-19} M level sensitivity was achieved, which is roughly 4 orders more sensitive then conventional ELISA. Antigens were captured with magnetic beads and partitioned into 50 fl reaction chambers for digital detection. (ref: David M Rissin, et al. Nature Biotechnology, 2010.)

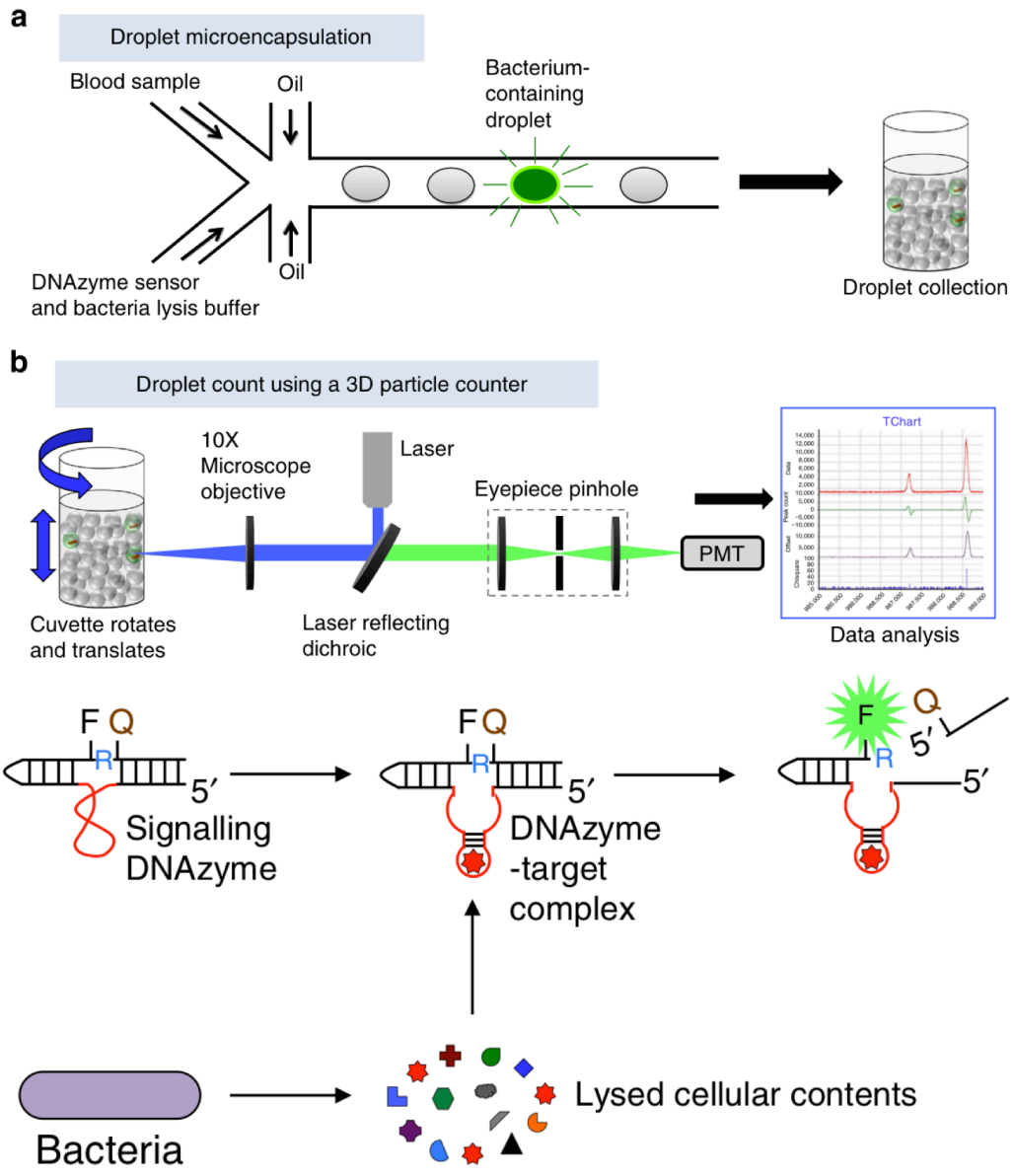

Figure 7 The Integrated Comprehensive Droplet Digital Detection (IC 3D) platform for single bacteria detection in unprocessed blood. 1 to 10,000 bacteria per ml can be detected using a DNAzyme-based sensor in 1.5~4 hr. DNAzymes are single stranded DNA oligonucleotides that are similar to enzymes in the sense that they have catalytic activity. In this case, the DNAzyme cleaves the ribonulceotide junction (R) when bacteria lysate binds to the DNAzyme. (ref: Dong-Ku Kang, et al. Nature communications, 2014.)

Table 18 Comparison of digital amplification platforms. (ref: Elizabeth Day, dfet al. Methods, 2013).

Platform	Description	Number of reactions	Aliquot volume	Analysis	Published sensitivity for rare variants	Integrated thermocycling and analysis	Commercial availability
Microdroplets							
ddPCR, BioRad	Microdroplets are generated in an emulsion and transferred to 96 well plates for cycling then to the custom analysis unit (QX100 droplet reader). The reader unpacks the emulsion to single droplets for analysis.	20,000 per 20 µl sample	1 nL	Automated droplet flow cytometer (two colors) with Taqman probes	0.001%	No	Yes QX100 Droplet digital PCR System
RainDrop, raindance technologies	Microdroplets, are generated in an emulsion, collected and transferred for thermocycled. The emulsion is then injected onto a microfluidic device and each droplet is analysed	Continuous flow	9 pL	End point analysis with TaqMan probes	0.0005%	No	Yes RainDrop digital PCR system
BEAMing (beads, emulsion, amplification, magnetics)	Microdroplets containing magnetic beads are generated in an emulsion and transferred to 96 well plates for thermocycling. The emulsion is dispersed and the beads separated. A circularizable probe is hybridized to the sequences on the beads and the changes of interest are labeled with fluorescently labeled dideoxynucleotide terminators	5×10^7 beads	9 µm diameter	Labeled beads are analyzed by flow cytometry	0.01%	No	No
Microfluidic chambers							
MegaPixel digital PCR	Surface tension based sample partitioning creates aliquots that are thermocycled and analyzed on the device. Fluorescent probes are annealing during thermocycling to enable analysis	1×10^6	10 pL	Microarray scanner	0.001%	Yes	No
Spinning disk platform	Aliquots are generated by passive compartmentalization through centrifugation. These are thermocycled and analysed on the device	1,000	33 nL	CCD camera – end point melting curve analysis	–	Yes	No
OpenArray Life technologies/ ABI	Microfluidc reaction chambers are loaded, thermocycled and analysed using the OpenArray system. Chambers may be preloaded with the assay of choice	3,072	33 nL	CCD camera – real time PCR end point melting curve analysis	–	Yes	Yes OpenArray Real-Time PCR platform
Digital array chip, fluidigm	Microfluidic reaction chambers are loaded, thermocycled and analysed using the BioMark system	9,180 (12×765) Prototype $2 \times 100{,}893$	6 nL	CCD camera – real time PCR end point melting curve analysis		Yes	Yes BioMark HD system

Notes and references

1. Posthuma-Trumpie, G. A., Korf, J. & Van Amerongen, A. Lateral flow (immuno)assay: its strengths, weaknesses, opportunities and threats. A literature survey. *Analytical and Bioanalytical Chemistry* **393,** 569–582 (2009).
2. Choi, D. H. *et al.* A dual gold nanoparticle conjugate-based lateral flow assay (LFA) method for the analysis of troponin I. *Biosensors and Bioelectronics* **25,** 1999–2002 (2010).
3. Jaroenram, W. & Owens, L. Recombinase polymerase amplification combined with a lateral flow dipstick for discriminating between infectious Penaeus stylirostris densovirus and virus-related sequences in shrimp genome. *Journal of Virological Methods* **208,** 144–151 (2014).
4. Mens, P. F., Van Amerongen, A., Sawa, P., Kager, P. A. & Schallig, H. D. F. H. Molecular diagnosis of malaria in the field: development of a novel 1-step nucleic acid lateral flow immunoassay for the detection of all 4 human Plasmodium spp. and its evaluation in Mbita, Kenya. *Diagnostic Microbiology and Infectious Disease* **61,** 421–427 (2008).
5. Rohrman, B. A., Leautaud, V., Molyneux, E. & Richards-Kortum, R. R. A Lateral Flow Assay for Quantitative Detection of Amplified HIV-1 RNA. *PLoS ONE* **7,** e45611 (2012).
6. Rohrman, B. & Richards-Kortum, R. Inhibition of Recombinase Polymerase Amplification by Background DNA: A Lateral Flow-Based Method for Enriching Target DNA. *Analytical Chemistry* **87,** 1963–1967 (2015).
7. Wang, Y. & Nugen, S. R. Development of fluorescent nanoparticle-labeled lateral flow assay for the detection of nucleic acids. *Biomedical Microdevices* **15,** 751–758 (2013).
8. Martinez, A. W. *et al.* Programmable diagnostic devices made from paper and tape. *Lab Chip* (2010). doi:10.1039/c0lc00021c
9. Hu, J. *et al.* Advances in paper-based point-of-care diagnostics. *Biosensors and Bioelectronics* **54,** 585–597 (2014).
10. Allen, P. B., Arshad, S. A., Li, B., Chen, X. & Ellington, A. DNA circuits as amplifiers for the detection of nucleic acids on a paperfluidic platform. *Lab on a Chip* (2012). doi:10.1039/c2lc40373k
11. Liu, H. & Crooks, R. M. Paper-Based Electrochemical Sensing Platform with Integral Battery and Electrochromic Read-Out. *Analytical Chemistry* **84,** 2528–2532 (2012).
12. Rohrman, B. A. & Richards-Kortum, R. R. A paper and plastic device for performing recombinase polymerase amplification of HIV DNA. *Lab on a Chip* **12,** 3082 (2012).
13. Schilling, K. M., Lepore, A. L., Kurian, J. A. & Martinez, A. W. Fully Enclosed Microfluidic Paper-Based Analytical Devices. *Analytical Chemistry* **84,** 1579–1585 (2012).
14. Wang, X., Hagen, J. A. & Papautsky, I. Paper pump for passive and programmable transport. *Biomicrofluidics* **7,** 014107 (2013).

15. Yetisen, A. K., Akram, M. S. & Lowe, C. R. Paper-based microfluidic point-of-care diagnostic devices. *Lab on a Chip* **13,** 2210 (2013).
16. Chin, C. D. *et al.* Microfluidics-based diagnostics of infectious diseases in the developing world. *Nat Med* **17,** 1015–1019 (2011).
17. Gervais, L., De Rooij, N. & Delamarche, E. Microfluidic Chips for Point-of-Care Immunodiagnostics. *Advanced Materials* **23,** H151–H176 (2011).
18. Jayamohan, H., Sant, H. J. & Gale, B. K. in *Microfluidic Diagnostics* (eds. Jenkins, G. & Mansfield, C. D.) **949,** 305–334 (Humana Press, 2013).
19. Rivet, C., Lee, H., Hirsch, A., Hamilton, S. & Lu, H. Microfluidics for medical diagnostics and biosensors. *Chemical Engineering Science* **66,** 1490–1507 (2011).
20. Lee, D.-S. *et al.* Construction of Membrane Sieves Using Stoichiometric and Stress-Reduced Si_3N_4 /SiO_2 /Si_3N_4 Multilayer Films and Their Applications in Blood Plasma Separation. *ETRI Journal* **34,** 226–234 (2012).
21. Fan, R. *et al.* Integrated barcode chips for rapid, multiplexed analysis of proteins in microliter quantities of blood. *Nature Biotechnology* **26,** 1373–1378 (2008).
22. Kersaudy-Kerhoas, M. & Sollier, E. Micro-scale blood plasma separation: from acoustophoresis to egg-beaters. *Lab on a Chip* (2013). doi:10.1039/c3lc50432h
23. Clack, N. G., Salaita, K. & Groves, J. T. Electrostatic readout of DNA microarrays with charged microspheres. *Nature Biotechnology* **26,** 825–830 (2008).
24. Dufva, M. Fabrication of high quality microarrays. *Biomolecular Engineering* **22,** 173–184 (2005).
25. Fang, S., Lee, H. J., Wark, A. W. & Corn, R. M. Attomole Microarray Detection of MicroRNAs by Nanoparticle-Amplified SPR Imaging Measurements of Surface Polyadenylation Reactions. *Journal of the American Chemical Society* **128,** 14044–14046 (2006).
26. Jung, J. H., Choi, S. J., Park, B. H., Choi, Y. K. & Seo, T. S. Ultrafast Rotary PCR system for multiple influenza viral RNA detection. *Lab on a Chip* **12,** 1598 (2012).
27. Neuzil, P. Ultra fast miniaturized real-time PCR: 40 cycles in less than six minutes. *Nucleic Acids Research* **34,** e77–e77 (2006).
28. Wheeler, E. K. *et al.* Under-three minute PCR: Probing the limits of fast amplification. *The Analyst* **136,** 3707 (2011).
29. Asiello, P. J. & Baeumner, A. J. Miniaturized isothermal nucleic acid amplification, a review. *Lab Chip* **11,** 1420 (2011).
30. Buates, S. *et al.* Development of a reverse transcription-loop-mediated isothermal amplification (RT-LAMP) for clinical detection of Plasmodium falciparum gametocytes. *Parasitology International* **59,** 414–420 (2010).
31. Craw, P. & Balachandran, W. Isothermal nucleic acid amplification technologies for point-of-care diagnostics: a critical review. *Lab on a Chip* **12,** 2469 (2012).
32. Fang, X., Liu, Y., Kong, J. & Jiang, X. Loop-Mediated Isothermal Amplification Integrated on Microfluidic Chips for Point-of-Care Quantitative Detection of Pathogens. *Anal. Chem.* **82,** 3002–3006 (2010).

33. Francois, P. *et al.* Robustness of a loop-mediated isothermal amplification reaction for diagnostic applications. *FEMS Immunology & Medical Microbiology* **62,** 41–48 (2011).
34. Hakenberg, S. *et al.* A phaseguided passive batch microfluidic mixing chamber for isothermal amplification. *Lab on a Chip* **12,** 4576 (2012).
35. Iseki, H. *et al.* Evaluation of a Loop-Mediated Isothermal Amplification Method as a Tool for Diagnosis of Infection by the Zoonotic Simian Malaria Parasite Plasmodium knowlesi. *Journal of Clinical Microbiology* **48,** 2509–2514 (2010).
36. Kim, H.-J. *et al.* A rapid and simple isothermal nucleic acid amplification test for detection of herpes simplex virus types 1 and 2. *Journal of Clinical Virology* **50,** 26–30 (2011).
37. Lucchi, N. W. *et al.* Real-Time Fluorescence Loop Mediated Isothermal Amplification for the Diagnosis of Malaria. *PLoS ONE* **5,** e13733 (2010).
38. Rane, T. D., Chen, L., Zec, H. C. & Wang, T.-H. Microfluidic continuous flow digital loop-mediated isothermal amplification (LAMP). *Lab Chip* **15,** 776–782 (2015).
39. Tao, Z.-Y. *et al.* Adaptation of a visualized loop-mediated isothermal amplification technique for field detection of Plasmodium vivax infection. *Parasites & Vectors* **4,** 115 (2011).
40. Wang, C.-H., Lien, K.-Y., Wu, J.-J. & Lee, G.-B. A magnetic bead-based assay for the rapid detection of methicillin-resistant Staphylococcus aureus by using a microfluidic system with integrated loop-mediated isothermal amplification. *Lab on a Chip* **11,** 1521 (2011).
41. Rapid Diagnosis of Human Herpesvirus 6 Infection by a Novel DNA Amplification Method, Loop-Mediated Isothermal Amplification.
42. Niemz, A., Ferguson, T. M. & Boyle, D. S. Point-of-care nucleic acid testing for infectious diseases. *Trends in Biotechnology* **29,** 240–250 (2011).
43. Piepenburg, O., Williams, C. H., Stemple, D. L. & Armes, N. A. DNA Detection Using Recombination Proteins. *PLoS Biology* **4,** e204 (2006).
44. Tomita, N., Mori, Y., Kanda, H. & Notomi, T. Loop-mediated isothermal amplification (LAMP) of gene sequences and simple visual detection of products. *Nature Protocols* **3,** 877–882 (2008).
45. Nge, P. N., Rogers, C. I. & Woolley, A. T. Advances in Microfluidic Materials, Functions, Integration, and Applications. *Chemical Reviews* **113,** 2550–2583 (2013).
46. Dentry, M. B., Friend, J. R. & Yeo, L. Y. Continuous flow actuation between external reservoirs in small-scale devices driven by surface acoustic waves. *Lab on a Chip* **14,** 750 (2014).
47. Shi, J. *et al.* Three-dimensional continuous particle focusing in a microfluidic channel via standing surface acoustic waves (SSAW). *Lab on a Chip* **11,** 2319 (2011).
48. Yeo, L. Y. & Friend, J. R. Ultrafast microfluidics using surface acoustic waves. *Biomicrofluidics* **3,** 012002 (2009).
49. Aeinehvand, M. M. *et al.* Latex micro-balloon pumping in centrifugal microfluidic platforms. *Lab on a Chip* **14,** 988 (2014).

50. Chen, Y., Wu, T.-H. & Chiou, P.-Y. Scanning laser pulses driven microfluidic peristaltic membrane pump. *Lab on a Chip* **12,** 1771 (2012).
51. Cui, J. & Pan, T. A vacuum-driven peristaltic micropump with valved actuation chambers. *Journal of Micromechanics and Microengineering* **21,** 065034 (2011).
52. Ehrenberg, O. & Kosa, G. Analysis of a novel piezoelectric micro-pump for drug delivery in a medical integrated micro system. in 467–472 (IEEE, 2012). doi:10.1109/BioRob.2012.6290893
53. Rhie, W. & Higuchi, T. Design and fabrication of a screw-driven multi-channel peristaltic pump for portable microfluidic devices. *Journal of Micromechanics and Microengineering* **20,** 085036 (2010).
54. Wang, X., Cheng, C., Wang, S. & Liu, S. Electroosmotic pumps and their applications in microfluidic systems. *Microfluidics and Nanofluidics* **6,** 145–162 (2009).
55. Siegel, A. C. *et al.* Foldable Printed Circuit Boards on Paper Substrates. *Advanced Functional Materials* **20,** 28–35 (2010).
56. Osborn, J. L. *et al.* Microfluidics without pumps: reinventing the T-sensor and H-filter in paper networks. *Lab on a Chip* **10,** 2659 (2010).
57. Novo, P., Volpetti, F., Chu, V. & Conde, J. P. Control of sequential fluid delivery in a fully autonomous capillary microfluidic device. *Lab on a Chip* **13,** 641 (2013).
58. Safavieh, R. & Juncker, D. Capillarics: pre-programmed, self-powered microfluidic circuits built from capillary elements. *Lab on a Chip* **13,** 4180 (2013).
59. Dimov, I. K. *et al.* Stand-alone self-powered integrated microfluidic blood analysis system (SIMBAS). *Lab Chip* **11,** 845 (2011).
60. Jixiao Liu *et al.* Microfluidic Solution Isolated Pumping (uSIP). *uTAS* 17th International Conference on Miniaturized Systems for Chemistry and Life Sciences, Freiburg, Germany (2013).
61. Arata, H., Komatsu, H., Han, A., Hosokawa, K. & Maeda, M. Rapid microRNA detection using power-free microfluidic chip: coaxial stacking effect enhances the sandwich hybridization. *The Analyst* **137,** 3234 (2012).
62. Hosokawa, K., Sato, K., Ichikawa, N. & Maeda, M. Power-free poly(dimethylsiloxane) microfluidic devices for gold nanoparticle-based DNA analysisElectronic supplementary information (ESI) available: Sample movie used for flow characterization, mathematical details of the one-dimensional diffusion model, and time course of the gold nanoparticle deposition. See http://www.rsc.org/suppdata/lc/b4/b403930k/. *Lab on a Chip* **4,** 181 (2004).
63. Hosokawa, K., Omata, M. & Maeda, M. Immunoassay on a Power-Free Microchip with Laminar Flow-Assisted Dendritic Amplification. *Analytical Chemistry* **79,** 6000–6004 (2007).
64. Hosokawa, K., Omata, M., Sato, K. & Maeda, M. Power-free sequential injection for microchip immunoassay toward point-of-care testing. *Lab on a Chip* **6,** 236 (2006).
65. Okada, H., Hosokawa, K. & Maeda, M. Power-Free Microchip Immunoassay of PSA in Human Serum for Point-of-Care Testing. *Analytical Sciences* **27,** 237 (2011).

66. Sato, K., Hosokawa, K. & Maeda, M. Rapid Aggregation of Gold Nanoparticles Induced by Non-Cross-Linking DNA Hybridization. *Journal of the American Chemical Society* **125,** 8102–8103 (2003).
67. Sato, Y., Sato, K., Hosokawa, K. & Maeda, M. Surface plasmon resonance imaging on a microchip for detection of DNA-modified gold nanoparticles deposited onto the surface in a non-cross-linking configuration. *Analytical Biochemistry* **355,** 125–131 (2006).
68. Li, G., Luo, Y., Chen, Q., Liao, L. & Zhao, J. A 'place n play' modular pump for portable microfluidic applications. *Biomicrofluidics* **6,** 014118 (2012).
69. Zhang, H. *et al.* Direct detection of cancer biomarkers in blood using a 'place n play' modular polydimethylsiloxane pump. *Biomicrofluidics* **7,** 034105 (2013).
70. Liang, D. Y., Tentori, A. M., Dimov, I. K. & Lee, L. P. Systematic characterization of degas-driven flow for poly(dimethylsiloxane) microfluidic devices. *Biomicrofluidics* **5,** 024108 (2011).
71. Cira, N. J., Ho, J. Y., Dueck, M. E. & Weibel, D. B. A self-loading microfluidic device for determining the minimum inhibitory concentration of antibiotics. *Lab on a Chip* (2012). doi:10.1039/c2lc20887c
72. Ho, J. Y., Cira, N. J., Crooks, J. A., Baeza, J. & Weibel, D. B. Rapid Identification of ESKAPE Bacterial Strains Using an Autonomous Microfluidic Device. *PLoS ONE* **7,** e41245 (2012).
73. Han, Z. & Zheng, B. A poly(dimethylsiloxane) viscometer for microliter power law fluids. *Journal of Micromechanics and Microengineering* **19,** 115005 (2009).
74. Tang, X. & Zheng, B. A PDMS viscometer for assaying endoglucanase activity. *The Analyst* **136,** 1222 (2011).
75. Zhou, X., Lau, L., Lam, W. W. L., Au, S. W. N. & Zheng, B. Nanoliter Dispensing Method by Degassed Poly(dimethylsiloxane) Microchannels and Its Application in Protein Crystallization. *Analytical Chemistry* **79,** 4924–4930 (2007).
76. Nevill, J. T. *et al.* Vacuum soft lithography to direct neuronal polarization. *Soft Matter* **7,** 343 (2011).
77. Hitzbleck, M. & Delamarche, E. Reagents in microfluidics: an 'in' and 'out' challenge. *Chemical Society Reviews* **42,** 8494 (2013).
78. Vogelstein, B. Digital PCR. *Proceedings of the National Academy of Sciences* **96,** 9236–9241 (1999).
79. Selck, D. A., Karymov, M. A., Sun, B. & Ismagilov, R. F. Increased Robustness of Single-Molecule Counting with Microfluidics, Digital Isothermal Amplification, and a Mobile Phone versus Real-Time Kinetic Measurements. *Analytical Chemistry* **85,** 11129–11136 (2013).
80. Day, E., Dear, P. H. & McCaughan, F. Digital PCR strategies in the development and analysis of molecular biomarkers for personalized medicine. *Methods* **59,** 101–107 (2013).
81. Shen, F. *et al.* Digital Isothermal Quantification of Nucleic Acids via Simultaneous Chemical Initiation of Recombinase Polymerase Amplification Reactions on SlipChip. *Analytical Chemistry* 110408160603036 (2011). doi:10.1021/ac200247e
82. Gansen, A., Herrick, A. M., Dimov, I. K., Lee, L. P. & Chiu, D. T. Digital LAMP in a sample self-digitization (SD) chip. *Lab on a Chip* **12,** 2247 (2012).

83. Zhu, Q. *et al.* Self-priming compartmentalization digital LAMP for point-of-care. *Lab on a Chip* (2012). doi:10.1039/c2lc40774d
84. Rissin, D. M. *et al.* Single-molecule enzyme-linked immunosorbent assay detects serum proteins at subfemtomolar concentrations. *Nature Biotechnology* **28,** 595–599 (2010).
85. Kang, D.-K. *et al.* Rapid detection of single bacteria in unprocessed blood using Integrated Comprehensive Droplet Digital Detection. *Nature Communications* **5,** 5427 (2014).
86. Heyries, K. A. *et al.* Megapixel digital PCR. *Nature Methods* **8,** 649–651 (2011).

Chapter 2. Digital Micro-Patterning of Nucleic Acid Amplification Initiator

Abstract

Patterning of reagents is essential for microfluidic based point-of-care devices that need pre-storage or lyophilisation of reagents. However, common techniques such as mechanical contact printing is difficult to increase the density of samples, and inkjet printing or dispensers require costly specialized equipment and additional buffers which may not be compatible with subsequent biological reactions. Here we report the digital micro-patterning method that can create high-density micro patterns of nucleic acid amplification initiator with common lab equipment in few simple steps. By digital degas pumping, automatic reagent spotting was accomplished with minimal manual operation (<20 min). High-density patterning (~150 μm footprint) was possible by a micro-apex design that concentrates reagents via capillary guiding. Without any special solvents or buffers, it was demonstrated to be possible to pattern concentrated isothermal amplification initiator (MgOAc) into a microfluidic device that contained hundreds of microwells (650 μm diameter) and perform isothermal amplification directly. Since only common equipment is necessary, and pre-made patterning stencils (or molds of stencils) can be used on-site, this technique is ideal for patterning at low resource settings.

Introduction

Micro-patterning of reagents onto chips is a crucial technology for fabricating point-of-care devices that can be brought into the field. Current common techniques include examples such as inkjet printing[1], dispensers[2], and contact printing[3]. A review of reagent patterning methods has been done by Hitzbleck[4] et al. Inkjet printing work by using piezoelectric shockwaves to expel liquids through a nozzle head. Although this method is rapid, there are several drawbacks with inkjet printing. **Figure 1** shows some of the common reagent printing technique used.

Firstly, the cost for specialized biological compatible inkjet printers can be very high (e.g. Arrayjet machines can cost more than $70k, each service run cost ~$2k). Secondly, the cost of maintenance is high, as the most costly part—the print heads, can be easily damaged, clogged or contaminated with the printed medium. It is also risky to attempt to print new materials such as acid, bases, or solvents since these materials can damage the print heads. Thirdly, the final shape and footprint depends strongly on the hydrophilicity of the substrate and the viscosity of the ink medium. Due to uneven evaporation, coffee ring like concentration profiles are often observed at the outer boundaries of the printed pattern. Fourthly, to achieve high concentration spots, multiple print passes over the same area has to be done. However, each pass needs to wait until the previous run is dry before performing the next run if a small

footprint is desired. For example, 40 passes (~100 pl/pass) took 8 hours of machine time to complete with an Arrajet inkjet printer. Finally, inkjet printing often requires

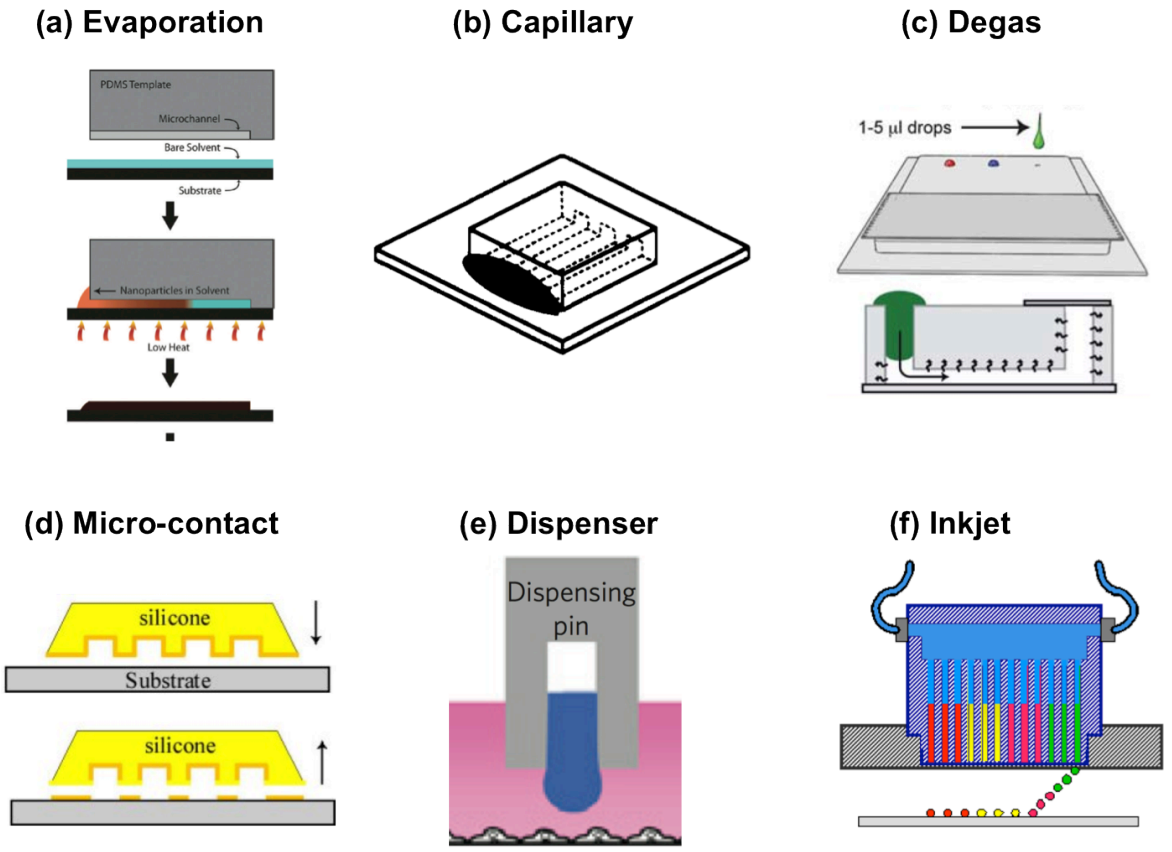

Figure 1 Examples of other common patterning techniques. Ref: (a)[14], (b)[9], (c)[15], (d)[3], (e)[2], (f) referenced from Arrayjet Limited).

special buffers or solvents to control the viscosity of the printed liquid, which may not be compatible with subsequent biological reactions such as nucleic acid amplification.

Another common technique is printing via robotic dispensers. These machines work by dispensing liquid onto substrates via pipetting action through needles or pipettes. The main drawback of this method is the lack of resolution to print into reagents into microfluidic structures. Smallest print volumes are typically in the range of tens or more nanoliters. Also as with inkjet printers, the robotic dispensers can be costly and not be part of a list of equipment that laboratories commonly possess.

Contact printing[5] is also a popular choice. These methods often involve using a substrate such as micropatterned PDMS to serve as a stamp to transfer inked material onto substrates. Another method is using capillary pins that resemble miniaturized fountain pens, and a robotic printer to draw desired patterns on substrates. Other methods use a direct writing[6,7] action using mechanical tips. However, a limitation with these methods is that it is very difficult to produce patterns

with high reagent concentration, because a limited volume is transferred during each pass. Specialized pin printers are also equipment that is not common to average laboratories.

Other printing methods such as capillary printing[8–10], microfluidic[11] networks, evaporation[12–14], or degas[15,16] based printing may be low cost, however, they all create continuous patterns defined by the fluidic channels. To our best knowledge, there have yet been examples demonstrating patterning of unconnected, discrete digitized islands of reagents via these techniques.

In this chapter, a new printing method termed “digital micro-patterning” is reported (**Fig.2**). The key advantage to this method is that it enables production of digitized

Table 1 Detailed comparison of common patterning techniques.

Method / Attributes	Evaporation	Capillary	Degas	Micro-contact printing	Dispensing	Inkjet	Digital Micro-patterning
Special solvents/ buffers needed	initial solvent layer	no	no	yes	no	yes	no
Digital compartmentalization	no	no	no	no	no	no	yes
Micro-Apex Reagent Concentration	no	no	no	no	no	no	yes
shape	continuous	continuous	continuous	discrete	discrete	discrete	discrete
PDMS substrate patterning	no	yes	no	yes	yes	yes	yes
On-site patterning	difficult	easy	easy	easy	difficult	difficult	easy
Other disadvantages	solvents needed	pumps,	continuous patterns	cannot concentrate samples, (pin printer)	high cost, footprint too large	high cost, print head contamination/ damage	NA

micro-p atterns of highly concentrated reagents into small footprints. Common laboratory equipment is used and no specialized solvents are needed. This research demonstrates it is possible to pattern magnesium acetate, an amplification initiator for isothermal nucleic acid amplification (recombinase polymerase amplification[17]), individually into hundreds of microwells and achieve isothermal amplification within these wells.

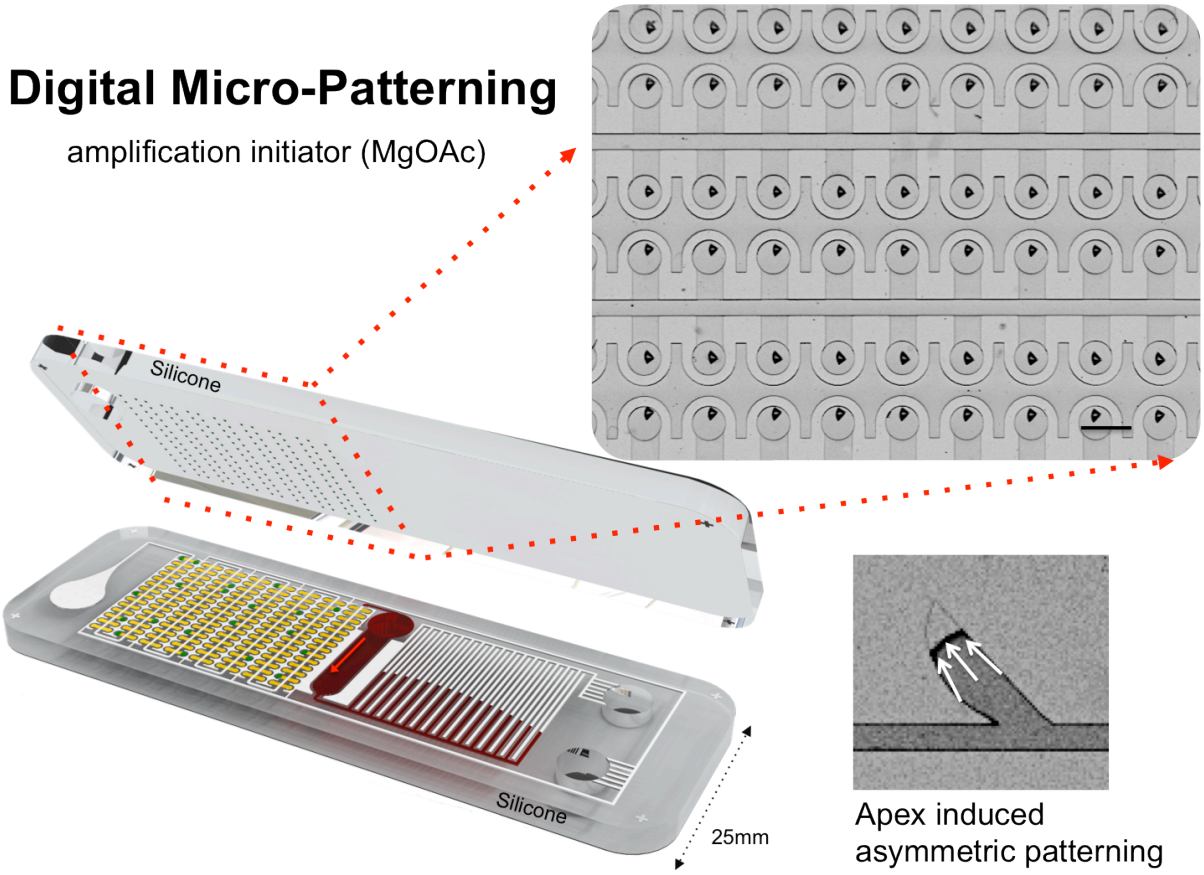

Figure 2 Digital micro-patterning of high density reagents for resource-limited settings. Digital micro-patterning enables patterning reagents into microfluidic wells. The small footprint and high concentration is ideal for subsequent bonding of the device. Digital micro-patterning is used to pattern magnesium acetate, an amplification initiator, into hundreds of micro-wells (650 µm) diameter each, and run isothermal amplification reactions (recombinase polymerase amplification) for nucleic acid detection in these wells. Scale bar= 1mm.

Methods

Fabrication of PDMS chips

A cross section of the bi-layer chip construction is shown in **Figure 2a**. The chips tested were fabricated using the standard soft lithography[18] process. Briefly, PDMS layers containing fluidic channels were made by casting PDMS on a silicon wafer that had protruding microfluidic channels created by photo-patterning (OAI Series 200 Aligner) SU-8 photoresist (Microchem). The digital micro-patterning channels were 30 µm high. The wells on the bottom fluidic PDMS chip were 300 µm in height. The inlets and outlets of the digital micro-patterning chip were fabricated by punching by punchers (Harris Uni-Core, Ted Pella). The outer boundary of the chips were kept consistent using a laser cut mold to mold the PDMS into 20x75 mm shapes. All chips had a total thickness of 3 mm. PDMS were cured for 4 hours at 60 °C.

Heat treatment of and surface activation of blank PDMS layer

The blank PDMS layer to be patterned with MgOAc was additionally heat treated at 100 °C for at least three days. The heat treatment prevents hydrophobic recovery of the plasma treated PDMS surface.

Digital Patterning

The heat treated blank PDMS was treated with oxygen plasma (PETS Reactive Ion Etcher, 100W, 120 mTorr O_2, 50 s) to make the surface hydrophilic. After plasma treatment, the blank was immediately assembled with the patterning chip and vacuumed at 30 mTorr for 10 minutes. Then the outlets of the patterning chips were sealed with scotch tape and 2 µl of magnesium acetate solution (MgOAc 1M, Sigma Aldrich 63052) was pipetted to each of the inlets immediately (for the fluorescence pictures, fluorescein dye was added). After finishing autonomous loading by degas pumping (~10 min), the tape at the outlet was removed and excess MgOAc was aspirated. The chip was left to air dry in atmosphere for 1 day before peeling. After drying, the patterning chip was peeled off in the direction from the base of the leaf patterns to the tips of the leaf patterns (from right to left, in the dyed loaded chips shown in **Fig. 2a**). The patterned MgOAc remained on the blank chip.

Chip bonding.

After the blank PDMS chips were patterned with MgOAc, they were bonded to the chips that contained the microfluidic wells and channels for the digital plasma separation design using UV exposure (UVO cleaner, Jetlight, Model 42) for 3 minutes. The chips were aligned manually under a stereoscope. After UV bonding, the chips were immediately incubated at 60 °C for at least 20 minutes while applying ~0.5 kg to increase bonding strength. For the reconstitution test, the final assembled chips were incubated at -95 kPa overnight and water was loaded into the chip to

dissolve the MgOAc.

Quantification

All fluorescent images and bright field images of zoomed in regions were taken with a macroscope (Axiozoom Ems3/SyCoP3, AxioCamMR3 camera, Zeiss) at 7~20X zoom (PlanNeoFluar Z1.0x objective, Zeiss). I used the 38HE green fluorescence filter (Zeiss) for visualizing fluorescein dye. The bit depth was 12 bit, images were 692x520 pixels (2,2, binning mode). Acquisition of images and zoomed videos were done with Zen (v.2012, Zeiss) software. Imaging was done at room temperature. I used NIH imageJ and Zen software to quantify the fluorescence intensities, normalize contrast, and crop images. Time-lapse videos of the entire chip loading were acquired using the TimeLapse app (xyster.net LLC) using an iPhone 5 (Apple).

Statistical analysis

For experimental data, sample sizes are noted in the corresponding figure legends. All experimental data are shown as means, and error bars denote plus minus one standard deviation. Replicates represent technical replicates. For **Figure 2c**, and **2d**, the black curve was fitted by a normal distribution curve. I used OriginPro (version 9.0, OriginLab) for statistical analysis and scientific graphing.

Results

The location of the magnesium acetate that is patterned is shown in **Figure 2** (the fluidic functions of the bottom layer will be described in later chapters). The four main steps for digital micro-patterning is shown in **Figure 3~5**. In the first step- digitization (**Fig. 3**), It was able to separate the reagents into discrete islands (~2nl) automatically via a fluidic design that uses degas pumping[19]. Fluid is drawn into the microfluidic channels when pre-vacuumed air permeable PDMS material gradually sucks out trapped air pockets. The reagents are separated when liquid loading finishes and the trailing air gap physically separates each "leaf" pattern. This step usually takes less than ~15 minutes after loading.

The second step is concentrating the reagents asymmetrically into smaller footprints by drying (**Fig. 4**). The dried patterns have a footprint smaller than 200 μm

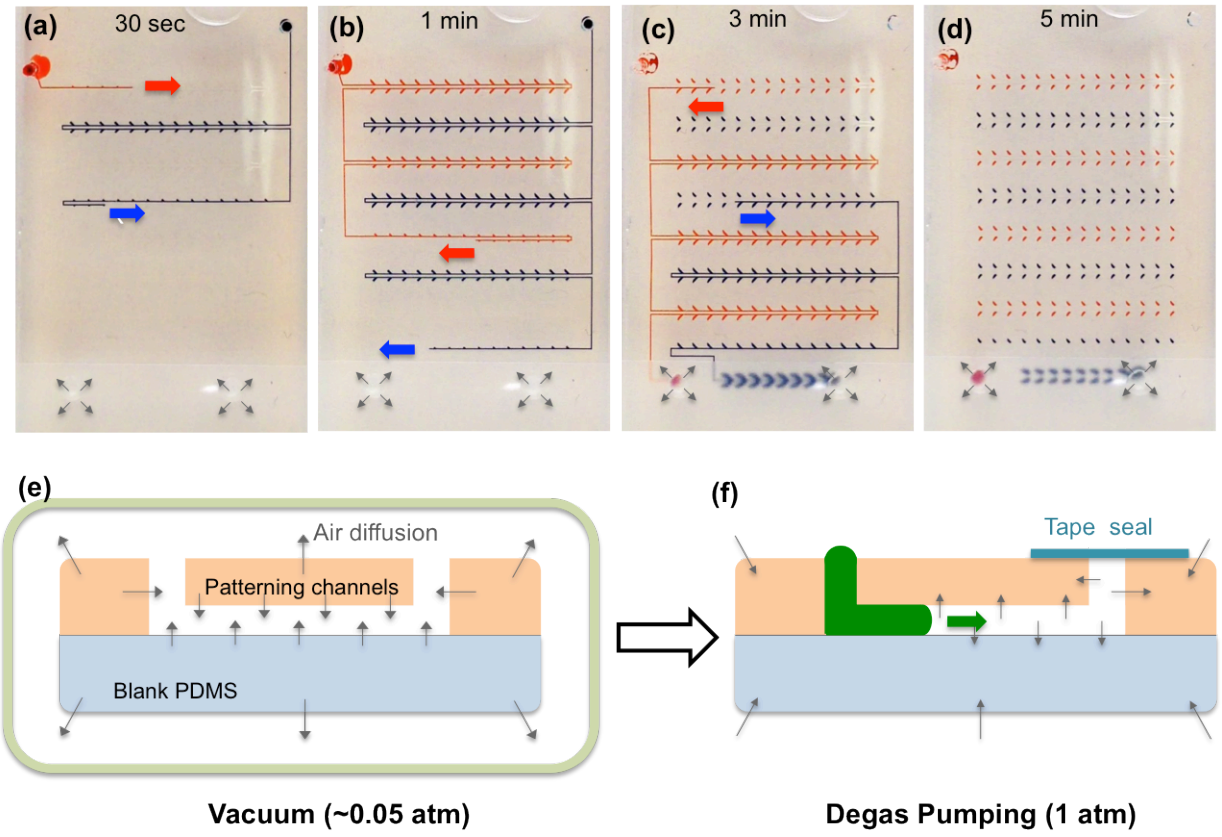

Figure 3 Minimal manual operation with automated digital loading. Amplification initiator (MgOAc) can be digitized into discrete samples by degas pumping. In these pictures, food-dye was used to visualize the digitization process. **(a)~(d)** shows the timelapse images of reagent loading and digitizing. **(e)** and **(f)** shows how degas pumping works by slowly sucking liquid when trapped air diffuses into pre-vacuumed gas permeable silicone (PDMS) material. Digitization occurs when the air interface trailing after liquid loading separates patterns into discrete islands. Both patterning channels and bottom blanks are made from PDMS.

in length. It was able to decrease the footprint by a factor of 2 after drying. For visualization, fluorescein or food dye was added for imaging. These results show it was possible to reduce the footprint and solidify MgOAc by simply by air-drying in atmosphere overnight. Drying under house vacuum further decreased the time needed to dry to a few hours.

The third step is peeling off the patterning layer (**Fig. 5**). It was able to asymmetrically pattern all of the MgOAc patterns onto the blank PDMS layer by

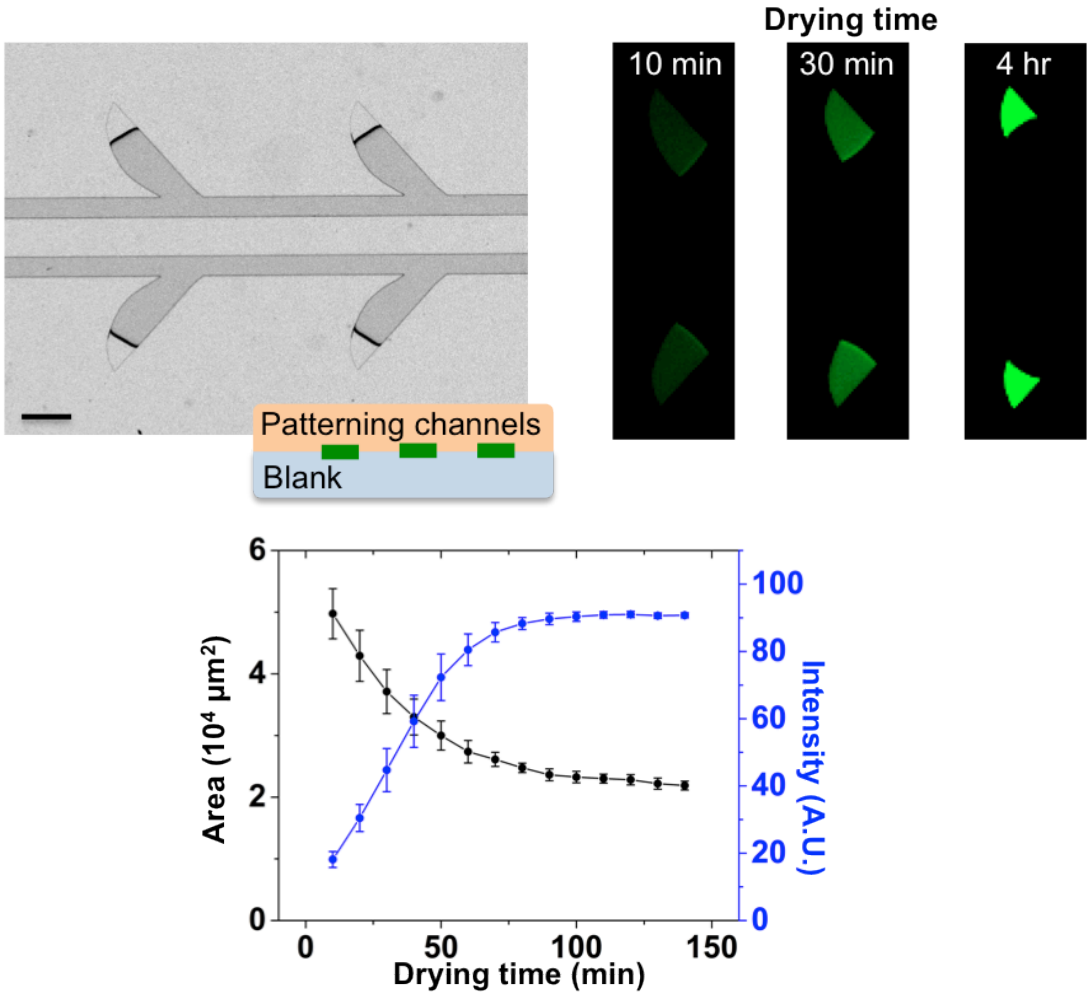

Figure 4 Increasing reagent density by micro-apex induced asymmetric patterning. In step **(b),** reagents are further packed into a smaller footprint by capillary guiding and air-drying. Fluorescein was added for visualization. Reagents concentrate toward the tip asymmetrically via capillary tension. A small reagent footprint prevents bonding problems and false positives. False positives can happen if contaminating reagents causes unwanted reactions outside the wells. (mean ± s.d., n=16). Black scale bars are 250 µm.

creating a difference in surface energy. The blank surface was pre-treated with heat at 100 °C for at least three days, then exposed to oxygen plasma immediately before performing the first step digitization. The plasma treatment made the blank PDMS surface hydrophilic and the heat treatment[20] prevented the PDMS surface returning to a hydrophobic state. Since the top patterning PDMS remained hydrophobic, the MgOAc preferentially sticks to the hydrophilic bottom blank surface. In addition, it was found that peeling in the direction away from the sharp tips gives better yields. The micro-patterned MgOAc showed a very uniform shape and area under the microscope (average area was $2.3x10^4$ μm^2, and standard deviation was $0.1x3x10^4$ μm^2). No residue of MgOAc was observed in unwanted regions.

The final step is assembling the MgOAc patterned layer with the microwell layer (**Fig. 6**). UV bonding and manual alignment was used under a stereoscope for

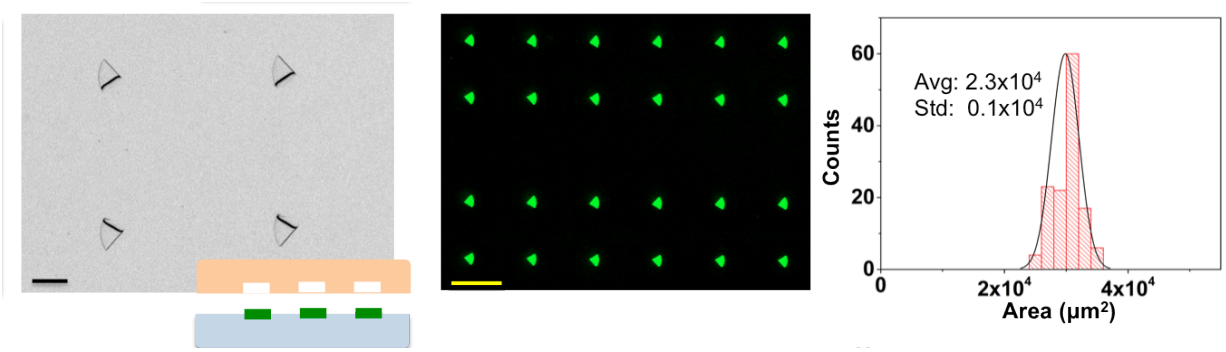

Figure 5 After peeling patterning stencil layer off. Left figure shows bright field image of patterns, no residue is observed at undesired regions. Middle figure shows fluorescence image. Right figure shows the results of area distribution. n=140. In stepd **(d),** the MgOAc patterned PDMS is flipped, aligned, and bonded on top of the bottom half of the iMDx chip. n=140. Black scale is 250 μm. Yellow scale bar is 1 mm.

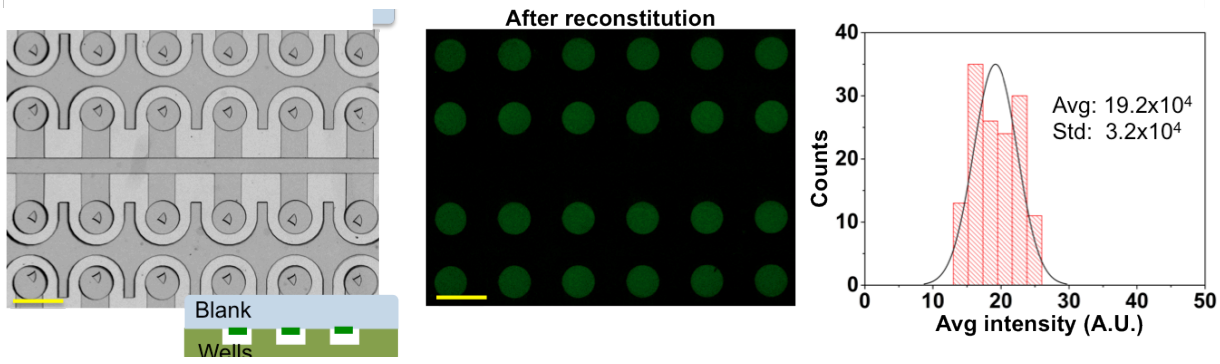

Figure 6 Chip bonding and reconstitution. Left figure shows bonded chip with microwells. The MgOAc patterned PDMS is flipped, aligned, and bonded on top of the bottom half of the iMDx chip. The middile figure shows the result of uniform reconstitution after loading the microwells with water. Right figure shows the distribution of average intensity of fluorescence from each reconstituted well. n=140. Yellow scale bars are 1 mm.

bonding. The reduced footprint of the MgOAc prevented the patterns overlapping with the bonding areas, thus leaks were avoided. The patterning channels were designed to not have any overlaps with the fluidic channels, therefor even if there were any residue outside of the desired patterning areas, it would not come in contact with the fluidic channels (**Fig. 7**). After bonding, the reconstitution uniformity was tested by loading water into the patterned microwells using degas loading. The reconstituted fluorescence intensity distribution was more spread than after the concentrated MgOAc after the drying step, but still within tolerable ranges as subsequence RPA reactions were still viable. This may be caused from degradation of the fluorescein during the UV bonding step. The results for the RPA isothermal tests will be shown in the following chapters.

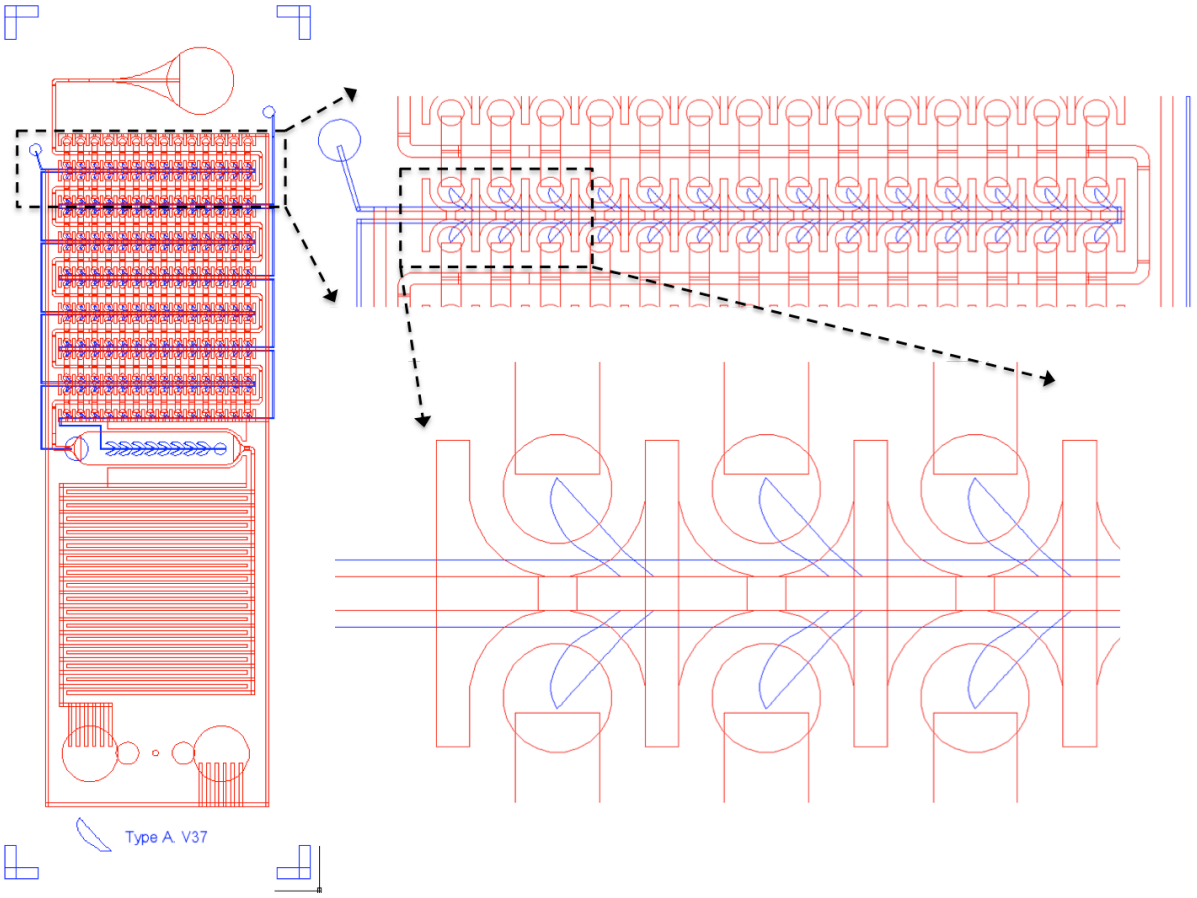

Figure 7 Alignment of the patterned reagents and iMDx chip. The blue layer represents the fluidic design for the patterning layer. The red layer represents the fluidic design for the bottom of the iMDx chip. Note that the patterning layer never has overlaps with fluidic channels in the iMDx layer. The patterning layer only routes through the vacuum lines of the iMDx chip, this further decreases the risk for residue contamination of reagents in the main channel.

Discussion

This project was initially developed because there were no biological grade inkjet printers, dispensers, or contact printing robots available in the lab to print micro-patterns of reagents into microfluidic devices. It was necessary to brainstorm methods to make these micropatterns with simple steps and current available lab infrastructure. The method developed—digital micro-patterning—requires only common lab equipment such as a vacuum source and UV light source. The oxygen plasma machine is optional and only needed to render hydrophobic substrates such as PDMS to a hydrophilic surface, if the substrate is inherently hydrophilic (e.g. glass), then plasma is not required. Due to the low requirements of infrastructure, digital micro-patterning can be easily performed in any lab that has these equipment. The patterning PDMS molds containing microfluidic patterns can be fabricated by facilities that have lithography capability and sent to the laboratories mentioned above for in-house PDMS replication molding. Thus, this technique is well suited for low resource settings for micro-patterning of highly concentrated reagents.

Another merit of this technique is that unlike inkjet printers that require addition of viscosity/evaporation modulation buffers, digital micro-patterning does not require any special solvents. That means there is less chance for interference with downstream assays (e.g. PCR or isothermal amplification). In this system, only water was used as the solvent. That being said, this does not limit the system for testing other types of solvents or materials. A big advantage of this system is that it is possible to boldly try new reagents and solvents because each chip costs only a few cents of PDMS material, whereas replacing a damaged inkjet print head may cost several thousand dollars.

Magnesium acetate, an amplification initiator, was needed to be patterned into the wells because if it were contaminate any of the main fluidic channels in the final assembled chip, isothermal amplification would commence prematurely and cause false positive signals. Magnesium acetate starts recombinase polymerase amplification reaction because the polymerase needs a certain concentration of magnesium ions to be active. For this reason, it is crucial to have a small footprint so that magnesium acetate do not contaminate outside of the microwells. Also a small footprint avoids bonding issues because reagents do not interfere with PDMS contact during bonding. Finally, a high density of reagents was desired, and this method was unique in the sense that it made it possible to pack reagents in a 3D block with a very clear and defined footprint. Contact printing cannot achieve this kind of 3D stacking, and inkjet printing's footprint starts to smear out when high volume of liquid is printed.

Conclusion

In summary, this research demonstrates a new technique that can produce dense micro patterns of reagents with common laboratory equipment. For the first time, it has been shown that reagents can be patterned by degas-based sample digitization, and further concentrated asymmetrically into micro-apex structures via capillary drying. The major merits of this system are that no special solvents and special robotic equipment are needed. A detailed comparison of technologies is shown in and **Table 1**. As a proof of concept, this work demonstrates that it is possible to pattern magnesium acetate into hundreds of microfluidic wells. In later chapters, the results of isothermal amplification (via recombinase polymerase amplification) will be shown. Due to the versatility of this technique, it may be highly valuable for patterning of reagents for microfluidic point-of-care devices in the future.

Notes and references

1. Singh, M., Haverinen, H. M., Dhagat, P. & Jabbour, G. E. Inkjet Printing-Process and Its Applications. *Advanced Materials* **22,** 673–685 (2010).
2. Tavana, H. *et al.* Nanolitre liquid patterning in aqueous environments for spatially defined reagent delivery to mammalian cells. *Nature Materials* **8,** 736–741 (2009).
3. Geissler, M. & Xia, Y. Patterning: Principles and Some New Developments. *Advanced Materials* **16,** 1249–1269 (2004).
4. Hitzbleck, M. & Delamarche, E. Reagents in microfluidics: an ‘in’ and ‘out’ challenge. *Chemical Society Reviews* **42,** 8494 (2013).
5. Loo, Y.-L., Willett, R. L., Baldwin, K. W. & Rogers, J. A. Interfacial Chemistries for Nanoscale Transfer Printing. *Journal of the American Chemical Society* **124,** 7654–7655 (2002).
6. Huang, N. F. *et al.* A matrix micropatterning platform for cell localization and stem cell fate determination. *Acta Biomaterialia* **6,** 4614–4621 (2010).
7. Gong, J. *et al.* Micro- and Nanopatterning of Inorganic and Polymeric Substrates by Indentation Lithography. *Nano Letters* **10,** 2702–2708 (2010).
8. Suh, K.-Y., Park, M. C. & Kim, P. Capillary Force Lithography: A Versatile Tool for Structured Biomaterials Interface Towards Cell and Tissue Engineering. *Advanced Functional Materials* **19,** 2699–2712 (2009).
9. Kim, E., Xia, Y. & Whitesides, G. M. Polymer microstructures formed by moulding in capillaries. *Nature* **376,** 581–584 (1995).
10. Cuvelier, D., Rossier, O., Bassereau, P. & Nassoy, P. Micropatterned ‘adherent/repellent’ glass surfaces for studying the spreading kinetics of individual red blood cells onto protein-decorated substrates. *European Biophysics Journal* **32,** 342–354 (2003).

11. Delamarche, E. Patterned Delivery of Immunoglobulins to Surfaces Using Microfluidic Networks. *Science* **276,** 779–781 (1997).
12. Demko, M. T., Cheng, J. C. & Pisano, A. P. High-Resolution Direct Patterning of Gold Nanoparticles by the Microfluidic Molding Process. *Langmuir* **26,** 16710–16714 (2010).
13. Demko, M. T., Cheng, J. C. & Pisano, A. P. Rigid, Vapor-Permeable Poly(4-methyl-2-pentyne) Templates for High Resolution Patterning of Nanoparticles and Polymers. *ACS Nano* **6,** 6890–6896 (2012).
14. Demko, M. T., Choi, S., Zohdi, T. I. & Pisano, A. P. High resolution patterning of nanoparticles by evaporative self-assembly enabled by in situ creation and mechanical lift-off of a polymer template. *Applied Physics Letters* **99,** 253102 (2011).
15. Nevill, J. T. *et al.* Vacuum soft lithography to direct neuronal polarization. *Soft Matter* **7,** 343 (2011).
16. Luo, C., Ni, X., Liu, L., Nomura, S. M. & Chen, Y. Degassing-assisted patterning of cell culture surfaces. *Biotechnology and Bioengineering* n/a–n/a (2009). doi:10.1002/bit.22586
17. Piepenburg, O., Williams, C. H., Stemple, D. L. & Armes, N. A. DNA Detection Using Recombination Proteins. *PLoS Biology* **4,** e204 (2006).
18. Xia, Y. & Whitesides, G. M. SOFT LITHOGRAPHY. *Annual Review of Materials Science* **28,** 153–184 (1998).
19. Sato, K., Hosokawa, K. & Maeda, M. Rapid Aggregation of Gold Nanoparticles Induced by Non-Cross-Linking DNA Hybridization. *Journal of the American Chemical Society* **125,** 8102–8103 (2003).
20. Eddington, D. T., Puccinelli, J. P. & Beebe, D. J. Thermal aging and reduced hydrophobic recovery of polydimethylsiloxane. *Sensors and Actuators B: Chemical* **114,** 170–172 (2006).

Chapter 3. Vacuum Battery for Portable Microfluidic Pumping

Abstract

Low cost pumping is essential to enable microfluidic devices functioning in the field. However, common techniques such as capillary fibres used in lateral flow assays hinder quantitative optical sensing, and previous degas pumping lacks robustness. Herein this report presents the vacuum battery system, which is highly robust, portable, and can be easily integrated in chips for advanced microfluidic function. Robustness is achieved by pre-storing large amounts of vacuum potential in a void chamber, and discharging the vacuum over gas permeable lung-like structures to drive flow (~8 times less loading time standard deviation, and faster pumping compared to previous degas pumping). Fully portable tubeless pumping was possible without any external power sources or control sources (>2 hours operational time, 140 µl). To demonstrate advanced fluidic integration potential, this pumping method was integrated seamlessly with sample preparation, optical readout, and digital amplification modules into a single quantitative nucleic acid detection chip. This simple, low cost pumping design provides a promising fundamental building block for future portable microfluidic devices.

Introduction

Low cost, power-free, portable, and controlled microfluidic pumping are critical traits needed for next generation disposable point-of-care medical diagnostic chips. Ideally, the pumping system should enable disposable chips to perform on-site testing, where there may be poor infrastructure (i.e. trained technicians, power source, or equipment). Furthermore, the pumping system should provide a platform that is compatible with common quantitative analysis techniques that are usually done in centralized labs such as the Enzyme-Linked Immunosorbent Assay (ELISA) or Polymerase Chain Reaction (PCR). Preferably, the pumping system should also have good optical characteristics so various types of optical detection can be utilized. Finally, it should be simple and robust enough so it can be operated with minimal or no training.

Microfluidic pumping is basically a method to drive fluid flow in miniaturized fluidic systems. Microfluidic pumping can be divided into two main categories: active or passive pumping, depending on whether the pumping uses external power sources. There are several extensive reviews[1–5] on microfluidic pumping. Active pumping

examples include the syringe pumps, peristaltic pumps[6–10], membrane based pneumatic valves[11,12], centrifugal pumps[13], electro-wetting on dielectrics (EWOD)[14,15], electrosmosis[16], piezoelectric pumps[17,18], and surface acoustic wave actuation methods[19,20]. Typically active pumping systems have more precise flow control and generally larger flow volumes compared to passive systems. However, the requirement of external power sources, peripheral control systems, or mechanical parts makes the devices more bulky, complex, or costly. These barriers make active pumping systems far less feasible for low cost disposable point-of-care systems.

In passive pumping, there are two main types: capillary or degas pumping. These two types are termed passive because these systems typically do not require power sources or peripheral equipment for pumping, thus they are ideal for low cost point-of-care assays. For capillary systems, the lateral flow assay (e.g. pregnancy dipstick tests) is a prevalent commercial example. These assays use fibrous materials to wick bodily fluids in for immunoassays. In academia, researchers also often use fibrous materials such as paper[21–23] or even threads[24] to drive fluid. However, the opaque or reflective fibres can obstruct optical path, or cause higher background noise in fluorescent detection. These reasons make transmission type optical detection, such as fluorescence, phase contrast, and dark-field microscopy difficult to perform in paper capillary formats.

There is also capillary pumping in plastic formats. Glucose test strips are a very common commercial example of this category. These test strips wick blood into a plastic slit for electrochemical detection. In academia, others have also developed capillary pumping in plastic[25], silicone[26–28], and silicon[29–31] formats. However, since capillary force is dependent on geometry, there are intrinsic limitations in design. For example, channels cannot be too thick, therefore deep (mm scale) optically clear wells with large diameters are not compatible with capillary designs. Flow channels also cannot be too wide, as bubbles may be easily trapped. Periodic structures have been used to prevent bubbles from being trapped[32], but these structures make the fluidic regions not flat and are less desirable for optical detection, as they can cause excessive scattering; for instance, in dark-field microscopy or total internal reflection microscopy. Furthermore, special surface treatment steps are often needed to render the surfaces hydrophilic/hydrophobic, and flow speeds are highly sensitive to surface tension differences among liquids.

Finally, in all capillary formats, it is not possible to have complete dead-end loading or post degassing to remove bubbles. Dead-end loading is useful in nucleic acid amplification applications as it prevents evaporation. However, dead-end loading cannot be done in capillary systems because an outlet vent for air is always necessary. Dead-end loading and the removal of bubbles are of critical importance if elevated heat processes are involved, such as heat cycling during PCR, since bubbles can expand and cause a catastrophic expulsion of the fluids in the device.

These drawbacks have been alleviated by the other more recent example of passive pumping, which is called degas pumping[33]; here, fluid flow is driven when air pockets diffuse into the surrounding air permeable pre-vacuumed silicone materials, such as polydimethylsiloxane (PDMS). It is analogous to a dry sponge soaking in water, but instead of water, air is diffused into the vacuumed silicone and draws fluid

movement. The main advantages of degas loading are the ability to load dead-end chambers, have great optical clarity, and allow for more flexibility in design geometries, as deep and wide structures can be loaded without air bubbles. However, the main drawback is the lack of flow control, and fast exponential decay of flow rate when the device is taken out of vacuum.

Since the first demonstration of degas pumping in 2004 by Hosokawa[33], numerous applications with this kind of pumping have been developed. Such examples include various immunoassays[34–37], DNA/RNA hybridization assays[33,38], bacterial resistance assays[39], digital DNA amplification assays[40,41], PCR assays[42], viscosity assays[43,44], Surface Plasmon Resonance (SPR) assays[45], mercury detection assays[46], and protein crystallization assays[47]. There also has been shear-free cell loading[48] and cell patterning[49] applications. An approach using a modular plug-and-play method of placing vacuumed PDMS blocks in the outlet to drive flow was also demonstrated[34,50]. This research has also demonstrated trench[51] or filter[52] based plasma separation modules with degas pumping for point-of-care devices. Degas pumping has been systematically characterized[53] and used to pattern biomolecules to guide neuron growth[54]. Additionally, a modification of degas pumping was demonstrated by using a thumb-pump[55] to create a vacuum and actuate flow across a diffusion barrier instead of pre-storing vacuum as in degas pumping. Another recent example from these experiments shows one-step integration of sample preparation with digital isothermal amplification of DNA[56].

This report presents a new “Vacuum Battery System” design, which is the first design to use voids to pre-store vacuum potential and gradually discharge vacuum via air diffusion through alveoli-like structures to drive flow. Its main advantages over conventional degas pumping is that it provides more extended (~2 hrs) and reliable flow (~8 times less standard deviation in loading time). Loading speed can be easily tuned and enhanced up to 10 times by varying the diffusion area of vacuum lungs or changing the size of the vacuum void. This pumping mechanism can load at least 140 µl of liquid, and compartmentalize liquids into hundreds of dead-end wells for digital amplification or multiplexed assay applications. Since vacuum batteries can be easily integrated into optically clear microfluidic circuits while leaving design flexibility for different geometry, this platform is very valuable for controlled pumping in low cost power-free handheld devices. It would be particularly useful in point-of-care diagnostics as this system is robust and requires no technical skill or extra peripheral equipment/power sources for operation. A detailed comparison with previous technologies is described in **Table 1**.

Table 1 Pumping technology comparisons. Red labels highlight the disadvantages compared to this work.

	active systems	capillary Loading	conventional degas flow[33]	μSIP[55]	Vacuum Battery System
examples	syringe pumps, quake pumps	pregnancy test strips	SIMBAS[51] system	Microfluidic Solution Isolated Pumping	this work
mechanism	external power source	wicking by capillary action	degas through permeable materials	degas through membrane	void space stores vacuum and degas through lung like structures
portability	difficult	yes	yes	yes	yes
cost	high	low	low	low	low
optical properties	NA	fibers are opaque or cause autofluorescence	transparent	transparent	transparent
flow control	excellent	superior than degas	flow has fast exponential decay	depends on thumb pumping	5 times longer decay time constant than degas flow
flow speed	nl~ml/min	μl~ml/min	~μl/min	~nl/min	10 times faster than degas, also faster than μSIP. (nl~μl/min)
dead end loading	no	no	yes	yes	yes
loading volume	not limited	μl-ml	nl-μl	nl-μl	nl-ml
operation time	not limited	secs~mins	mins	depends on thumb pumping	hours
geometrical constraints	NA	no deep height channels	none	none	none
surface treatment	none	need to be hydrophillic	none	none	none
equipment/ power free	no	yes	yes	need thumb pressing	none
construction	complex with peripherals	simple	simple	extra valve and thumb pump needed.	simple

Mechanism of the vacuum battery system

The vacuum battery system is physically separated from the fluid lines

The actual chip design using the vacuum battery system is depicted in **Figure 1**. The comparison with conventional degas pumping is in **Figure 2**. Basic vacuum battery is defined to include a “vacuum battery” and “vacuum lung” component with an optional waste reservoir (**Fig. 2 bottom**). The vacuum battery and vacuum lung components are connected to each other, but not physically connected to the fluid lines. The vacuum battery void component is simply a punched void volume that stores vacuum potential and is connected to the vacuum lungs. The “vacuum lungs” component mimics lung alveoli gas exchange by allowing air to diffuse through thin gas permeable silicone (PDMS) walls across from the fluid lines into the vacuum battery. It is important to note that the vacuum battery system is not connected to fluid lines as vacuum would be instantly lost once the device is taken out of a vacuum environment if it was connected. Instead, gas diffusion is controlled across air permeable silicone material by design to regulate flow properties. These two components—the vacuum battery and the vacuum lungs—greatly improve the pumping characteristics compared to conventional bulk degas pumping in terms of robustness, speed, and operation time. `

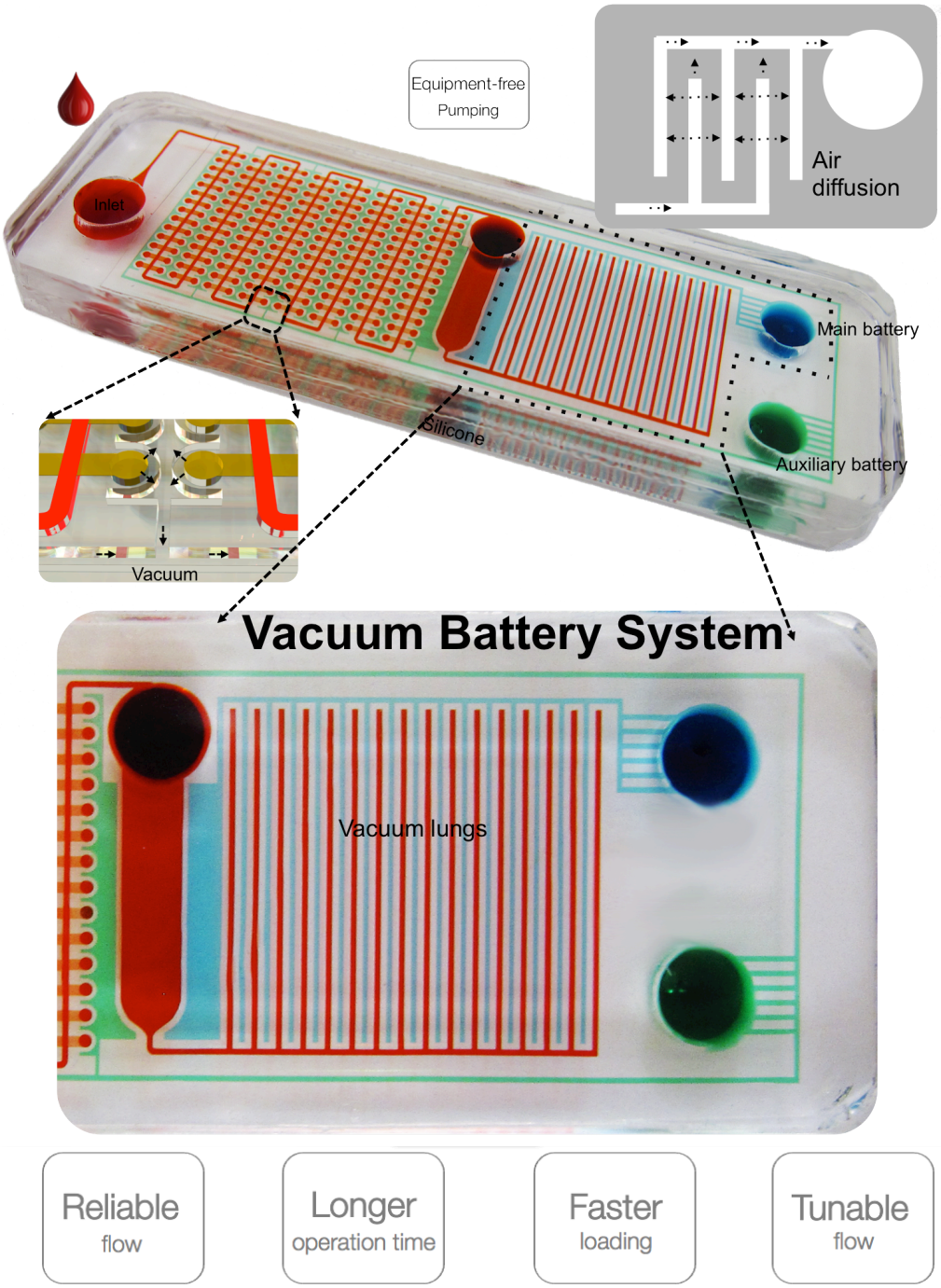

Figure 1 The low cost integrated vacuum battery system designed for portable equipment-free pumping. The above chip was loaded with food dye to highlight the microfluidic design. Red color shows where the fluid flows. Blue color shows where the main vacuum battery and the vacuum lung structures are. Green color shows where the vacuum lines connect to the auxiliary battery to assist micro-well loading. Compared with conventional degas flow, the merits are outlined in the boxes below.

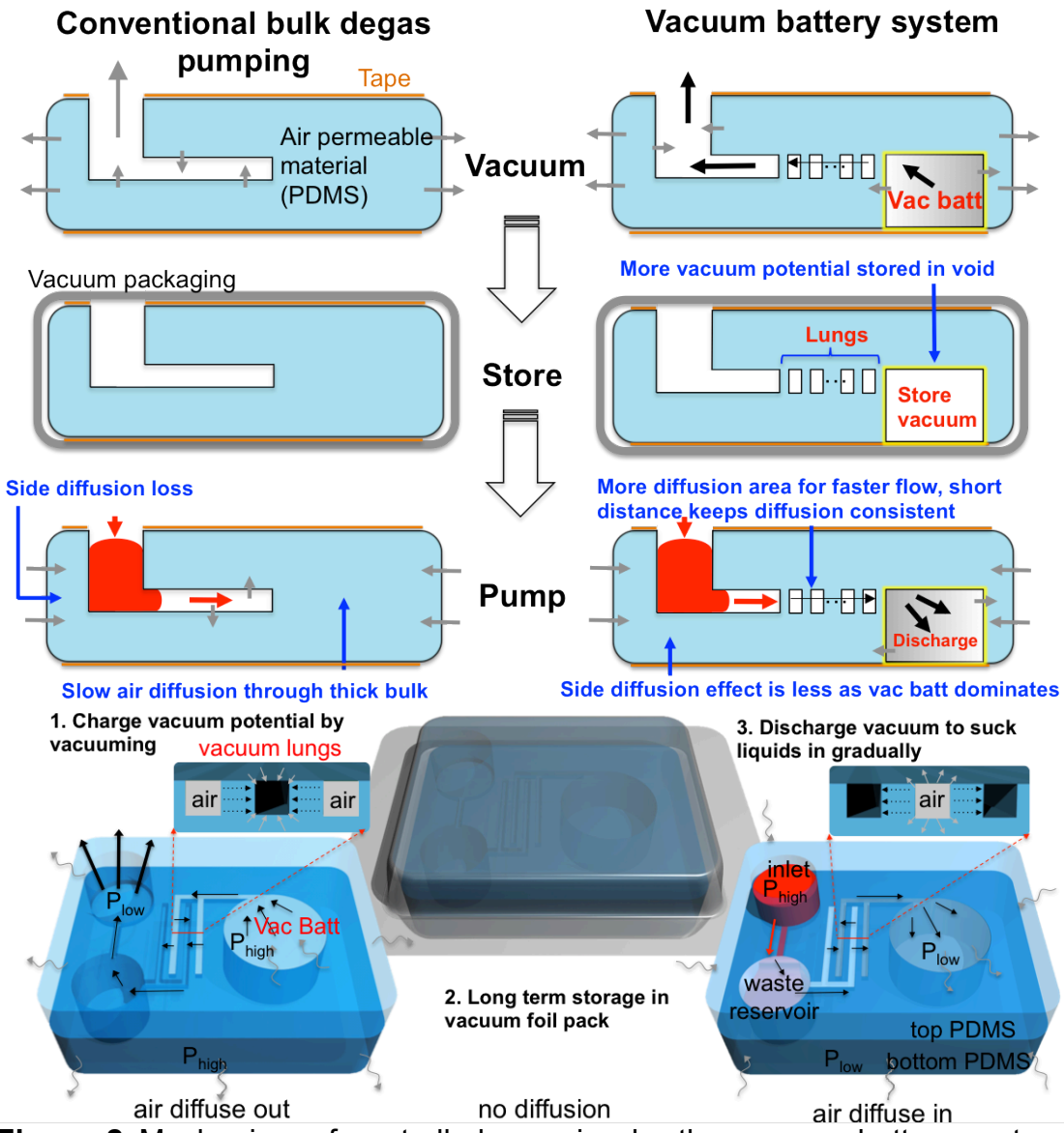

Figure 2 Mechanism of controlled pumping by the vacuum battery system. The top schematic shows the side view comparison with conventional bulk degas pumping. The vacuum battery system pumps fluid by slowly releasing stored vacuum potential via air diffusion over the vacuum lung structures. This system is able to deliver more stable and faster flow, over a longer duration of time because more vacuum potential can be stored in the void battery space. The bottom schematic shows a top view of the basic unit of the vacuum battery system. Black arrows depict air diffusing across the vacuum lungs. Grey arrows depict air diffusing from bulk PDMS. Flow rate can be tuned easily by varying the battery size and lung surface area.

There are four main reasons for these improved characteristics; firstly, the vacuum battery void can provide more vacuum potential storage than bulk PDMS and therefore more air can be outgassed and resulting in more liquid being sucked in. Since more vacuum is accumulated, a longer operation time is possible. This is analogous to the arranging batteries in parallel to discharge longer. Secondly, since the main vacuum potential is stored in the vacuum batteries, instead of the bulk PDMS, the system is less susceptible to losing vacuum power from the sides of the devices. This contributes to the higher consistency of fluid loading. Thirdly, air no longer has to diffuse through bulk PDMS material, but only through a thin PDMS wall. This translates into faster and more consistent flow. In conventional bulk degas diffusion, there is a characteristic initial sharp exponential drop in flow rate as air diffuses into the surface layers of PDMS, but becomes much slower afterwards as air takes much longer to diffuse into the bulk material (**Fig. 2**). More consistent flow is possible since vacuum diffuses with a more constant pressure drop across the vacuum lung thin PDMS walls as the vacuum battery provides a large capacitance for vacuum energy storage. Fourthly, the flow rate can be easily tuned and increased by modifying the surface area of the vacuum lung diffusion area or increasing the vacuum battery volume. The combined effects of the vacuum battery system plus bulk degas pumping also help increase the flow rate.

Charging, storage, and discharging vacuum potential

The basic components of the vacuum battery system and operation steps are depicted in the bottom of **Figure 2**. There are three cycles. The first cycle is the charging phase, where the device is put in a vacuum environment and the air from the vacuum battery slowly diffuses out. Air also degasses out of the bulk PDMS material from the sides of the chip. This step is termed the “charging vacuum potential” step. In the second step, if long-term storage is needed, the device is packed with a vacuum-sealing machine in aluminium pouches. The devices can be stored indefinitely and transported easily in these pouches (**Fig. 3**), which is a desirable attribute for point-of-care diagnostic devices. No observable loading speed differences were found with devices that were stored in these pouches for up to a year. In the last step, the user simply opens the pouch and loads the liquid sample; this is termed the “discharging” step. This step is simple and straightforward, so no special training is required to perform it.

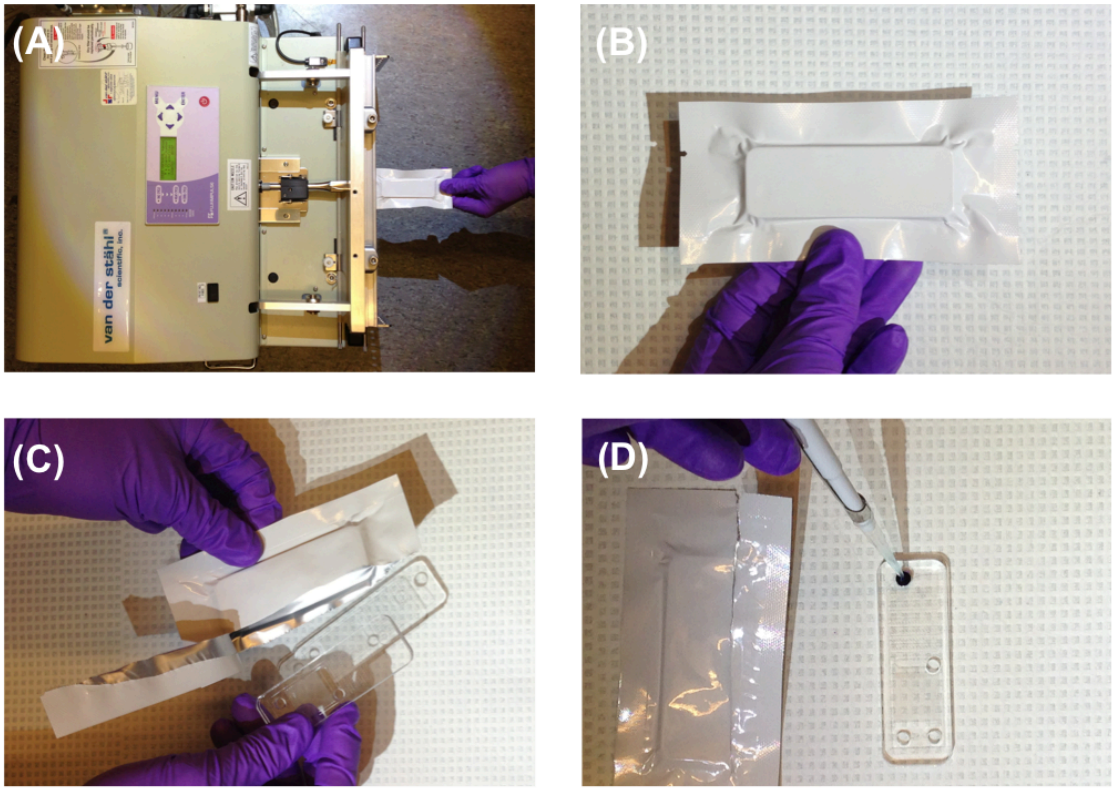

Figure 3 Chip operation protocol. (A) After the chips are incubated in vacuum overnight, it is sealed in an aluminum pouch with a vacuum sealer. It takes only several seconds to seal each pouch. There is a layer of plastic laminated on the inside of the aluminum seals, and by heating the seams up, it can melt and seal the pouch. (B) Zoom in on the sealed pouch. This pouch can be stored indefinitely and transported easily to remote areas. (C) The user simply rips the seal open and load samples in. (D) Loading samples in. With the vacuum battery system, there is a long loading window of 40 minutes (data shown in Fig. 2) for the user to load the chip.

Governing equations

A simplified 2-D diffusion model was built with the COMSOL simulation software using the convection diffusion equation. The detailed model setup and general assumptions are explained in **Fig. 4**.

The air diffusion across from the fluid channels through the PDMS vacuum lungs into the vacuum battery space can be described with the convection-diffusion equation[57]:

$$\frac{\partial c_i}{\partial t} = \nabla \cdot (D_i \nabla c_i) - \nabla \cdot (\vec{u} c_i) \quad (1)$$

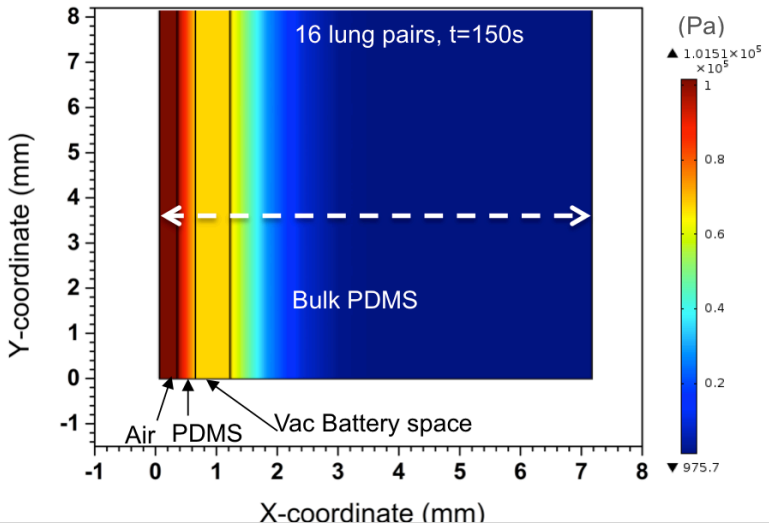

Figure 4 Simplified 2D simulation model. The vacuum battery system was simplified into a 2D model with four regions, from left to right, the fluid channel where air is being drawn out, the thin PDMS membrane of the vacuum lungs to control diffusion speed, the vacuum battery void space to store vacuum potential, and the surrounding bulk PDMS material. The convection-diffusion model was used in COMSOL to simulate this setup. Within the PDMS regions, no convection was assumed. Air diffuses gradually from the left to right regions.

Where c_i denotes the concentration species of air in the fluid channel, PDMS, or vacuum battery. D_i is the diffusion constant of air in each regime, and $\vec{u}$ is the convection velocity vector in the fluid channel and vacuum battery. In the bulk PDMS, there is no convection, therefore the equation simplifies into Fick's second law[58]:

$$\frac{\partial c_i}{\partial t} = D\nabla^2 c_i \tag{2}$$

The pressure in the fluid channels and vacuum battery can be found by correlating the gas concentration via the ideal gas law:

$$P = \frac{n}{V}RT = cRT \tag{3}$$

where P is the pressure, V is the volume, n is number of moles, R is the Avogadro number, and T is the temperature. The volume of liquid being sucked in the device is the same volume of air that has diffused into the vacuum battery and PDMS. This volume can be calculated by integrating the flux of air concentration being degassed over time and surface area. Pressure changes against time plots are shown in **Fig. 5**.

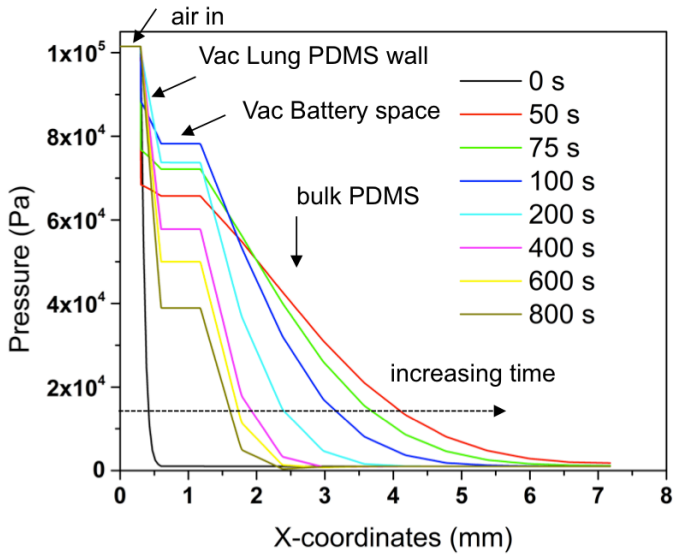

Figure 5 Simulated pressure profile of dashed line in Supplementary Fig. 2. As time increases, the vacuum battery void space first fills with air, then it gradually diffuses into the bulk PDMS. The bulk PDMS degassing follows a characteristic exponential decay in pressure.

Design of microfluidic chip

The main battery and auxiliary well-loading battery for vacuum storage

The two vacuum battery systems that are included on the chip (**Fig 1**) serve different purposes. The main vacuum battery system (top void) connects to the vacuum lungs, and draws air in from the fluid line via diffusion across the vacuum lungs. It pumps the main fluid flow that goes from the inlet into the waste reservoir from left to right. The auxiliary well-loading vacuum battery system (bottom void) is connected to the vacuum lines adjacent to the dead-end wells; as in the main battery system, they are both not physically connected to the fluid channels, they draw air in via diffusion across the PDMS wall, and assist in making the dead-end well's loading speed faster. The auxiliary well-loading battery is optional since conventional degas pumping can still cause the wells to be loaded, though at a slower speed. For experiments, the auxiliary battery has always been kept at a constant size (100 µl), while varying the main battery size to characterize its effect on flow. Though simple, the vacuum batteries voids are the key in enabling large vacuum potential storage in the devices to drive flow.

Vacuum lung design mimicking alveoli gas diffusion

This experiment mimicked gas exchange of the lung alveoli by designing closely staggered fluid channels and vacuum channels in an array where a 300 μm thin PDMS membrane separates them (**Fig. 1**). It is important to note that the fluid and vacuum channels do not physically connect with each other as all pressure differences is actuated by gas diffusion across the thin PDMS wall. This is similar to the concept that of that blood vessels do not connect with the atmospheric environment in alveoli, but rely on diffusion for gas exchange. Both the fluid channels and vacuum channels are 300 μm in width and height. One lung pair is defined as one pair of fluid channel plus one pair of vacuum channel, having a 10 mm^2 diffusion cross section area. The number of lung pairs, which determines the diffusion cross section, is proportional to the flow speed. Air is able to diffuse through the permeable PDMS membrane from the fluid channel into the vacuum lungs and then into the main vacuum battery, thus sucking the fluid in. The fluid will never cross into the vacuum battery system as the fluid channels and vacuum channels are not physically connected.

Deep reservoirs for large loading volume and transmission optics

In contrast to capillary pumping, the vacuum battery system enables more flexibility in the design of geometries. To demonstrate this, a deep reservoir (5 mm diameter, 3 mm height, **Fig. 1**) was designed to retain the excess of pumped liquid. This reservoir enables large loading volumes of liquid to be continuously pumped in. The device can pump in at least 140 μl, and volume can be easily be further increased by punching larger waste reservoirs and vacuum batteries. This is possible because the vacuum battery significantly adds to the vacuum capacity of the device compared to bulk degassing systems. This additional capacity is the driving force that helps outgas the remaining air volume. The reservoir also helps prevent liquid from immediately flowing into the vacuum lung area, thus preventing the flow rate to be affected prematurely when the liquid covers the surface area for gas diffusion. The capacity for large and deep reservoirs is also advantageous for fluorescent or transmission type optical detection as the Beer Lambart law can be fully utilized since the optical path length is longer. For example, Enzyme-Linked Immunosorbent Assays (ELISA), or real-time PCR assay are common examples that use transmission type optical detection, which can be benefit from this system.

Methods

Fabrication of microfluidic chips

The chips tested were fabricated using the standard soft lithography[59] process. The same design in **Fig. 1** was used for all of the experiments. Briefly, a master mold with protruding microfluidic channels were created by photo-patterning (OAI Series 200 Aligner) 300 μm of SU-8 photoresist (Microchem) onto silicon wafers. Then 3 mm of Polydimethylsiloxane (PDMS, Sylgard 184, Dow Corning) was poured and cured over the silicon wafer mold to replicate the microfluidic channels. All chips were made to the same size of 25 mm*75 mm by putting a laser cut acrylic cast around the silicone mould, which is the same footprint as a standard microscope glass slide. The waste reservoir was punched by a 5mm punch. A separate blank piece of 3mm PDMS would be bonded on the top side to seal the fluidic layer by oxygen plasma bonding by a reactive ion etching machine (PETS Reactive Ion Etcher). Finally, transparent pressure sensitive adhesives (MH 90880, Adhesive Research) were taped on both the bottom and top surface of the chip to prevent excess gas diffusion. New chips were used for each experiment. A cross section of the chip construction is shown in **Figure 6**.

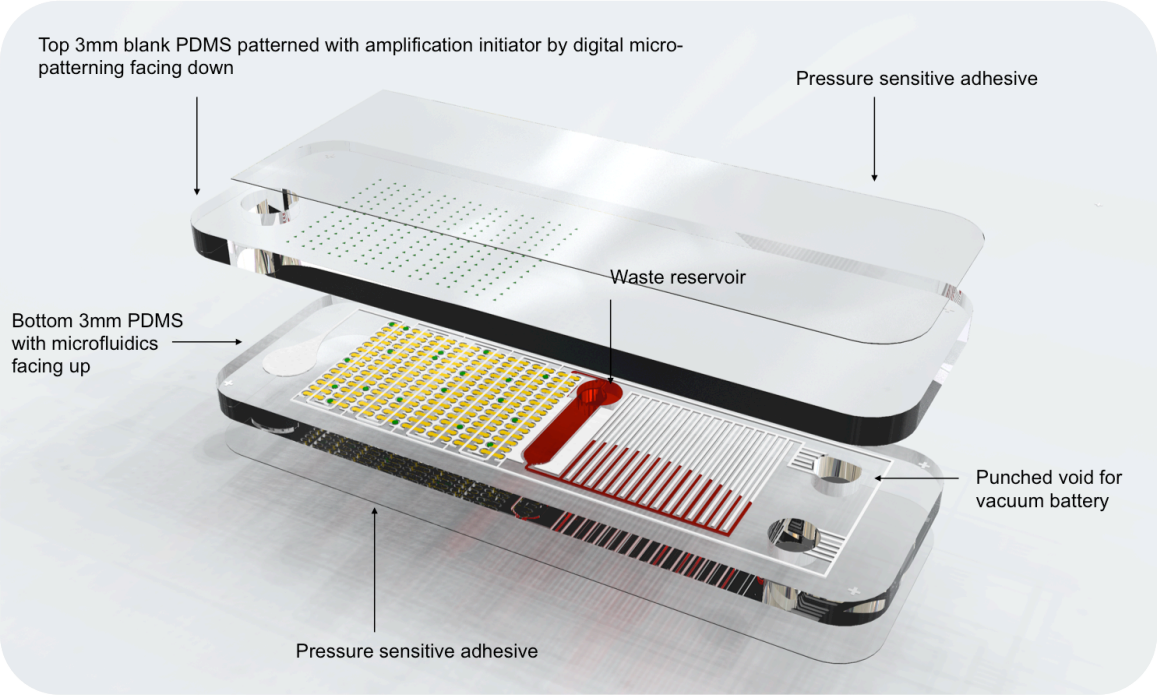

Figure 6 Simple construction of the device. Only two layers of air permeable silicone material (PDMS) are needed. These two layers are bonded together by exposing UV light to the PDMS. The bottom layer consists of the fluidic components; the large waste reservoir and vacuum battery voids were punched with punchers. The top piece is a blank PDMS that has been patterned with amplification initiator (MgOAc) on the bottom bonding surface. Transparent pressure sensitive adhesive is added on the top and bottom to prevent excess air diffusion from the top and bottom surfaces of PDMS. Microfluidic channels are highlighted with colors to show different functional parts. Red is the blood sample; white are empty channels and vacuum lines. The footprint of this device is 25*75 mm, which is the same as a standard microscope slide.

Master mold replication

To increase the device assembly throughput, the master silicon mold was replicated by casting urethane plastic (Smooth-Cast 327, Smooth-on, Inc.) over the molded PDMS devices placed in square petri dishes. A thin layer of release agent (Ease Release, Smooth-on Inc.) was applied to the surface of the petri dishes to prevent urethane from sticking. The PDMS devices and urethane resin were degassed before casting, so no air bubbles would be trapped. The first hour of curing was done at 4°C to lower viscosity and slow curing of the urethane resin thus further avoiding air bubbles. Afterwards, the resin was left to cure at room temperature

overnight and removed from the petri dishes. PDMS was poured into the hardened urethane molds to make devices.

Fabrication of vacuum battery void

The vacuum battery void would be fabricated by simply punching the 3 mm PDMS fluidic layer with through holes before bonding the top and bottom PDMS layers. Different diameters of punchers (Harris Uni-Core, Ted Pella) would be used to fabricate desired vacuum battery volumes. Pressure sensitive adhesive tape used to cover the top and bottom sides would seal these battery voids into compartments.

Vacuum charging and storage

The devices would be incubated at -95 kPa for 24 hours in a vacuum chamber before liquid loading experiments. The devices would be sealed in aluminium vacuum packs by a vacuum sealer (V-402, Van der Stahl Scientific) if long-term storage was necessary.

Statistical analysis

For experimental data, sample sizes are noted in the corresponding figure legends. Experiments were repeated in the lab at least three times. All experimental data are shown as means, and error bars denote plus minus one standard deviation. Replicates represent technical replicates. The Shapiro-Wilk test was used for normality testing and verified the data was normally distributed. For the **Figure 4a** and **Figure 4b**, the inset data was fitted with an inverse function $y=a+b*(x+c)^{-1}$. For both cases, Adj. R-Square=0.99, and $P<0.01$ (ANOVA). For **Figure 5a**, the data was fitted with an exponential function $y=a*\exp(b*x)$. Adj. R-Square was found to be 0.99 (conv. degas), 0.92 (vac batt sys.), 0.93 (inset), and $P<0.01$ (ANOVA). OriginPro (version 9.0, OriginLab) was used for statistical analysis.

Time gap out of vacuum experiments

The devices were taken out of the vacuum chamber and 100µl of diluted blue food dye (Assorted Food Colors, Safeway) was pipetted to the inlet at set time intervals with a dilution ration in water of 1:25 (**Fig. 3A**). A video time lapse was taken and the flow rate was analysed with ImageJ and Aegisub software. Full loading was defined when the dye reaches the end of the vacuum lung structures. The no-battery devices were pre-degased and had PDMS poured into all the vacuum lines to fill the vacuum battery structure, then it was left to cure at room temperature for 2 days. The no-battery and with-battery fluidic channels were exactly identical, except that the no-battery device had all of the vacuum lines and battery voids filled with PDMS. For each data point, at least three repeats were performed.

Vacuum battery and lung surface area experiments

200 µl of diluted blue food dye was pre-loaded into PTFE tubes (Microbore PTFE Tubing, 0.03” ID, Cole Parmer) that had a steel tubing connector (SC20/15, Instech Solomon) connected to one side. The tubing were connected to the inlet of the devices at 15 and 5 minutes after taking the devices out of vacuum respectively for the vacuum battery and lung surface area experiments. The volume of food dye left to be pumped was monitored by taking a time-lapse video. For each data point, at least three repeats were performed.

Flow rate vs. time characterization

The flow rate was extracted from the derivative of flow volume vs. time. Originpro software was used to extract the derivatives and also fit the flow rate with exponential decay curves.

Results

The effects of the vacuum battery system on flow rates were compared with conventional degas pumping. Parametric studies were performed by varying the operation time gaps, volume of vacuum battery, and surface area of the vacuum lung pairs. The results show that the vacuum battery system increases reliability of the flow, has longer loading windows, has faster loading, and is easy to tune flow.

More reliable, faster pumping, and longer operation time

The effect of the time gap between releasing the chip from vacuum and loading liquids was tested. The goal is to demonstrate that the vacuum system provides a sufficient long window of operation so users can load the samples at reasonable times after opening the vacuum seal. **Figure 7A** shows the experimental setup and how "fully loaded" is defined as liquid fills to the end of the vacuum lungs. It also shows how "digitization" is defined by the wells mean. Digitization is defined as complete when all 224 wells are filled and compartmentalized when the air gap comes in. A volume of 100 µl of blue food dye was loaded into the chips at different time gaps after the chip was taken out of the vacuum. **Figure 7B** shows a time-lapse comparison of actual loading. The vacuum battery system finished loading at 40 minutes while the conventional degas pumping system still had significant portions that were not loaded.

The vacuum battery system was found to be functional for a longer loading time gap for up to 40 minutes, whereas conventional degas pumping failed loading starting at 30 minutes (**Fig. 7C**). Even after idling in atmosphere for 40 minutes out of the vacuum, this system still remained functional and continued to pump for another 107 minutes (**Fig. 7C**). Thus, the conclusion is that this system can pump reliably for at least 2 hrs in total. Though the conventional degas pumping method could continue to load for longer times (50~200 min, **Fig. 7C**) after the liquid is loaded into the inlet, the more important factor is the length of the initial time gap that the user can load liquids in. Also, a longer post-loading pumping time indicates that conventional degas pumping is slower. Regardless of the time gap, loading speed was found to be much faster in the vacuum battery system (**Fig. 7C**). For example, at 5 minutes after releasing vacuum, the vacuum battery system was 4.5 times faster in loading. Furthermore, the vacuum battery system was much more robust, as it followed a linear trend nicely while conventional degas had much more variation, with r^2 values at 0.97 and 0.83, respectively. Finally, this system was found to be much more consistent in repeatability. The standard deviation of the loading time of the vacuum battery system was ~8 times less in average than conventional degassing (**Fig. 7D**). In characterizing digitization speed of the wells by varying the loading time gap (**Fig. 8**), the vacuum battery system was also found to enhance consistency and digitization speed. Compared to conventional degas pumping, the vacuum battery system provides faster loading, a significantly more robust system, and a longer window for user operation.

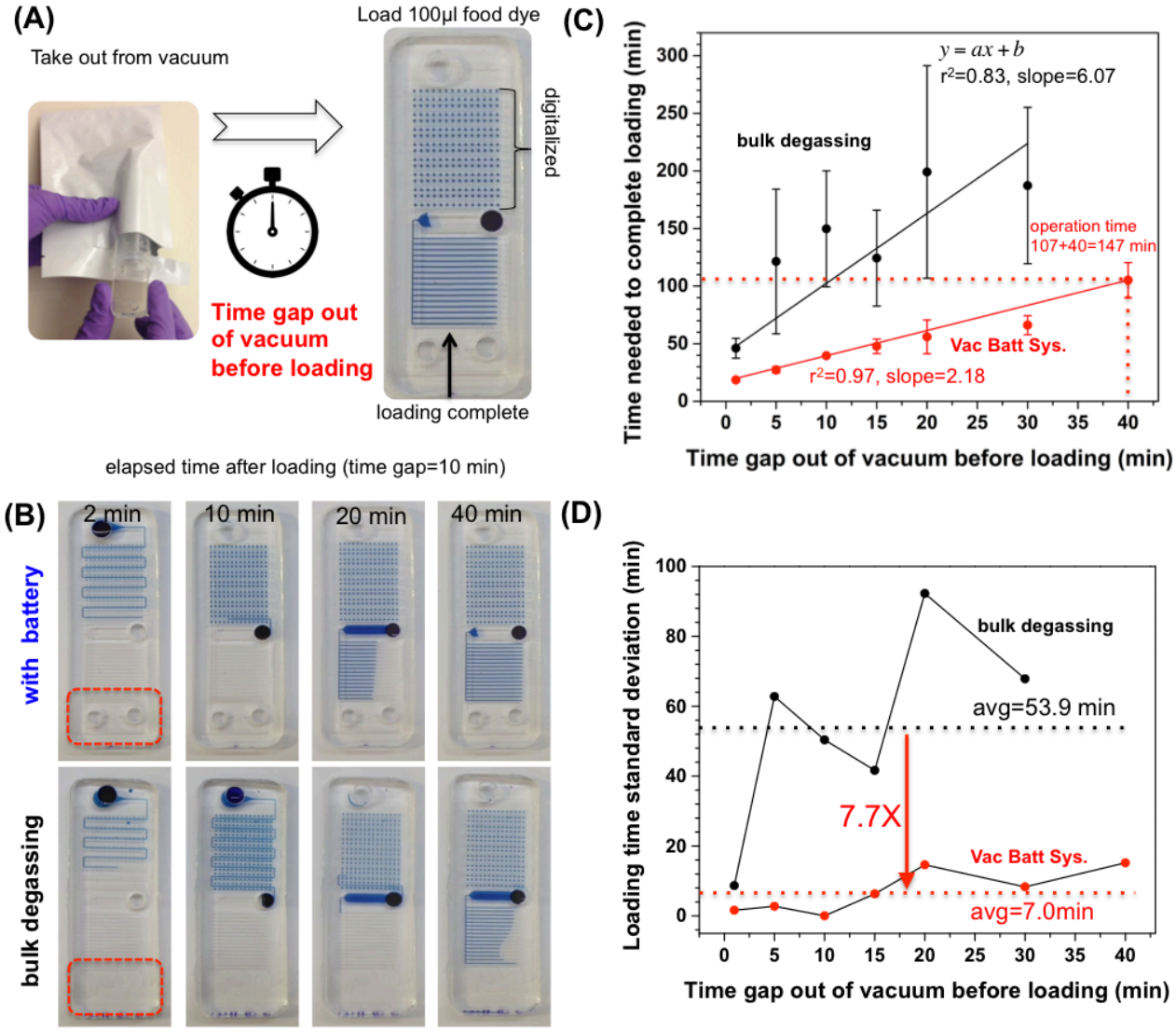

Figure 7 More reliable flow, faster flow, and longer operation time compared to conventional bulk degas pumping. (A) The experimental setup. (B) Time lapse images of loading. The front section of dead-end wells was compartmentalized to show adaptability for multiplexed reactions. The chips were loaded after being exposed to atmosphere for 10 minutes after taking out of vacuum. (C) The effect on flow speed by varying the time gap between taking the device out of vacuum and loading. The vacuum battery was significantly faster and more consistent. The vacuum battery void volume was kept consistent at 100 µl, n=3. (D) A comparison of the standard deviation of loading time extracted from (C).

Bubble free loading in wide optical windows

The possibility of designing wide fluidic channels (3x15 mm, 300 µm height) in this device and loading without any bubbles (**Fig. 8**) was demonstrated. This is difficult to perform in capillary or plastic microfluidic systems. In these systems, accidental trapping of bubbles is a common problem in wider geometries. It is critical to have minimal bubbles in microfluidic systems as they can easily clog channels, or cause catastrophic ejection of liquid when heated due to thermal expansion. This is a particular problem in PCR assays. The side vacuum lines were observably helpful in removing trapped bubbles much faster than regular bulk degassing in these large windows (**Fig. 7**).

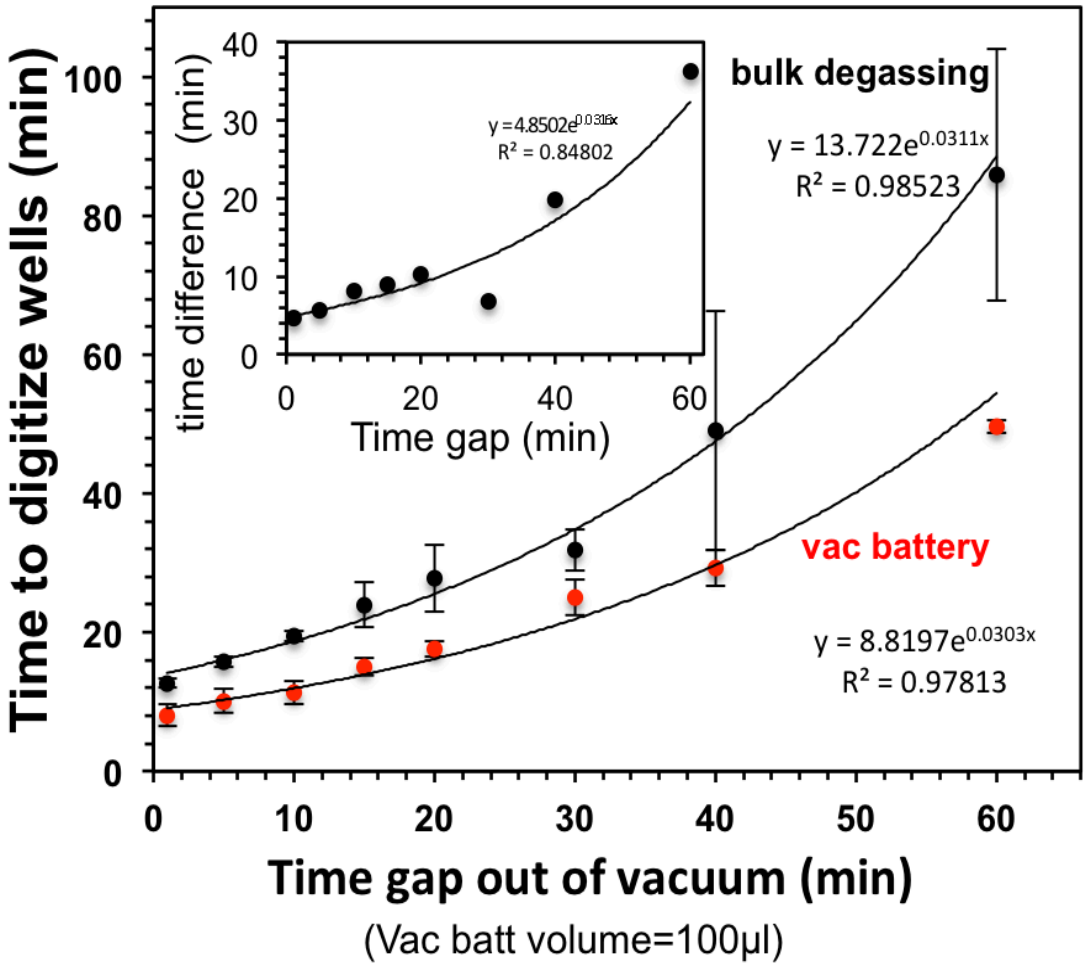

Supplementary Figure 8 More reliable and faster digitization compared to conventional bulk degas pumping. 100 µl of food dye was loaded into the chip. Time to digitize of a well is defined when all 224 wells are fully loaded with food dye and compartmentalized when the air plug from the inlet passes by. N=3 for all data points.

Varying vacuum battery void for fine flow tuning

Next up to test was the effect of changing vacuum battery size on the flow characteristics. Aside from increasing flow reliability and speed, a larger battery resulted in a faster flow rate (**Fig. 9**). However, flow rate saturated after the battery was increased to larger then 150 µl. There were not much difference in loading times between the 150 µl and 200 µl battery. The simulation results were plotted with dashed lines, and agreed well with experimental results that were in dots (**Fig. 9, inset**). The loading time was found to be inversely proportional to the volume of the vacuum battery, and reaches saturation as the volume gets larger. The flow rates were turned at finer increments from 9.0~16.7 µl/min. Tuning flow rates was easily accomplished by simply punching different diameter sizes for the vacuum void after the mold was already fabricated. This kind of post-processing is very convenient since the same mold could be used.

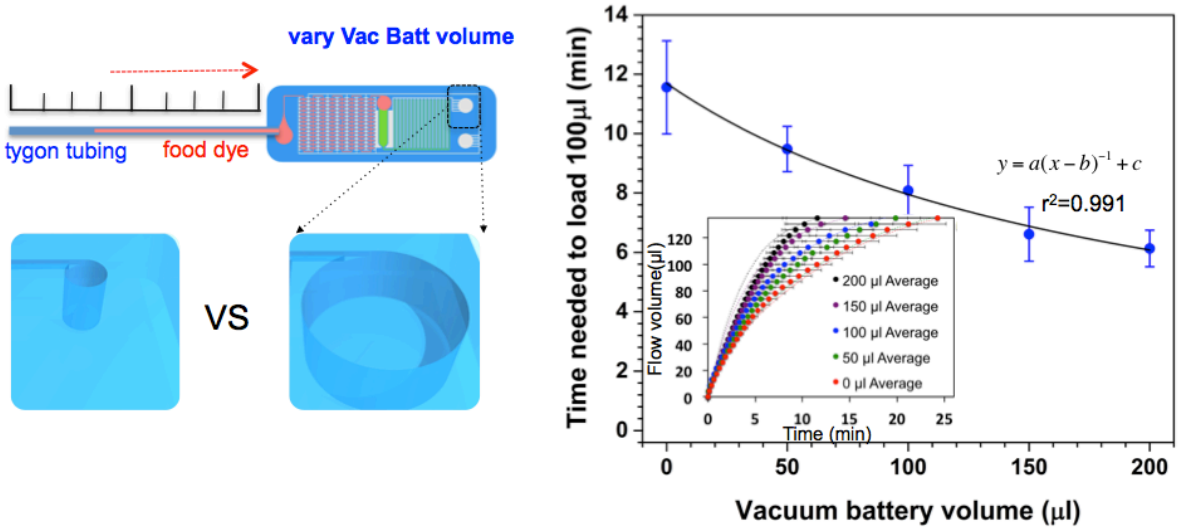

Figure 9 Fine tuning by varying the stored vacuum potential by changing vacuum battery volume. Time gap out of vacuum=10 min, n=3. The auxiliary vacuum battery was kept constant at 100 µl, while the main vacuum battery volume was varied.

Faster Dead-end loading for Digital PCR or multiplexed assays

Dead-end loading is especially useful for PCR reactions because it minimizes evaporation problems. Also, dead-end wells can be useful in digital PCR[60]

applications, where one PCR reaction is partitioned and compartmentalized into multiple smaller volumes of reactions, and each chamber is run until saturation for a digital readout. On the other hand, dead-end wells are also useful for multiplexed reactions, for example multiple diseases can be screened in different wells. However, dead-end wells would not be possible to load with capillary loading, and conventional degas pumping is slow. Consequently, this system's unique advantage is exhibited by demonstrating ~2 times faster dead-end loading (**Fig. 10**) compared to conventional degas pumping. The chip was designed with 224 dead-end wells, each having a diameter of 650 μm and a height of 300 μm. This translates to 100 nl of volume per well. The vacuum battery system enabled an increase in the loading speed of these wells. Vacuum channels, which connect to the vacuum battery, are adjacent to the dead-end wells. The wells are connected to the fluidic channels. They are separated by a 300 μm PDMS membrane (**Fig. 1, bottom zoom**). All wells were loaded and compartmentalized in 12 minutes with the vacuum battery, whereas well loading without the vacuum battery took 23 minutes.

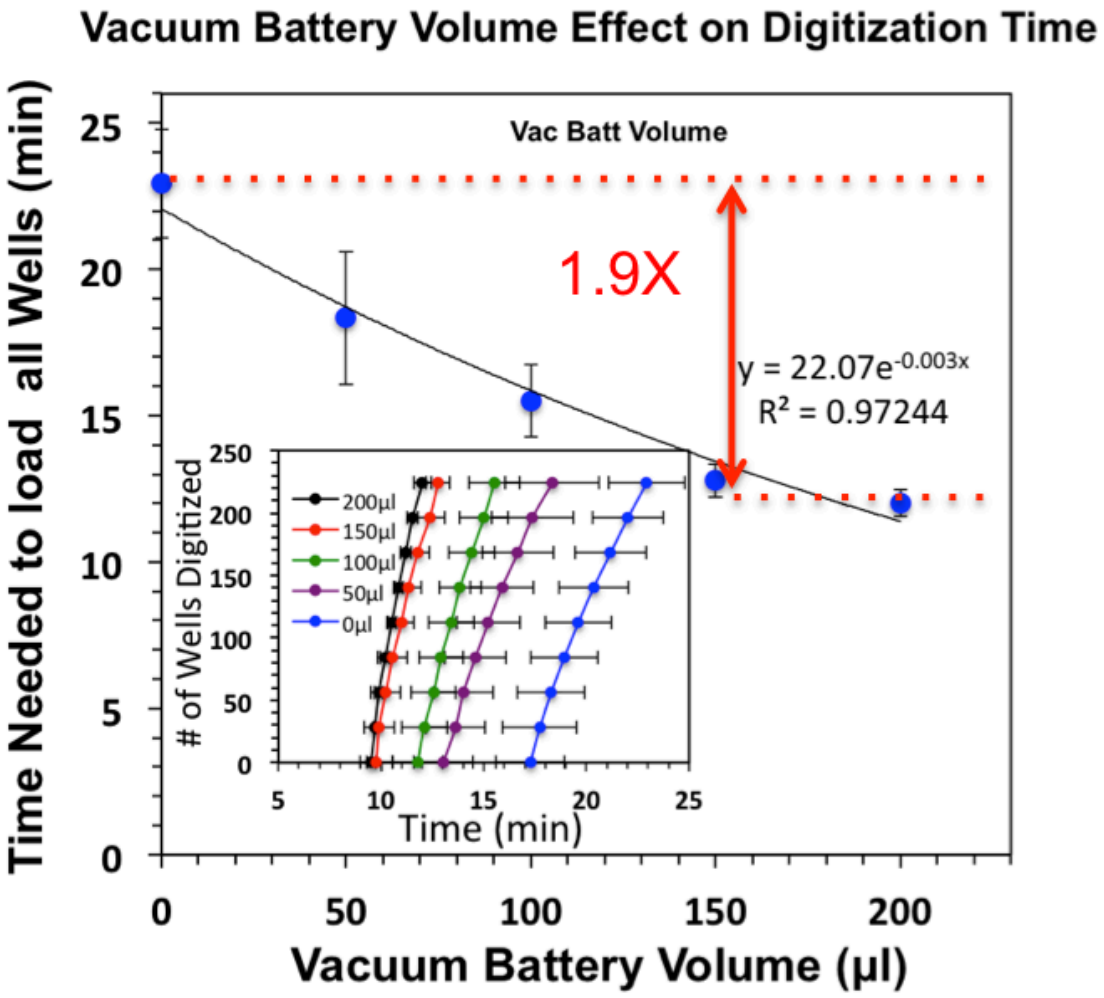

Figure 10 Faster compartmentalization (digitization) of the dead-end wells with larger vacuum batteries**.** 100 µl of food dye was loaded into the chip. Digitization of a well is defined when a well is fully loaded with food dye and compartmentalized when the air plug from the inlet passes by. The chip was left in atmosphere pressure for 15 minutes before loading. The auxiliary vacuum battery was kept at 100 µl while the main battery volume was varied. N=3 for all data points.

Varying vacuum lungs for coarse flow tuning

Next up for testing was the effect of vacuum lung cross-section area on flow characteristics (**Fig. 11**). Simulation results were plotted with dashed lines, and agreed well with experimental results that were in dots (**Fig. 11, inset**). It was discovered that loading time was also inversely proportional to the surface area of

the diffusion cross-section area. It was possible to tune flow rates with a larger range from 1.6~18.2 µl/min by adding the number of "lung pairs". A lung pair is defined as one pair of vacuum and fluidic line (**Fig. 11, left**). The vacuum lungs had a more dramatic effect of increasing loading speed up to 10 times compared to chips that did not have any vacuum lungs. In order to tune flow rates, the mold has to be predesigned with the desired number of lung pairs.

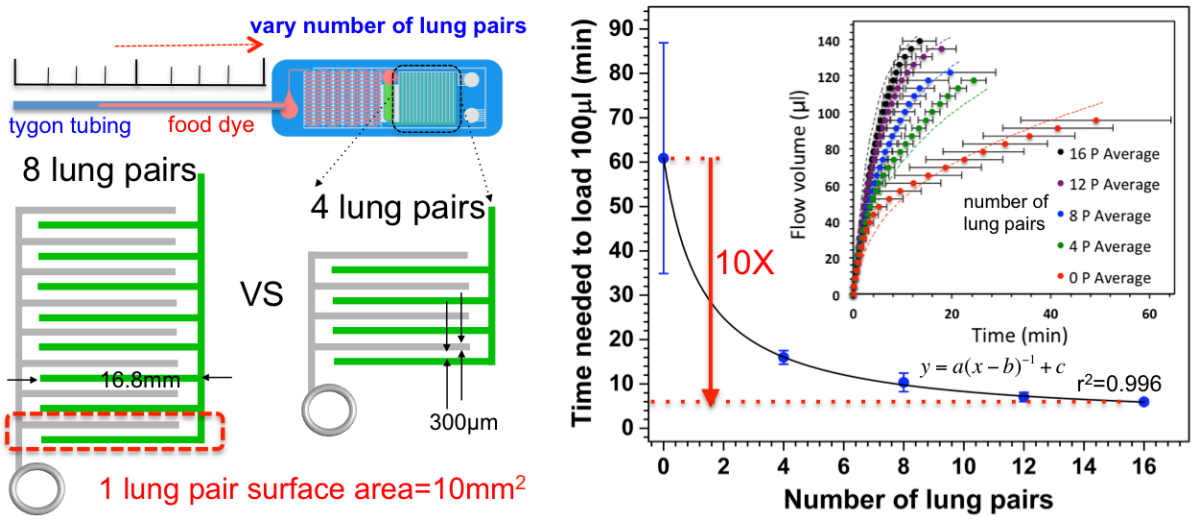

Figure 11 Coarse tuning by varying the diffusion surface area by changing the number of lung pairs. Time gap out of vacuum=15min, n=3. Channel height is 300 µm. Dashed lines in inset are simulation results. Solid dots show experimental results.

More consistent flow rates with vacuum battery system

Adding vacuum batteries and vacuum lungs contributed to more consistent flow rates, as the slope of loading was more linear (See insets of **Fig. 11, 12**). Additionally, the vacuum lungs increased not only the loading speed, but also the flow stability (**Fig. 13**). Flow rate followed the characteristic exponential decay over time as in conventional degas pumping, however, the flow rate decay could be made much slower when there are more lung pairs. The exponential decay time constant was increased ~5 times with this prototype. It is anticipated that further optimization of the vacuum battery system is possible: adding extra vacuum batteries would allow decay time to be constant even longer, while additional secondary degas lungs to degas and stabilize the primary vacuum battery.

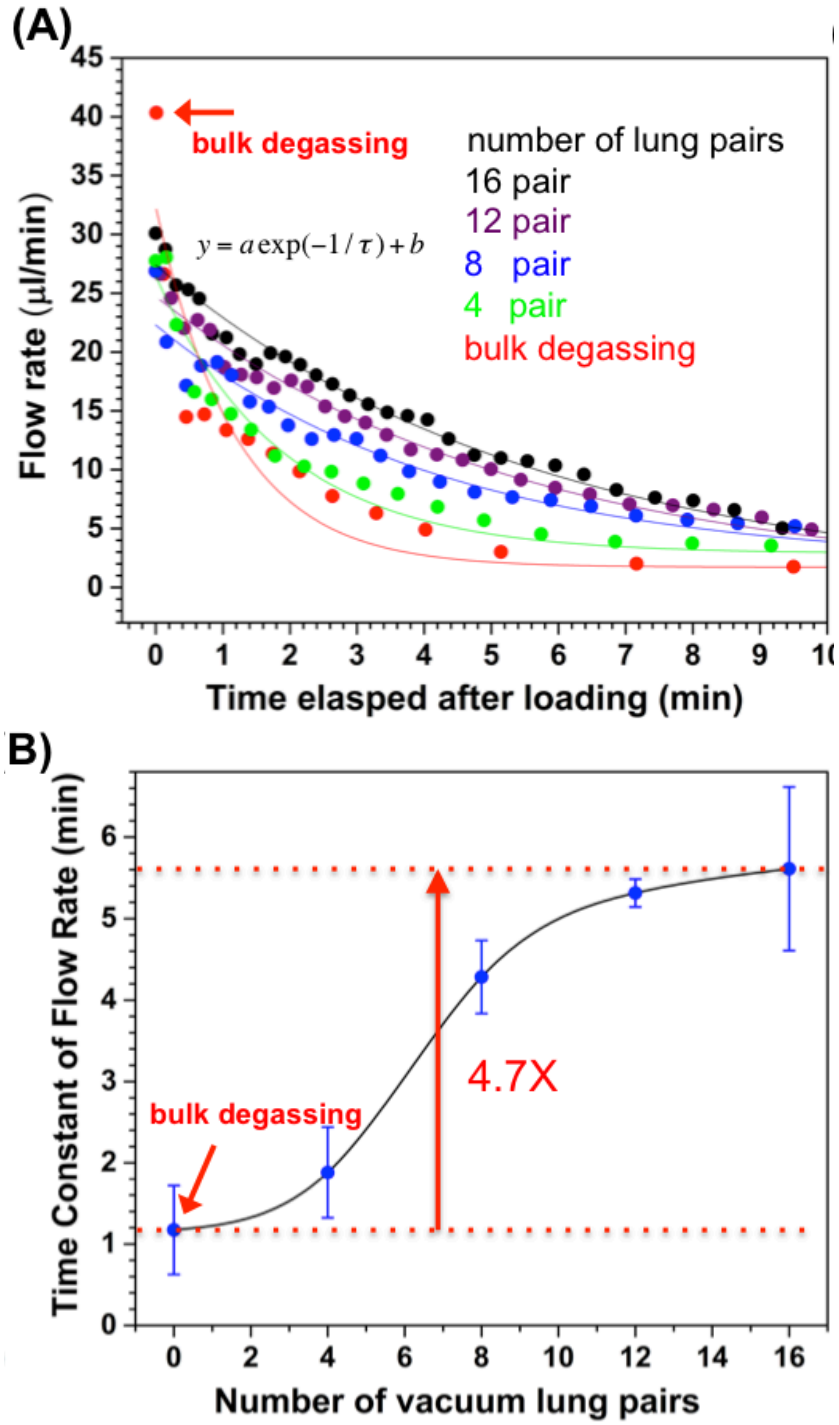

Figure 13 More constant flow rates with slower decay with the vacuum battery system. (A) Flow rates decay slower with the vacuum battery system when there are more lung pairs. Time gap out of vacuum =15 min. (B) Exponential decay time constant is 5 times slower with the vacuum battery system compared to conventional degas pumping. Both vacuum batteries were kept constant at 100µl for all experiments, n=3.

Discussion

Herein is presented the new “vacuum battery system” design, the first demonstration of pumping via a vacuum void to store vacuum potential for controlled microfluidic pumping in conjunction with biomimetic vacuum lungs. With the new design, this research makes advancements in four key areas of flow control compared to conventional degas pumping. It also demonstrates that this system can be adopted for digital amplification assays. (1) It is possible to attain more stable flow, with ~8 times less deviation in loading time and up to ~5 times increase of the decay time constant for a much slower and stable exponential decay in flow rate. (2) This system can perform reliable pumping for up to 2 hours without any external power sources or extra peripheral equipment. (3) It is able to increase loading speed to up to 10 times, with a large loading capacity of at least 140 µl. (4) The system is possible to easily tune flow and increase flow consistency by varying the vacuum battery volume or vacuum lung surface area.

This research further improves the distinct advantages of existing degas loading traits over capillary pumping. Loading a large array of dead-end wells (224 in total) without trapping any bubbles was demonstrated at up to twice the speed. These dead-end wells can be adopted for future multiplexed assays or digital PCR assays. Faster bubble-free loading of large optical windows and deep wells were shown. These are useful in transmission type optical detection, but would be challenging for capillary systems to perform. The vacuum battery system does not require any special surface treatment and has more flexibility for channel geometry design, as it does not rely on surface tension or capillary action to drive flow.

It is recommended for designers to follow these simple and straightforward steps for their own applications: (1) increase the vacuum battery void if longer operation time or sample volume is needed. (2) Increase the number of vacuum lung pairs if faster flow speed is desired. (3) Increase the waste reservoir volume if larger sample volumes are necessary. Further recommended is to conduct rapid prototyping over simulations, as empirical results are more accurate and the experiments are straightforward to conduct.

All pumping components are directly integrated into the device and can be easily manufactured by molding. For mass production, PDMS can be replaced by the use of injection molding compatible gas permeable elastomers (e.g. liquid silicone, TPE[61], etc.). The straightforward construction only requires two layers thus it can be manufactured at low cost. The current limitations of this system is the eventual drop of the flow rate over time, however the vacuum battery system is already significantly more stable than conventional degas pumping. It is believed that flow rate can be further stabilized by adding second order vacuum battery systems to degas the first battery system.

Conclusion

In conclusion, compared to conventional degas loading, the vacuum battery system provides significantly more reliable flow, longer operational time, faster flow, and easy tunablity of flow rates. In addition, it overcomes several limitations of

capillary loading. The vacuum battery system is able to load dead-end wells, load deep or wide geometries without bubbles, and has excellent transparent optical properties. This simple system is easy to operate, can be stored for long term, is convenient to transport, and can be operated on-site without any external power sources or equipment. This translates into exciting opportunities for applications such as performing on-site ELISA, digital PCR, or multiplexed digital nucleic acid amplification. For these reasons, the vacuum battery system is an ideal alternative platform technology from capillary systems or conventional degas pumping for future handheld point-of-care devices.

Notes and references

1. Laser, D. J. & Santiago, J. G. A review of micropumps. *Journal of Micromechanics and Microengineering* **14,** R35–R64 (2004).
2. Haeberle, S. & Zengerle, R. Microfluidic platforms for lab-on-a-chip applications. *Lab on a Chip* **7,** 1094 (2007).
3. Zhang, C., Xing, D. & Li, Y. Micropumps, microvalves, and micromixers within PCR microfluidic chips: Advances and trends. *Biotechnology Advances* **25,** 483–514 (2007).
4. Iverson, B. D. & Garimella, S. V. Recent advances in microscale pumping technologies: a review and evaluation. *Microfluidics and Nanofluidics* **5,** 145–174 (2008).
5. Gervais, L., De Rooij, N. & Delamarche, E. Microfluidic Chips for Point-of-Care Immunodiagnostics. *Advanced Materials* **23,** H151–H176 (2011).
6. Yi, H., Pan, J.-Z., Shi, X.-T. & Fang, Q. Automated liquid operation method for microfluidic heterogeneous immunoassay. *Talanta* **105,** 52–56 (2013).
7. Chen, Y., Wu, T.-H. & Chiou, P.-Y. Scanning laser pulses driven microfluidic peristaltic membrane pump. *Lab on a Chip* **12,** 1771 (2012).
8. Cui, J. & Pan, T. A vacuum-driven peristaltic micropump with valved actuation chambers. *Journal of Micromechanics and Microengineering* **21,** 065034 (2011).
9. Rhie, W. & Higuchi, T. Design and fabrication of a screw-driven multi-channel peristaltic pump for portable microfluidic devices. *Journal of Micromechanics and Microengineering* **20,** 085036 (2010).
10. Skafte-Pedersen, P., Sabourin, D., Dufva, M. & Snakenborg, D. Multi-channel peristaltic pump for microfluidic applications featuring monolithic PDMS inlay. *Lab on a Chip* **9,** 3003 (2009).
11. Grover, W. H., Skelley, A. M., Liu, C. N., Lagally, E. T. & Mathies, R. A. Monolithic membrane valves and diaphragm pumps for practical large-scale integration into glass microfluidic devices. *Sensors and Actuators B: Chemical* **89,** 315–323 (2003).
12. Unger, M. A. Monolithic Microfabricated Valves and Pumps by Multilayer Soft Lithography. *Science* **288,** 113–116 (2000).

13. Aeinehvand, M. M. *et al.* Latex micro-balloon pumping in centrifugal microfluidic platforms. *Lab on a Chip* **14,** 988 (2014).
14. Sista, R. *et al.* Development of a digital microfluidic platform for point of care testing. *Lab on a Chip* **8,** 2091 (2008).
15. Moon, H., Cho, S. K., Garrell, R. L. & Kim, C.-J. 'CJ'. Low voltage electrowetting-on-dielectric. *Journal of Applied Physics* **92,** 4080 (2002).
16. Wang, X., Cheng, C., Wang, S. & Liu, S. Electroosmotic pumps and their applications in microfluidic systems. *Microfluidics and Nanofluidics* **6,** 145–162 (2009).
17. Ehrenberg, O. & Kosa, G. Analysis of a novel piezoelectric micro-pump for drug delivery in a medical integrated micro system. in 467–472 (IEEE, 2012). doi:10.1109/BioRob.2012.6290893
18. Johnston, I. D., Tracey, M. C., Davis, J. B. & Tan, C. K. L. Microfluidic solid phase suspension transport with an elastomer-based, single piezo-actuator, micro throttle pump. *Lab on a Chip* **5,** 318 (2005).
19. Dentry, M. B., Friend, J. R. & Yeo, L. Y. Continuous flow actuation between external reservoirs in small-scale devices driven by surface acoustic waves. *Lab on a Chip* **14,** 750 (2014).
20. Yeo, L. Y. & Friend, J. R. Ultrafast microfluidics using surface acoustic waves. *Biomicrofluidics* **3,** 012002 (2009).
21. Yuen, P. K. Fluid control in microfluidic devices using a fluid conveyance extension and an absorbent microfluidic flow modulator. *Lab on a Chip* **13,** 1737 (2013).
22. Wang, X., Hagen, J. A. & Papautsky, I. Paper pump for passive and programmable transport. *Biomicrofluidics* **7,** 014107 (2013).
23. Osborn, J. L. *et al.* Microfluidics without pumps: reinventing the T-sensor and H-filter in paper networks. *Lab on a Chip* **10,** 2659 (2010).
24. Reches, M. *et al.* Thread as a Matrix for Biomedical Assays. *ACS Applied Materials & Interfaces* **2,** 1722–1728 (2010).
25. Tsougeni, K., Papageorgiou, D., Tserepi, A. & Gogolides, E. 'Smart' polymeric microfluidics fabricated by plasma processing: controlled wetting, capillary filling and hydrophobic valving. *Lab on a Chip* **10,** 462 (2010).
26. Li, C., Liu, C., Xu, Z. & Li, J. A power-free deposited microbead plug-based microfluidic chip for whole-blood immunoassay. *Microfluidics and Nanofluidics* **12,** 829–834 (2011).
27. Novo, P., Volpetti, F., Chu, V. & Conde, J. P. Control of sequential fluid delivery in a fully autonomous capillary microfluidic device. *Lab on a Chip* **13,** 641 (2013).
28. Safavieh, R. & Juncker, D. Capillarics: pre-programmed, self-powered microfluidic circuits built from capillary elements. *Lab on a Chip* **13,** 4180 (2013).
29. Gervais, L., Hitzbleck, M. & Delamarche, E. Capillary-driven multiparametric microfluidic chips for one-step immunoassays. *Biosensors and Bioelectronics* **27,** 64–70 (2011).
30. Gervais, L. & Delamarche, E. Toward one-step point-of-care immunodiagnostics using capillary-driven microfluidics and PDMS substrates. *Lab on a Chip* **9,** 3330 (2009).

31. Juncker, D. *et al.* Autonomous Microfluidic Capillary System. *Analytical Chemistry* **74,** 6139–6144 (2002).
32. Zimmermann, M., Schmid, H., Hunziker, P. & Delamarche, E. Capillary pumps for autonomous capillary systems. *Lab on a Chip* **7,** 119 (2007).
33. Hosokawa, K., Sato, K., Ichikawa, N. & Maeda, M. Power-free poly(dimethylsiloxane) microfluidic devices for gold nanoparticle-based DNA analysisElectronic supplementary information (ESI) available: Sample movie used for flow characterization, mathematical details of the one-dimensional diffusion model, and time course of the gold nanoparticle deposition. See http://www.rsc.org/suppdata/lc/b4/b403930k/. *Lab on a Chip* **4,** 181 (2004).
34. Zhang, H. *et al.* Direct detection of cancer biomarkers in blood using a 'place n play' modular polydimethylsiloxane pump. *Biomicrofluidics* **7,** 034105 (2013).
35. Okada, H., Hosokawa, K. & Maeda, M. Power-Free Microchip Immunoassay of PSA in Human Serum for Point-of-Care Testing. *Analytical Sciences* **27,** 237 (2011).
36. Hosokawa, K., Omata, M. & Maeda, M. Immunoassay on a Power-Free Microchip with Laminar Flow-Assisted Dendritic Amplification. *Analytical Chemistry* **79,** 6000–6004 (2007).
37. Hosokawa, K., Omata, M., Sato, K. & Maeda, M. Power-free sequential injection for microchip immunoassay toward point-of-care testing. *Lab on a Chip* **6,** 236 (2006).
38. Arata, H., Komatsu, H., Han, A., Hosokawa, K. & Maeda, M. Rapid microRNA detection using power-free microfluidic chip: coaxial stacking effect enhances the sandwich hybridization. *The Analyst* **137,** 3234 (2012).
39. Ho, J. Y., Cira, N. J., Crooks, J. A., Baeza, J. & Weibel, D. B. Rapid Identification of ESKAPE Bacterial Strains Using an Autonomous Microfluidic Device. *PLoS ONE* **7,** e41245 (2012).
40. Zhu, Q. *et al.* Self-priming compartmentalization digital LAMP for point-of-care. *Lab on a Chip* (2012). doi:10.1039/c2lc40774d
41. Gansen, A., Herrick, A. M., Dimov, I. K., Lee, L. P. & Chiu, D. T. Digital LAMP in a sample self-digitization (SD) chip. *Lab on a Chip* **12,** 2247 (2012).
42. Trung, N. B. *et al.* Multi-chamber PCR chip with simple liquid introduction utilizing the gas permeability of polydimethylsiloxane. *Sensors and Actuators B: Chemical* **149,** 284–290 (2010).
43. Tang, X. & Zheng, B. A PDMS viscometer for assaying endoglucanase activity. *The Analyst* **136,** 1222 (2011).
44. Han, Z. & Zheng, B. A poly(dimethylsiloxane) viscometer for microliter power law fluids. *Journal of Micromechanics and Microengineering* **19,** 115005 (2009).
45. Sato, Y., Sato, K., Hosokawa, K. & Maeda, M. Surface plasmon resonance imaging on a microchip for detection of DNA-modified gold nanoparticles deposited onto the surface in a non-cross-linking configuration. *Analytical Biochemistry* **355,** 125–131 (2006).
46. He, S. *et al.* Design of a gold nanoprobe for rapid and portable mercury detection with the naked eye. *Chemical Communications* 4885 (2008). doi:10.1039/b811528a

47. Zhou, X., Lau, L., Lam, W. W. L., Au, S. W. N. & Zheng, B. Nanoliter Dispensing Method by Degassed Poly(dimethylsiloxane) Microchannels and Its Application in Protein Crystallization. *Analytical Chemistry* **79,** 4924–4930 (2007).
48. Kolnik, M., Tsimring, L. S. & Hasty, J. Vacuum-assisted cell loading enables shear-free mammalian microfluidic culture. *Lab on a Chip* **12,** 4732 (2012).
49. Luo, C., Ni, X., Liu, L., Nomura, S. M. & Chen, Y. Degassing-assisted patterning of cell culture surfaces. *Biotechnology and Bioengineering* n/a–n/a (2009). doi:10.1002/bit.22586
50. Li, G., Luo, Y., Chen, Q., Liao, L. & Zhao, J. A 'place n play' modular pump for portable microfluidic applications. *Biomicrofluidics* **6,** 014118 (2012).
51. Dimov, I. K. *et al.* Stand-alone self-powered integrated microfluidic blood analysis system (SIMBAS). *Lab Chip* **11,** 845–850 (2011).
52. Son, J. H. *et al.* Hemolysis-free blood plasma separation. *Lab on a Chip* **14,** 2287 (2014).
53. Liang, D. Y., Tentori, A. M., Dimov, I. K. & Lee, L. P. Systematic characterization of degas-driven flow for poly(dimethylsiloxane) microfluidic devices. *Biomicrofluidics* **5,** 024108 (2011).
54. Nevill, J. T. *et al.* Vacuum soft lithography to direct neuronal polarization. *Soft Matter* **7,** 343 (2011).
55. Jixiao Liu *et al.* Microfluidic Solution Isolated Pumping (uSIP). *uTAS* 17th International Conference on Miniaturized Systems for Chemistry and Life Sciences, Freiburg, Germany (2013).
56. Erh-Chia Yeh & Luke P. Lee. One-Step Digital Plasma Separation for Molecular Diagnostics. *uTAS* 17th International Conference on Miniaturized Systems for Chemistry and Life Sciences 27–31 October 2013, Freiburg, Germany (2013).
57. Bird, R. B., Stewart, Warren E & Lightfoot. *Transport phenomena*. (J. Wiley, 2002).
58. Crank, J. *The mathematics of diffusion*. (Clarendon Press, 1975).
59. Xia, Y. & Whitesides, G. M. SOFT LITHOGRAPHY. *Annual Review of Materials Science* **28,** 153–184 (1998).
60. Vogelstein, B. Digital PCR. *Proceedings of the National Academy of Sciences* **96,** 9236–9241 (1999).
61. Roy, E., Galas, J.-C. & Veres, T. Thermoplastic elastomers for microfluidics: Towards a high-throughput fabrication method of multilayered microfluidic devices. *Lab on a Chip* **11,** 3193 (2011).

Chapter 4. Digital Plasma Separation for One-step Integrated Molecular Diagnostics

Abstract

Simple, portable, and quantitative, on-site nucleic acid detection is crucial for next generation point-of-care diagnostics. However, complex sample preparation and costly/bulky equipment such as real-time PCR machines are required for nucleic acid assays. Herein this report documents the digital plasma separation module, which enables on-site quantitative nucleic acid detection directly from blood in one-step. This design facilitates autonomous sample preparation by removing >90% of blood cells without hemolysis. Automatic compartmentalization of samples (224 micro-wells, 100 nl/well) via vacuum battery pumping enables digital nucleic acid amplification. Quantitative digital isothermal amplification of nucleic acid directly from human blood mixed with reagents was possible in one-step (10~10^5 copies DNA/µl, via recombinase polymerase amplification, ~30 min). Integration of amplification initiator pre-patterning, pumping, and plasma separation resulted in a portable, low cost diagnostic chip (iMDx) that can perform quantitative nucleic acid detection directly from blood samples.

Introduction

Next generation point-of-care medical diagnostic assays would ideally be low cost, portable, simple, fast, and capable of quantitative nucleic acid detection. Current commercially available lateral flow assays (e.g. pregnancy test strips) have many of these traits, but typically they are neither quantitative nor capable of nucleic acid amplification, providing only positive or negative readouts. Nucleic acid based detection is superior in sensitivity and selectivity than immunoassays. However, real-time PCR, the current standard, is not suited for low cost field-testing. This is because it typically involves expensive and bulky thermal cyclers that require external power sources, several hours of assay time, multiple manual sample preparation steps, or trained technicians. The key problems for on-site nucleic acid tests are (1) lack of integrated sample preparation mechanisms, (2) lack of low cost quantification methods, and (3) lack of robust portable pumping systems that can allow complex microfluidic actuation without external equipment/power sources.

New state-of-art commercial real-time PCR[1] machines (e.g. GeneXpert, Cepheid) have shown robotic automation for sample preparation, solving problem (1). However these systems still remain costly, have long assay times, and require external power sources, leaving problem (2) unsolved. On the other hand, new nucleic acid amplification technologies, such as isothermal amplification[1] and digital PCR[2], can help solve problem (2). Isothermal amplification does not require a thermal cycler because all amplification processes are performed via isothermal enzyme reactions, thus simplifying the equipment requirements. Digital

amplification's advantage is that it utilizes end-point detection, so no real time imaging equipment is necessary. It is also much more robust[3] than PCR, as environmental variations in temperature, kinetics, time, and imaging have less effect on end-point quantification. Digital amplification works by compartmentalizing one sample into many individual miniature PCR reactions and amplifying. Then, by counting the endpoint number of positive compartments fluorescing, one can determine the original template concentration. Previously, sample compartmentalization for digital amplification has been conducted via droplet microfluidics[4], or microfluidic wells[5–7]; however these techniques mentioned above do not address problem (1) as they do not integrate on-chip sample preparation.

Addressing problem (1) in the context of working with whole blood samples presents many obstacles. Newer polymerases such as the isothermal recombinase polymerase can amplify nucleic acid directly in complex solutions such as blood plasma[8], thus traditional phase separation or spin column purification can be bypassed. However, the protocol for blood cell removal must not cause hemolysis in the sample. Hemolyzed red blood cells releases hemoglobin, which can disrupt ion concentration via chelation, and inhibit polymerase activity[9]. Also, the opaqueness of blood cells also interferes with optical readout. Standard techniques for blood cell removal such as centrifugation are difficult to miniaturize. Other membrane or mechanical filter[10] methods are popular, but they often clog or cause hemolysis. Other microfluidic methods[11] that utilize hydrodynamic lift force, Zweifach-Fung effect[12], acoustics, or inertia forces require external power sources, pumps, or peripheral control systems. Sedimentation methods[13–16] have also been shown, however, there has yet to be examples that addresses problems (1), (2), and (3) together.

The "Integrated Molecular Diagnostics Chip (iMDx)" is presented in this work. It is designed to address problems (1), (2), and (3) simultaneously. Two novel technologies enable low cost, portable, point-of-care digital nucleic amplification directly from blood in one-step. First, the "Digital Plasma Separation" design facilitates blood cell removal and simultaneous sample compartmentalization for digital amplification. Second, the "Vacuum Battery System" (described in detail in **Chapter 3**), enables significantly more reliable and controlled flow compared to previous degas pumping technology, while retaining key benefits including clear optics and dead-end loading. In one step, it is possible for end-point quantitative digital detection of nucleic acid directly from human whole blood samples in ~30 minutes with the chip via isothermal Recombinase Polymerase Amplification (RPA). This chip is robust and requires no special technical skill. No extra peripheral equipment/power sources are needed for portable pumping. This is one of the unique examples for next generation nucleic acid testing; it demonstrates a very valuable platform technology for future point-of-care medical diagnostic devices.

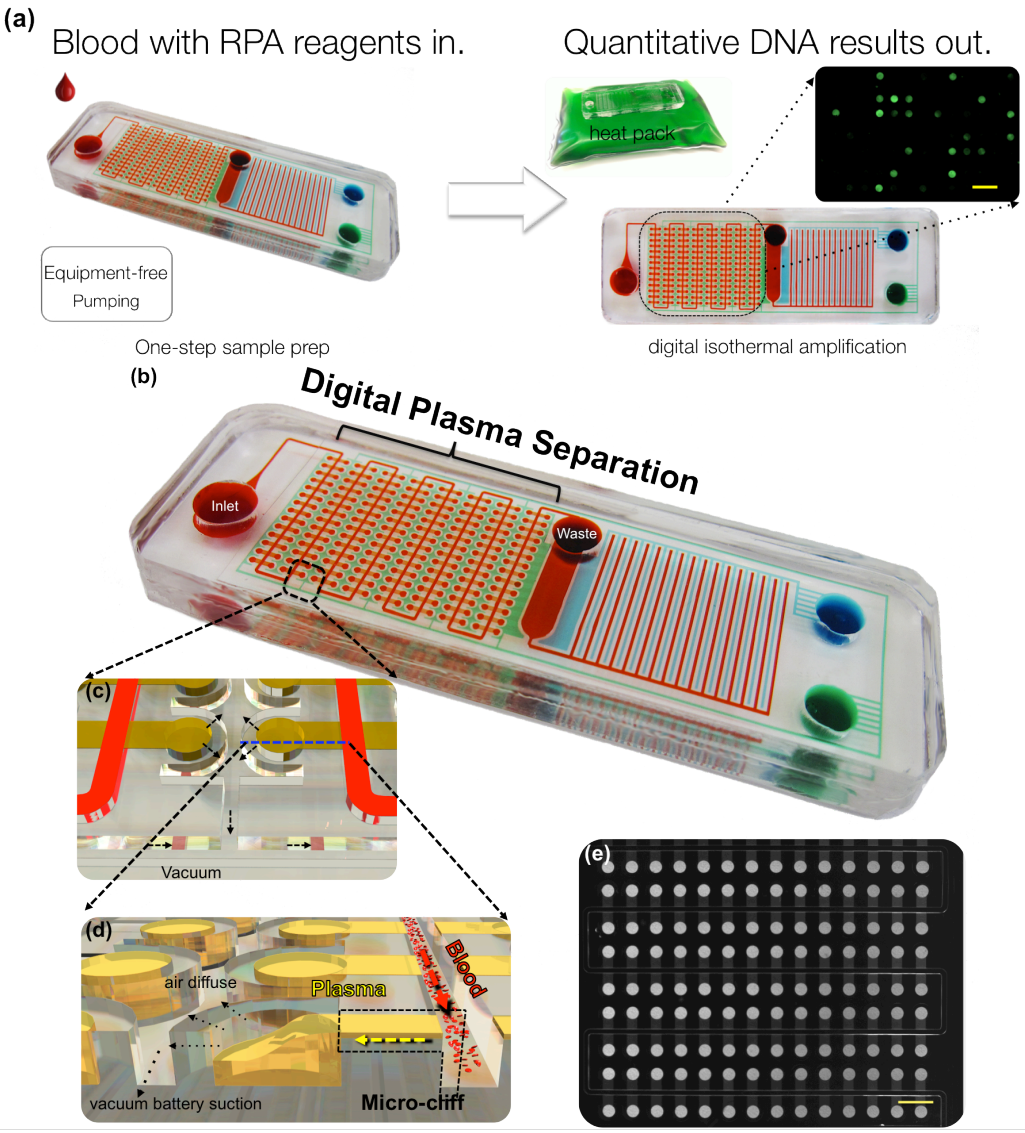

Figure 1 The Digital Plasma Separation design on the Integrated Molecular Diagnostics (iMDx) chip for low cost, quantitative, and portable nucleic acid testing. **(a)** The simple operation protocol requires minimal handling and no external pumps or power sources. Users simply drop blood mixed with amplification reagents into the inlet, then automatic plasma separation and sample compartmentalization is performed, the chip is then incubated on a reusable heat pack, and end-point isothermal digital amplification of nucleic acid is done. Left side shows a chip filled with dye. Right side shows result of digital amplification of 10^3 copies of Methicillin-Resistant Staphylococcus Aureus (MRSA) DNA directly from human blood using isothermal recombinase polymerase amplification (RPA). Scale bar =2 mm. **(b)** Schematic of the silicone (polydimethylsiloxane) microfluidic chip that was characterized in this study. **(c)** Top view of auxiliary vacuum lines to assist well loading. **(d)** Side view of the digital plasma separation design that removes blood cells via sedimentation, and skims plasma into dead-end wells for digital amplification. **(e)** Shows the result of compartmentalized microwells. Scale bar= 2mm.

Methods

Fabrication of microfluidic chips

The chips tested were fabricated using the standard soft lithography[17] process. Briefly, the bottom 3mm PDMS fluidic layer was made by casting PDMS on a silicon wafer that had protruding microfluidic channels created by photo-patterned (OAI Series 200 Aligner) SU-8 photoresist (Microchem). The main fluid and vacuum channels were 300 μm high. Heights of 40, 120, 170, 240, and 300 μm were made for the microcliff gap. The waste reservoir was punched by a 5mm punch (Harris Uni-Core, Ted Pella).

The vacuum battery void was fabricated by simply punching the bottom 3 mm PDMS fluidic layer with through holes. Different diameters of punchers (Harris Uni-Core, Ted Pella) were used to fabricate desired vacuum battery volumes. A separate top blank piece of 3mm PDMS was bonded on the top side to seal the fluidic layer by oxygen plasma bonding by a reactive ion etching machine (PETS Reactive Ion Etcher, at 100W, 120 mtorr O_2, 15 s). All chips were made the same size (25x75 mm), which is the same footprint as a standard microscope glass slide. For the RPA experiments, the blank chips were patterned with MgOAc, and passivated the microfluidic surfaces with an anti-biofouling surface treatment so non-specific adsorption of protein/DNA would be minimum. The patterning and passivation method will be described in a subsequent publication. Finally, transparent pressure sensitive adhesives (MH 90880, Adhesive Research) were taped on both the bottom and top surface of the chip to prevent excess gas diffusion and seal off the vacuum battery voids. New chips were used for each experiment.

Master mold replication

To increase the device assembly throughput, the master silicon mold was replicated by casting urethane plastic (Smooth-Cast 327, Smooth-on, Inc.) over the molded PDMS devices placed in square petri dishes. A thin layer of release agent (Ease Release, Smooth-on Inc.) was applied to the surface of the petri dishes to prevent urethane from sticking. The PDMS devices and urethane resin were degassed before casting, so no air bubbles would be trapped. The first hour of curing was done at 4°C to lower viscosity and slow curing of the urethane resin thus further avoiding air bubbles. Afterwards, the resin was left to cure at room temperature overnight and removed from the petri dishes. PDMS was poured into the hardened urethane molds to make devices.

Vacuum charging and storage

The devices were incubated at -95 kPa for 24 hours in a vacuum chamber before liquid loading experiments. The devices could be sealed in aluminium vacuum packs by a vacuum sealer (V-402, Van der Stahl Scientific) if long-term storage was necessary.

Quantification

All fluorescent images and bright field images of zoomed in regions were taken with a macroscope (Axiozoom Ems3/SyCoP3, AxioCamMR3 camera, Zeiss) at 7~20X zoom (PlanNeoFluar Z1.0x objective, Zeiss). The 38HE green fluorescence and 63HE red fluorescence filters (Zeiss) were used for visualizing fluorescein, FAM, Toto-1, and Cellmask orange dyes. The bit depth was 12 bit, images were 692x520 pixels (2,2, binning mode). Acquisition of images and zoomed videos were done with Zen (v.2012, Zeiss) software. Imaging was done at room temperature. The NIH imageJ and Zen software were used to quantify the fluorescence intensities, normalize contrast, crop images, and merge channels. Time-lapse videos of the entire chip loading were acquired using the TimeLapse app (xyster.net LLC) using an iPhone 5 (Apple).

Statistical analysis

For experimental data, sample sizes are noted in the corresponding figure legends. Experiments were repeated in the lab at least three times. All experimental data are shown as means, and error bars denote plus minus one standard deviation. Replicates represent technical replicates. The Shapiro-Wilk test for normality testing was used to verify that the data was normally distributed. For **Figure 6**, Pearson Correlation = 0.99, Sig<0.01, two tailed test of significance was used, n=6. For **Figure 18b**, P<0.05, power= 0.999, two tailed t-test. Statistical analysis was done using OriginPro (version 9.0, OriginLab).

Digital plasma separation

For the experiments in **Figure 5 and 6**, the main channel flow rate was kept at 5 µl/min by a syringe pump (NE-1600, New Era Pump Systems Inc.), the flow rate into the wells was precisely controlled by tuning the vacuum strength to the auxiliary battery, a schematic of the setup and correlation of flow rate vs auxiliary battery pressure can be found in **Figure 2**. DNA was fluorescently dyed green (Toto-1 Iodide, Invitrogen), by mixing DNA (10^{13} copies/ µl, MRSA) with 400X Toto-1 (diluted in 3.5 X TBE) at a ratio of 1:50, and then incubated for 1 hour at 55 °C. Human whole blood (HMWBACD, Bioreclaimation) was fluorescently dyed orange (Cellmask orange C10045, Invitrogen), by mixing 2X Cellmask dye (diluted in 3.5X TBE) into human whole blood (4:9 ratio), and incubated at 37 °C for 20 minutes. The dyed blood was centrifuged 5 times (1300 rcf, 5 mins); the supernatant was removed each time and replaced with fresh 3.5X TBE buffer. Finally the stained DNA was added to the stained blood to make a final mixture that had 20% blood. This mixture was loaded into the iMDx chip and the separation efficiency was quantified. Separation efficiency was calculated as 1-(blood intensity in well-background intensity)/(blood intensity in main channel-backgorund intensity). For data in **Figure 6**, 5 chips that had different microcliff gaps (40,120,170,240,300 µm) were used. Images were

taken via a fluorescence macroscope (Axiozoom, Ziess).

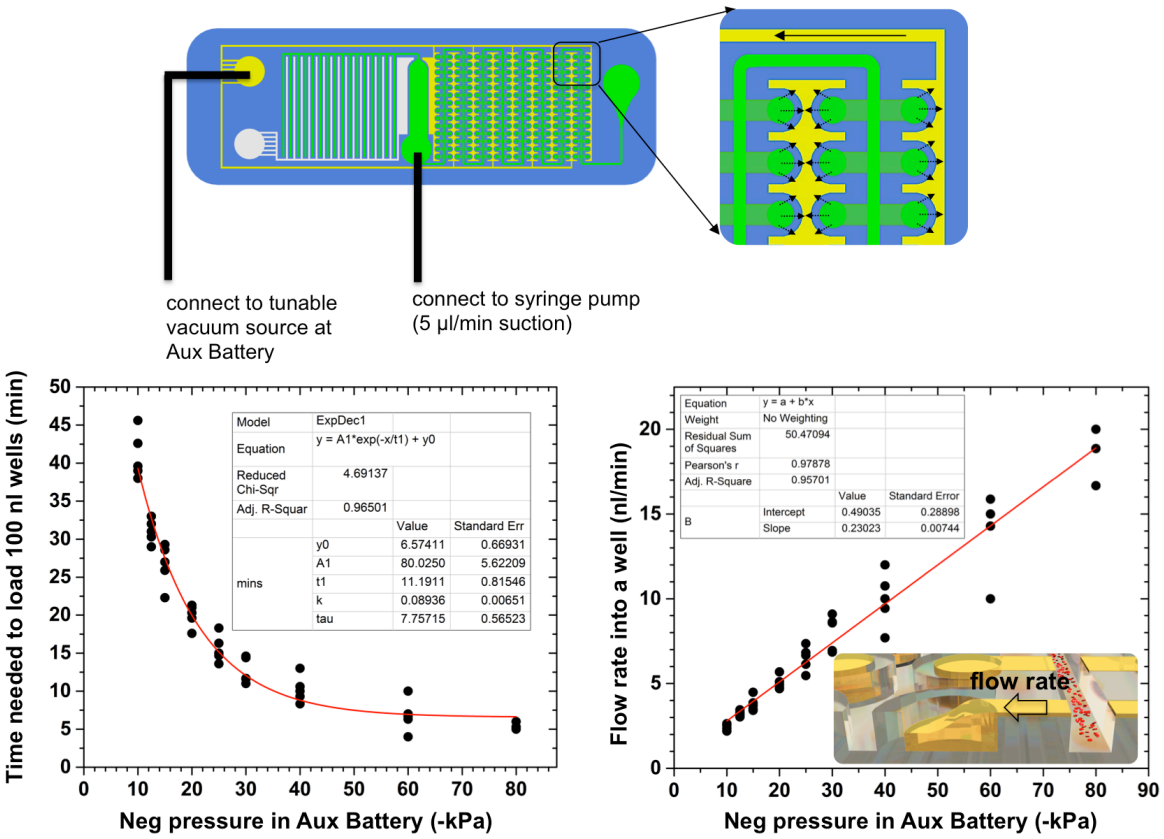

Figure 2 Gradual tuning of microwell filling speed is possible by varying vacuum strength. This was the experimental setup for data sets involved with controlled flow rates across microcliff gaps. A vacuum source was directly connected to the auxiliary battery, applying variable vacuum pressure to characterize the effect on microwell filling speed. Flow through the main channel was kept constant using a syringe pump. Black dots denote experimental results. Red curve denotes fitting results. n=5.

Hemolysis test

For the ultrasound treated control, a blood sample (20% human whole blood in PBS) was lysed with 120 W 40 Hz ultrasound (GB-2500B, Greenultrsonic) for 90 minutes. This was then loaded into the chip. For the centrifuge control, the same blood sample was centrifuged for 10 minutes at 1300 RCF. Plasma supernatant extracted therefrom was loaded into the chip. For the digital plasma separation control, the same blood sample was dropped directly into the chips. All chips were of the 40 μm microcliff gap, 16 lung pair, 100 μl vacuum battery design and incubated at -95 kpa vacuum for 24 hrs before the test. The absorbance inside a microwell was measured with a spectrometer (USB 2000, Ocean Optics) mounted to a microscope (BX51, Olympus) at 50x zoom. The background was normalized to a chip loaded with only PBS.

Isothermal digital amplification

All DNA (MRSA) detection experiments were done with the RPA EXO kit (Twistdx, UK). RNA (HIV-1) experiments were done with the RPA RT EXO kit. Sequences for primers, FAM probes, and the template can be found in **Table 1**. These sequences were designed according to the original RPA publication[18] and ordered through Biosearch Technologies and Integrated DNA Technologies. Magnesium acetate was pre-patterned into the wells (described in **Chapter 2**).

For the reaction time experiment (**Fig. 18b**) with HIV-RNA, 10 μl of human whole blood (HMWBACD, Bioreclaimation) was mixed with a RPA mix (RPA RT-EXO enzyme pellet, 40 μl of primer/probe mix at 10 μM, 59 μl of rehydration buffer, 2 μl of 10%BSA, 8 μl of RNAsin, and 2 μl of spiked HIV-1 RNA at $2*10^5$ copies/μl). 100μl of blood/RPA mix was added into each chip and incubated at 40°C while fluorescent time-lapse images were taken with a macroscope (Axiozoom, Zeiss). n=5.

For the DNA quantification experiments (**Fig. 18c**), 2.5 μl of human whole blood was mixed with a RPA mix (RPA EXO enzyme pellet, 1.6μl of primer/probe mix at 100 uM, 59μl of rehydration buffer, 2μl of 10%BSA, 35μl of water, and 2.5μl of spiked MRSA DNA at desired concentration). 100μl of blood/RPA mix was added into each chip and incubated at 40°C on instant heat packs (HotSnapz) for 1 hour, then endpoint fluorescent images were taken with a macroscope. Contrast of images were enhanced using the auto-contrast algorithm in the Zeiss Zen software, and positively fluorescent wells above the baseline threshold were counted. n≥3.

Table 1 Primer, probe, and target sequences used for recombines polymerase amplification. Primers and target sequence ordered from Integrated DNA Technologies.

MRSA Forward primer (sccI/II)	**CTCAAAGCTAGAACTTTGCTTCACTATAAGTATTC**
MRSA Reverse Primer (orfX)	**CCCAAGGGCAAAGCGACTTTGTATTCGTCATTGG CGGATCAAACG**
MRSA II Probe sequence	**TGTTAATTGAACAAGTGTACAGAGCATT-T(FAM)-A-dSpacer-GA-T(BHQ-1)-TATGCGTGGAG** (ordered from Biosearch Technologies)
MRSA II target sequence	TTTAGTTGCAGAAAGAATTTT**CTCAAAGCTAGAACTTTGCTTCACTATAAGTATTC**AGTATAAAGAATATTTC GCTATTATTTACTTGAAATGAAAGACTGCGGAGGCT AACTATGTCAAAAATCATGAACCTCATTACTTATGATA AGCTTCTTAAAAACATAACAGCAATTCACATAAACCT CATATGTTCTGATACATTCAAAATCCCTTTATGAAGC GGCTGAAAAAACCGCATCATTTATGATATGCTT***CTC CACGCATAATCTTAAATGCTCTGTACACTTGTTCAA TTAACA***CAACCCGCATCATTTGATGTGGGAATGTCA TTTTGCTGAATGATAGTGCGTAGTTACTGCGTTGTA AGACGTCCTTGTGCAGGC**CGTTTGATCCGCCAATG ACGAATACAAAGTCGCTTTGCCCTTGGG**TCATGCG
HIV primers and probes	provided by Twistdx, probes are FAM probes for the RPA RT-exo kit.
HIV RNA	Seracare, 500405, Purified RNA, HIV-1 Group M, Subtype B

Results

The simple user protocol is shown in **Figure 1a**. The chip has a simple construction of two slabs of polydimethylsiloxane (PDMS). With a small footprint similar to glass slides (25x75 mm), this device can be stored indefinitely and transported easily in airtight aluminium vacuum seals.

Digital Plasma Separation design and mechanism

The Digital Plasma Separation sample preparation platform is designed specifically for (1) autonomous plasma separation and (2) autonomous sample compartmentalization for digital amplification (**Fig. 3**).

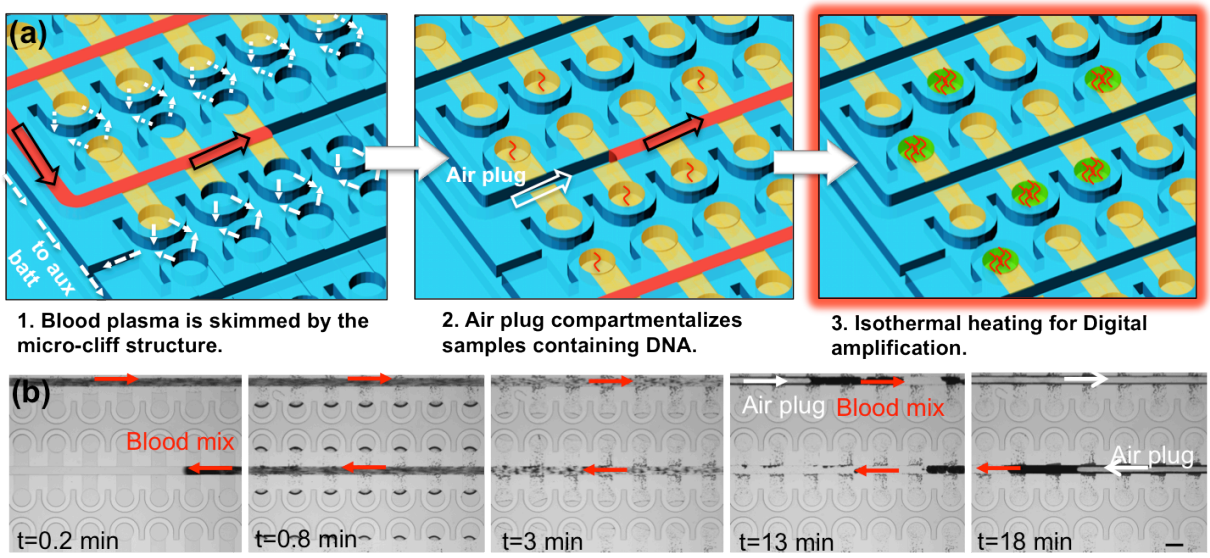

Figure 3 One-step autonomous sample preparation with the digital plasma separation design. **(a)** This design enables simultaneous plasma separation and sample compartmentalization for digital isothermal amplification. White dashed arrows depict air diffusion across the permeable silicone into the vacuum battery, driving the flow. Red S shaped lines in wells depicts target nucleic acid to be amplified with isotheral amplification. **(b)** Shows actual blood samples (mixed with RPA reagents) being separated into microwells. Blood cells are opaque and plasma is transparent in the wells.

Hemolysis free plasma separation by the micro-cliff structure

A novel "microcliff" structure facilitates plasma separation into the wells by taking advantage of blood cell sedimentation. The microcliff skims plasma near the top of the microchannel into the wells. Through Navier–Stokes equations[19], the flow field was computed. Thereafter, the particle trajectories were simulated by computing the gravity force and Stokes drag[20] that the blood cells experience. The resulting particle trajectories are plotted in **Figure 4**. Separating the blood cells ensured minimal optical obstruction of the fluorescence signal, and avoided polymerase inhibition from hemoglobin in red blood cells. Samples mixed with RPA reagents are compartmentalized automatically into the micro-wells. The micro-wells are pre-patterned with magnesium acetate, which initiates the RPA reaction when reconstituted. Next generation microfluidic pumping with the "vacuum battery system", described below, drives the microfluidic flow.

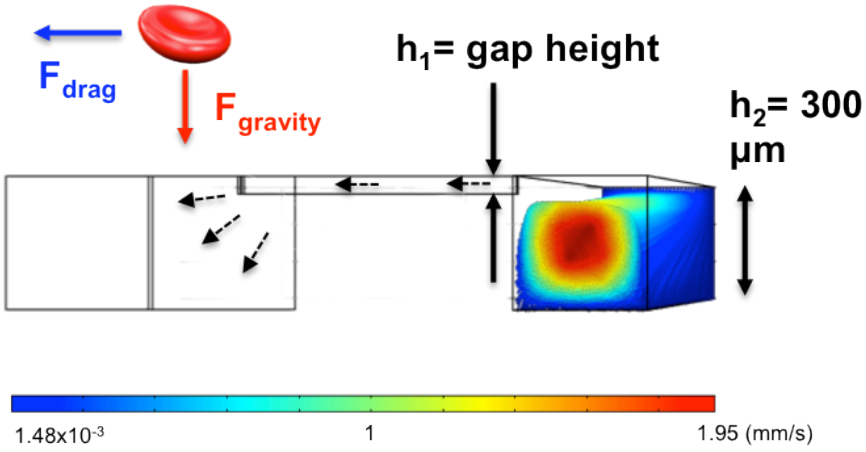

Supplementary Figure 4 Simulation of blood cell trajectories. Simulations were performed with COMSOL software. Flow is coming out perpendicular to this page. This figure shows plasma separation with a 40 µm microcliff gap, the top part of plasma is skimmed into the wells, while the blood cells sediments in the main channel. The main channel flow direction is towards the reader.

Simulation of particle trajectories

The COMSOL Multiphysics software was used to simulate the flow profile and particle trajectories. The first step was to simulate the fluid flow through the microfluidic device. The flow can be described with the Navier-Stokes equations. Equation (1) is a vector equation representing conservation of momentum:

$$\rho\frac{\partial\vec{u}}{\partial t}+\rho(\vec{u}\cdot\nabla)\vec{u}=\nabla\cdot[-pI+\tau]+F \qquad (1)$$

Where $\vec{u}$ is the velocity vector (m/s), ρ is the density of fluid (kg/m^3), p is the pressure (Pa), τ is the viscous stress tensor (Pa), and F is the volume force vector (N/m^3). Equation (2) is the continuity equation and describes conservation of mass:

$$\frac{\partial \vec{\rho}}{\partial t} + \nabla \cdot (\rho \vec{u}) = 0 \tag{2}$$

Assuming incompressible flow and steady state laminar flow (Reynolds number <1), no-slip boundary conditions were applied to the walls. The single-phase laminar flow module in COMSOL simulated the flow field, assuming that blood was diluted into PBS (20%), and ρ= 1004 kg/m^3.

Next, the flow field results were used to simulate the particle trajectories using the Particle Tracing for Fluid Flow module. The forces that the blood cells experience are drag and gravity forces. The total force experienced on each particle is the sum of drag forces and gravity forces:

$$\vec{F}_{total} = \vec{F}_{drag} + \vec{F}_{gravity} \tag{3}$$

The drag force on the blood cells can is governed by the following equation:

$$\vec{F}_{drag} = \frac{1}{\tau_p} m_p (\vec{u} - \vec{v}) \tag{4}$$

Where m_p is the particle mass (kg), τ_p is the particle velocity response time (s), $\vec{u}$ is the fluid velocity derived from the flow results (m/s), and $\vec{v}$ is the velocity of the particle (m/s). For simplicity, blood cells were approximated as spheres, and were assumed to experience Stokes drag, since the Reynolds number <1). Therefore, using Stoke's drag law:

$$\tau_p = \frac{\rho_p d_p^2}{18\mu} \tag{5}$$

Where ρ_p is the particle density (1125 kg/m^3), d_p is the diameter (6 μm), and μ is the dynamic viscosity (0.0016 Pa*s). Gravity forces on the blood cells can be described with the following equation:

$$\vec{F}_g = m_p \vec{g} \frac{(\rho_p - \rho)}{\rho_p} \tag{6}$$

Where g is the gravitational constant. Gravitation force is the main force that causes the blood cells sedimentation and allow for plasma skimming on the top edges of the main channels. Finally, the particle momentum can be described with Newton's second law, the rate of change of its momentum is equal to the net force the particle experiences:

$$\frac{d}{dt}(m_p \vec{v}) = \vec{F}_{drag} + \vec{F}_{gravity} \tag{7}$$

Using these equations, and the previously simulated flow field, the particle trajectories were simulated in a time dependent model. This simulation was set to release particles at the inlet simultaneously at a given time point.

Microcliffs for efficient, zero clogging, and hemolysis-free blood cell removal

Results show that the microcliff design drastically reduces blood cell entry into the wells and no clogging is observed (**Fig. 5**). More than 95% of blood cells can be removed, and separation efficiency increases when the h_1 microcliff gap or flow rate across cliff is reduced (**Fig. 6**). The parametric simulation result is shown in dashed lines and agrees well with experimental results. Increased concentration of blood cells in the microwells of the "without cliff" control was observed; this phenomenon is possibly due to inertial effects. The best separation efficiency is achieved with the 40 μm gap microcliff. There is no red blood cell hemolysis observed; the on-chip separated plasma showed indistinguishable quality from centrifuged plasma when absorbance was measured (**Fig. 7**). When blood cells enter the wells, the fluorescence signal from dyed DNA can be obstructed significantly (**Fig. 8**). Smaller microcliff gaps also make the separation efficiency much more consistent across the chip spatially (**Fig. 9**). This platform can separate blood cells while retaining biomarkers, as selective particle separation is possible according to size. Particles larger than 1 μm are separated and particles less than 100 nm are retained in the wells (**Fig. 10**). Plasma separation can be done within 12 minutes, with a total volume of ~22 μl plasma (**Fig. 11**).

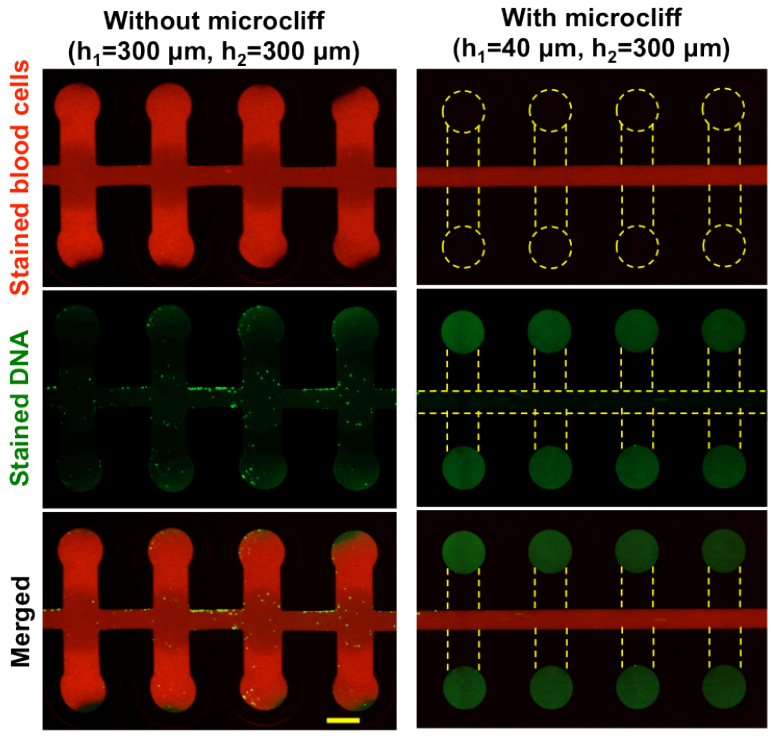

Figure 5 Fluorescence images of plasma separation of human blood mixed with stained DNA. Blood cells tend to obscure DNA readout if it is not separated. Contrast normalized. Scale bar=500 μm.

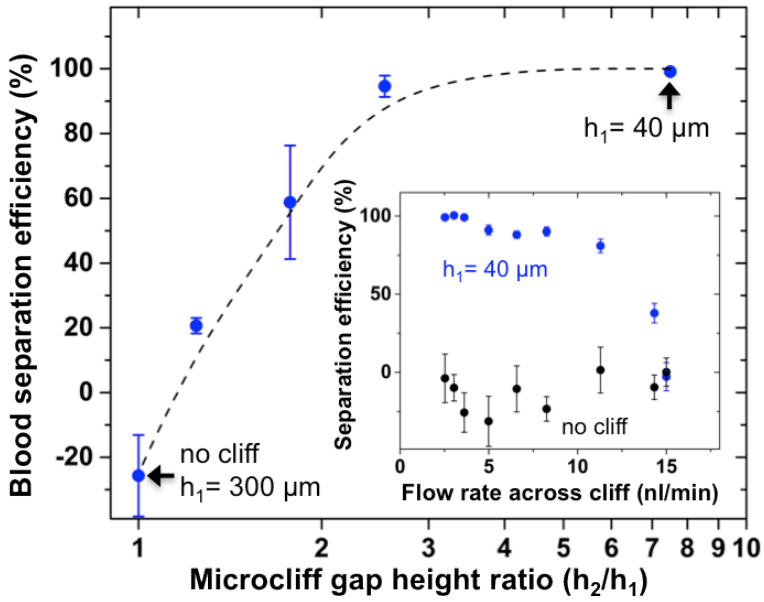

Figure 6 Smaller microcliff gaps and lower flow speed can remove >95% of blood cells. Dashed lines are simulation results. Solid dots show experimental results. (mean ± s.d., Pearson Corr= 0.99, $p<0.01$, two tail t-test, n=6).

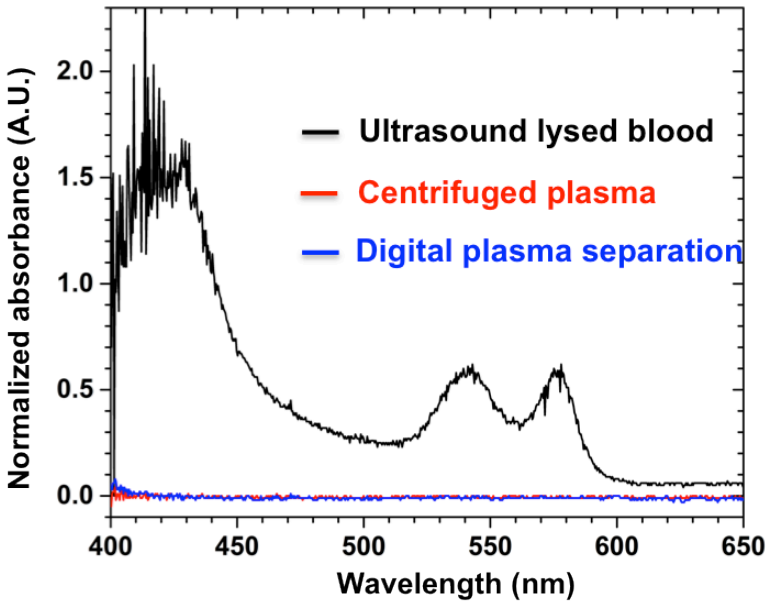

Figure 7 No hemolysis was observed using this design. Three chips were loaded separately with whole blood samples, ultrasound lysed blood, and plasma from centrifuged blood. Absorbance spectrum was taken from microwells in each set.

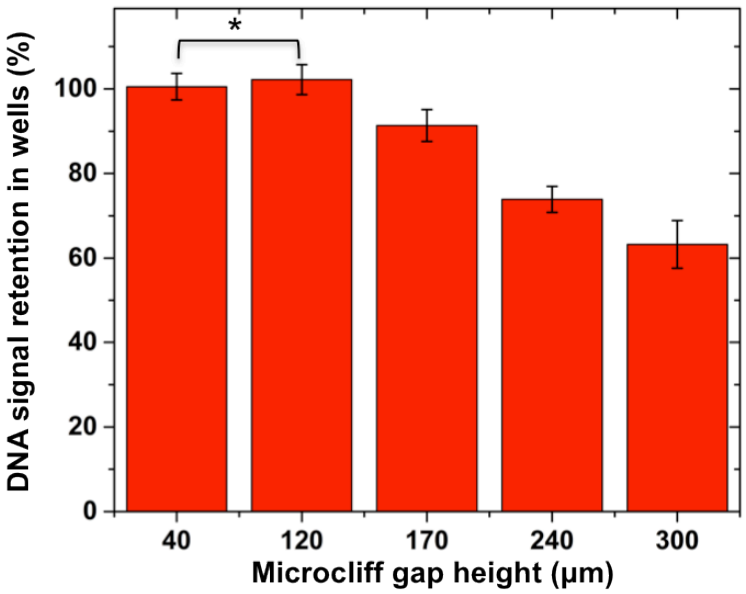

Figure 8 DNA signal is obstructed when blood cells are not removed. The quantitative results show that smaller microcliff gaps can retain higher DNA signal because of better blood cell separation. Flow rate across microcliff was kept at 3 nl/min. Flow rate in the main channel was 5 μl/min. (mean ± s.d., *not significantly different, all other pairs were significantly different with $p<0.05$, one-way ANOVA Sidakholm test, n=6)

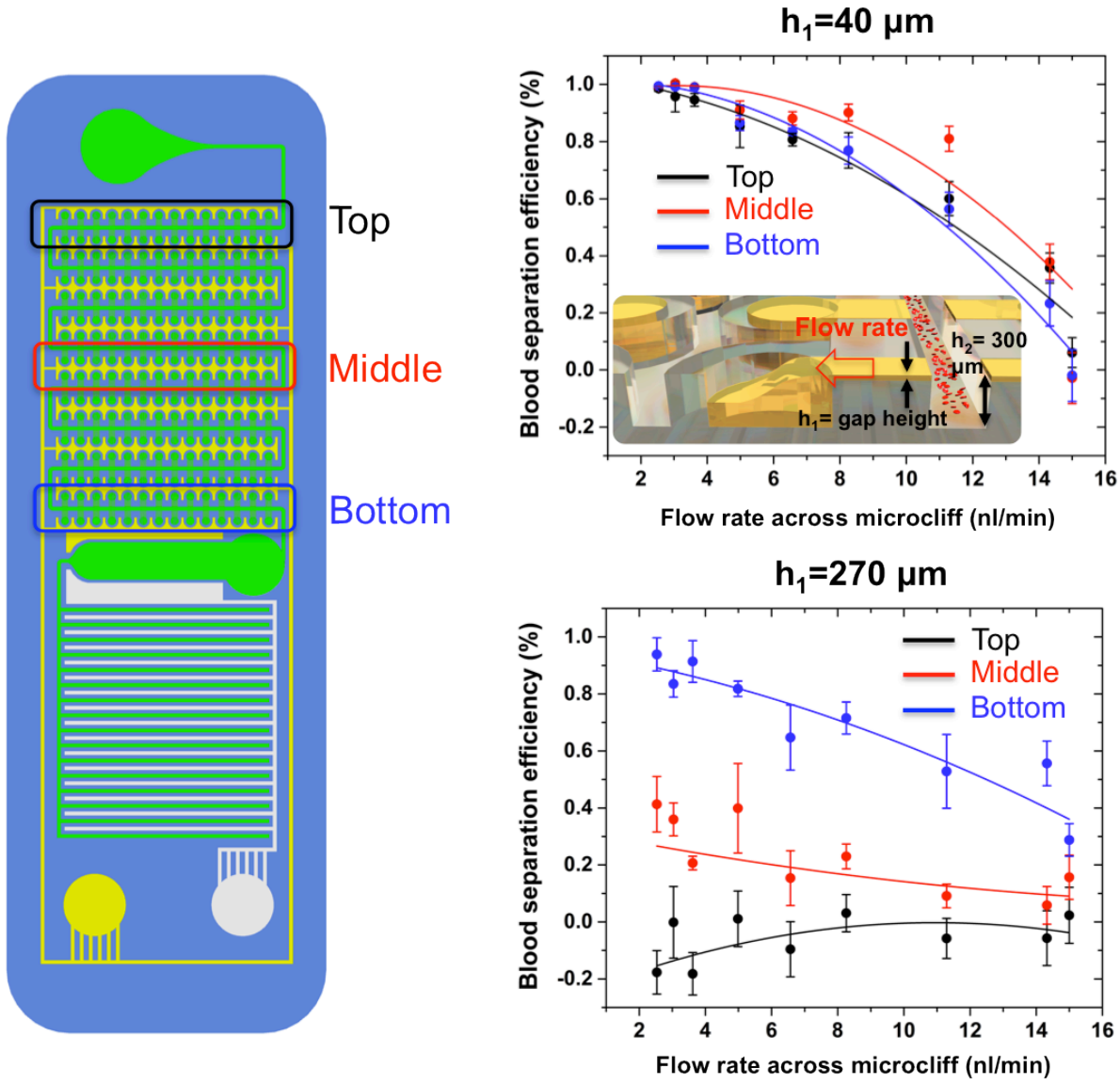

Figure 9 Smaller microcliff gap designs have much more robustness spatially. When the gap size of h_1 increases, the separation efficiency in the top wells near the inlet have very poor blood separation efficiency, this is because the blood cells do not have sufficient time to sediment in the main flow channel and get sucked into the wells. On the other hand, there is much less variation among top, middle, and bottom well separation efficiencies with a smaller microcliff gap design. (mean ± s.d., n=6 for all data points).

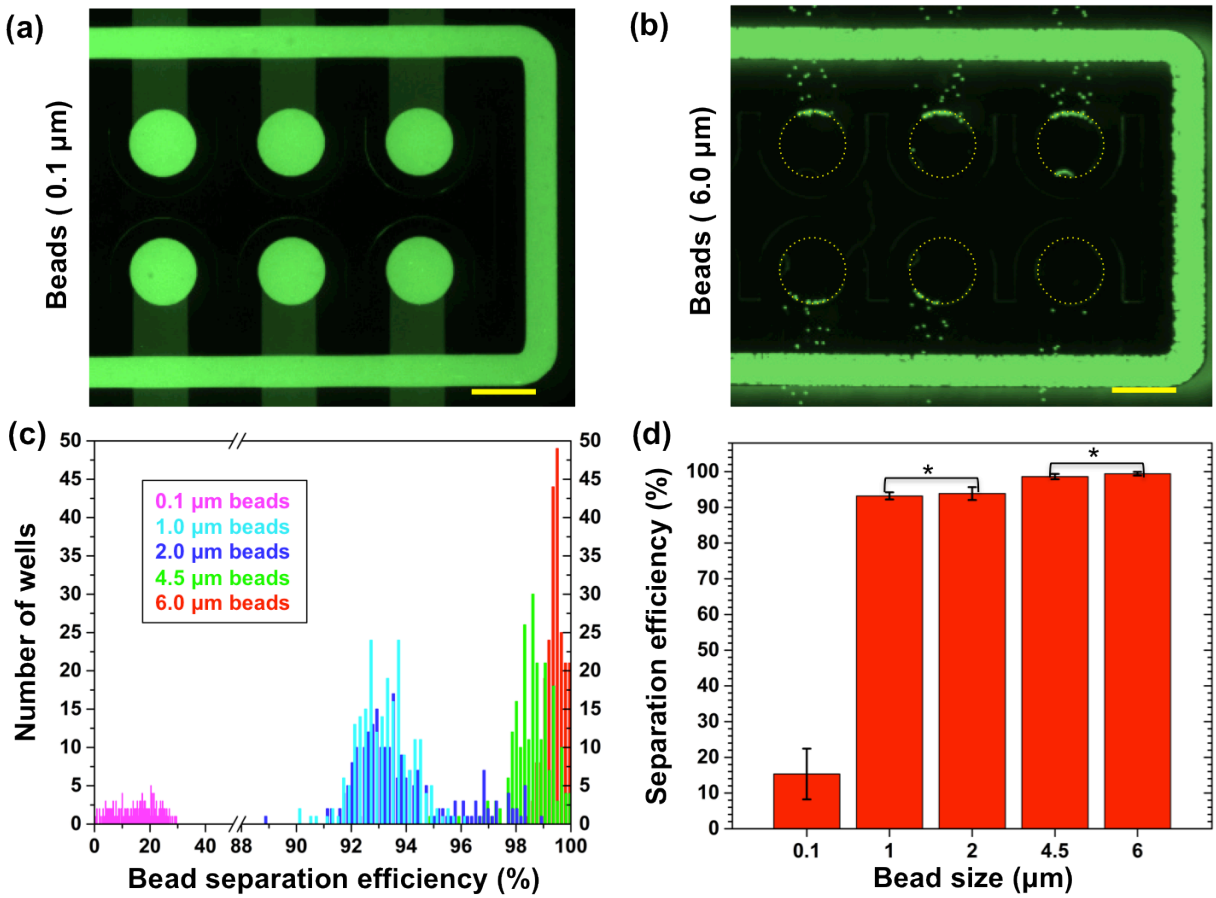

Figure 10 Selective particle separation according to size. The 40 µm micro-cliff gap design was tested to separate different sizes of polystyrene particles. It was found to be capable of separating >99% of 6 µm beads (which are similar size to red blood cells), while retaining >85% of the 0.1 µm beads (which are similar size to some viruses). Beads were polystyrene microspheres diluted in PBS. **(a)** and **(b)** show actual fluorescence pictures of bead separation results. Dashed yellow circles depict where the microwells are located. **(c)** Shows the histogram results and **(d)** shows the mean. Separation efficiency is defined as 1-(intensity in wells-background)/(intensity in main flow channel-background). (mean ± s.d., *not significantly different, all other pairs were significantly different with each other $p<0.05$, one-way ANOVA Sidakholm test, n=224 for all sets. Scale bar is 650 µm).

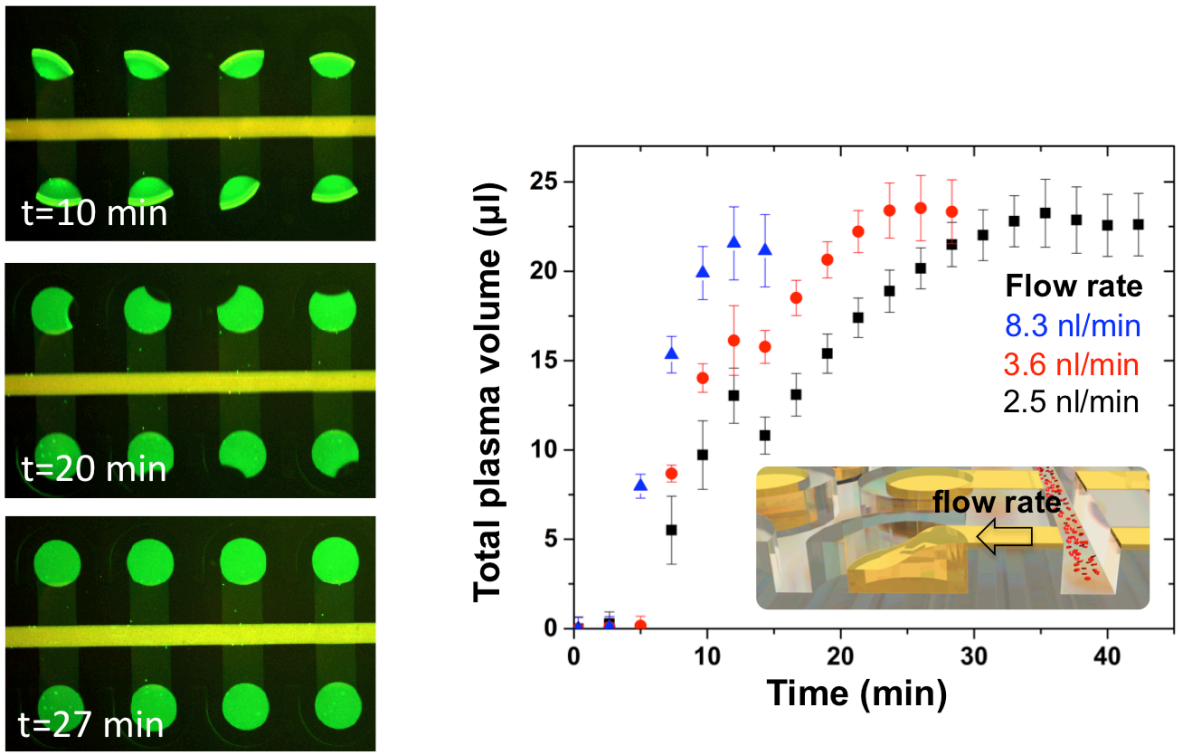

Figure 11 Total plasma volume separated. There are a total of 224 wells, each having a volume of 100 nl, which fills with plasma simultaneously. The flow rate into the wells was varied by controlling the negative pressure applied to the auxiliary vacuum battery. This data was taken from 40 µm microgap iMDx devices. The left figure shows human blood that has been spiked with green stained DNA (Toto-1), and the blood cells has been stained with red (Cell mask), -15 kPa was applied to the auxiliary vacuum battery. Plasma separation could be finished within 12 minutes. (mean ± s.d., n=6)

Integrated plasma separation and compartmentalization for digital amplification

This chip can perform autonomous plasma separation and compartmentalization in one-step (**Fig. 12**). Compartmentalization of samples makes each well an individual reaction and enables digital amplification. After loading, the receding air gap separates each well automatically and the samples are compartmentalized into 224 micro-wells (100 nl/well). Automatic loading is done via the vacuum battery system. Microcliff gaps smaller than 170 µm compartmentalize with 100% success rate (**Fig. 13)**.

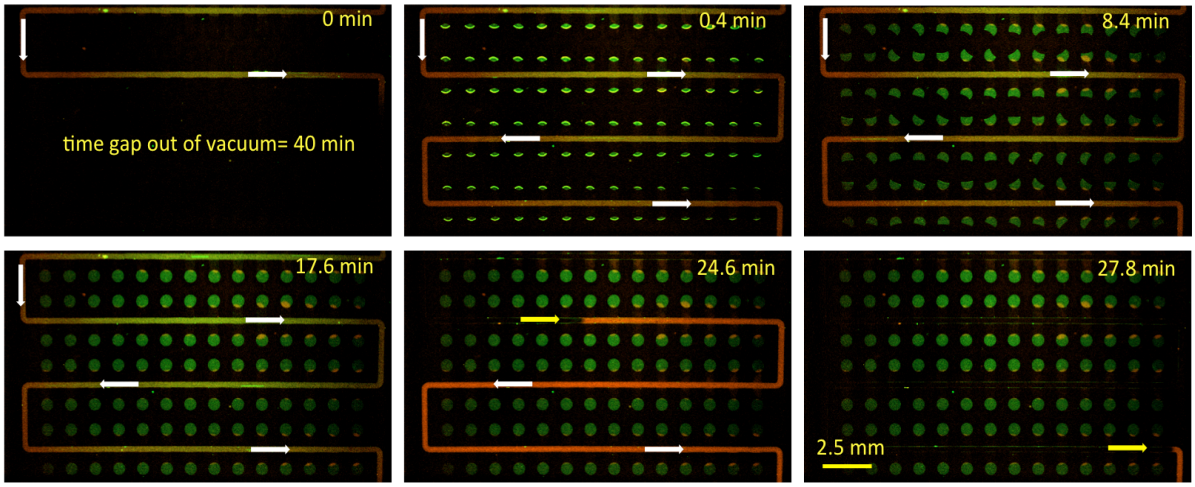

Figure 12 Time lapse of human blood cell separation from spiked Methicillin-Resistant Staphylococcus Aureus (MRSA) DNA without clogging. MRSA DNA was dyed with green fluorescence (Toto-1, LifeTechnologies), and human blood cells were dyed with red fluorescence (Cellmask orange, LifeTechnologies). Images show actual one-step plasma separation, compartmentalization, and retention of biomarkers in an automated manner. The unique design prevents clogging, which is a common problem with membrane filter based techniques. Clogging does not happen, as there are no micro-pore constrictions in any part of the design. Even the smallest microgap structure is much larger than blood cells, having a cross sectional area of 500 x 40 µm (red blood cells are approximately 6 µm in diameter).

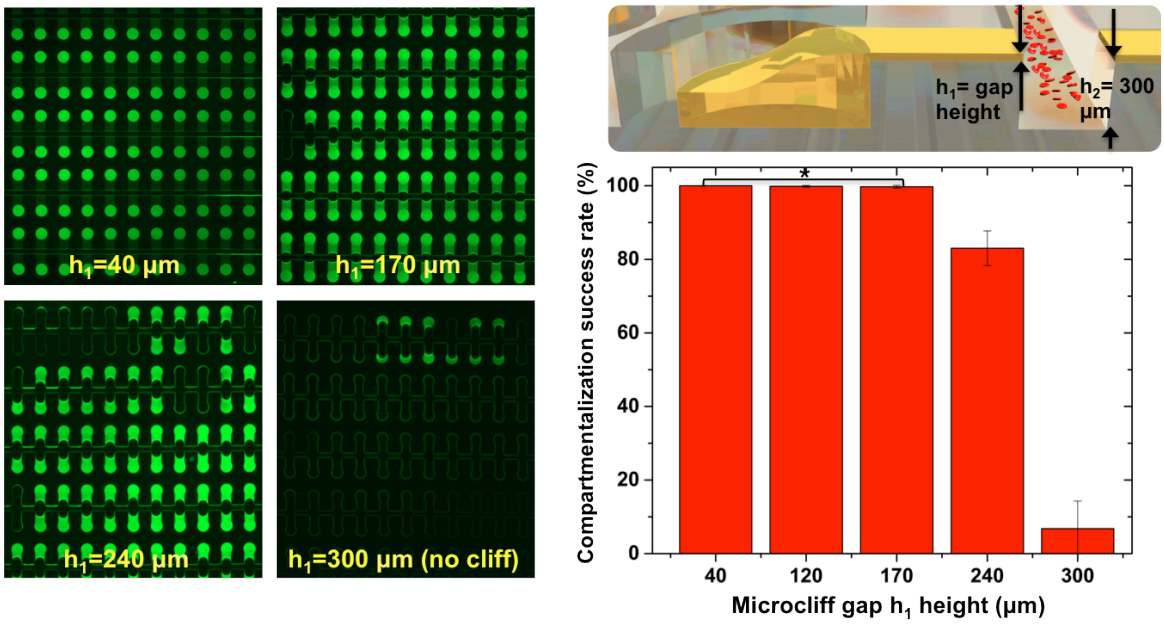

Figure 13 More reliable compartmentalization with smaller microcliff gap designs. Successful compartmentalization is defined as complete filling and retaining of liquids within a microwell after the air gap recedes and separates each well. An aliquot of 110 µl of human blood (20% blood in PBS) spiked with fluorescein was loaded into chips with different microcliff gap heights (h_1). (mean ± s.d., *not significantly different (40, 120, and 170 µm), all other pairs were significantly different with each other $p<0.05$, one-way ANOVA Sidakholm test, n=224 for all sets).

The Vacuum Battery System for robust equipment-free portable microfluidic pumping

The vacuum battery system was designed to deliver controlled and complex microfluidic flow without any external equipment or power sources. The basic vacuum battery system includes a "vacuum battery" and "vacuum lung" component with an optional waste reservoir. The "vacuum battery" is simply a punched void volume that stores vacuum potential and is connected to the vacuum lungs. The "vacuum lungs" mimic lung alveoli gas exchange by allowing air to diffuse through thin gas permeable silicone (PDMS) walls into the vacuum battery. More detail on the vacuum battery system is described in **Chapter 3**.

One-step quantitative isothermal digital amplification directly from human whole blood samples

Recombinase Polymerase Amplification[18] (RPA) was chosen because it is much more robust in plasma samples than PCR or Loop Mediated Isothermal Amplification (LAMP) (**Fig. 14**). RPA is also one of the fastest isothermal amplification technologies, and operates at lower temperatures (works at 25°C, ~39°C optimal). Using a fluorophore-quencher molecular probe (TwistAmp® exo Probe) that only fluoresces when amplicons with matched sequence are present minimized the possibility of false-positive signals. A reusable commercial sodium acetate instant heat pack can provide ~40°C heating at the microwells for up to an hour for isothermal amplification (**Fig. 15**). Using Poisson statistics, a simulation of digital amplification sensitivity range according to well size was done (**Fig. 16**). Two hundred twenty-four wells of 100 nl each were chosen, because this size allows a detection range that is physiologically relevant[21].

This research demonstrated quantitative digital nucleic acid detection directly from human blood samples with this chip. The concept and result of digital amplification[2] is shown on in **Figure 18**. It is possible to rapidly detect signals of HIV-1 RNA spiked in human blood ($2*10^5$ copies/µl) within 18 minutes. Quantitative detection of MRSA DNA (Methicillin-Resistant Staphylococcus Aureus) from $10\sim10^5$ copies/µl was possible in water (**Fig. 17**) and also directly from spiked human whole blood (**Fig. 18**).

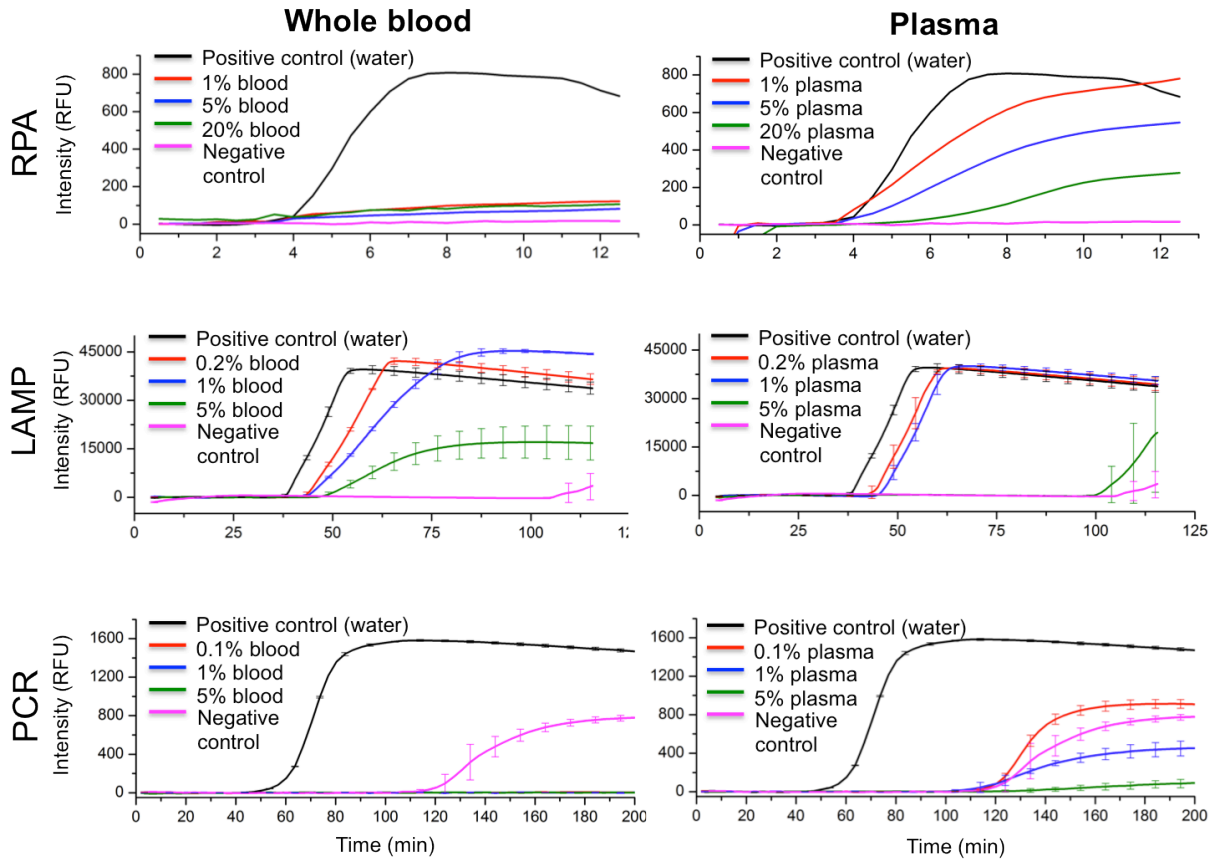

Figure 14 Recombinase polymerase amplification (RPA) is the more robust against plasma samples than loop-mediated isothermal amplification (LAMP) and polymerase chain reaction (PCR), but blood cells need to be removed. Off-chip tests were performed to determine the robustness of each nucleic acid amplification technique. Positive control had templates spiked in water, and negative control had no template spiked in water. The best case was demonstrated by RPA in plasma. Amplification directly from blood was generally very difficult. RPA also showed an extremely fast reaction rate, where the fluorescence signal starts to show up in 4 minutes. In addition, RPA showed much higher tolerance and remained functional at higher plasma concentrations. LAMP was able to amplify in some blood, but only up to 5% and gives false positives. On the other hand, the negative control in RPA never gave false positive signals. Due to these reasons, the decision was to use RPA to demonstrate the utility of the microfluidic plasma separation platform. The RPA-exo kit was used for experiments. Data was collected by a real-time PCR machine (CFX-96, BioRad).

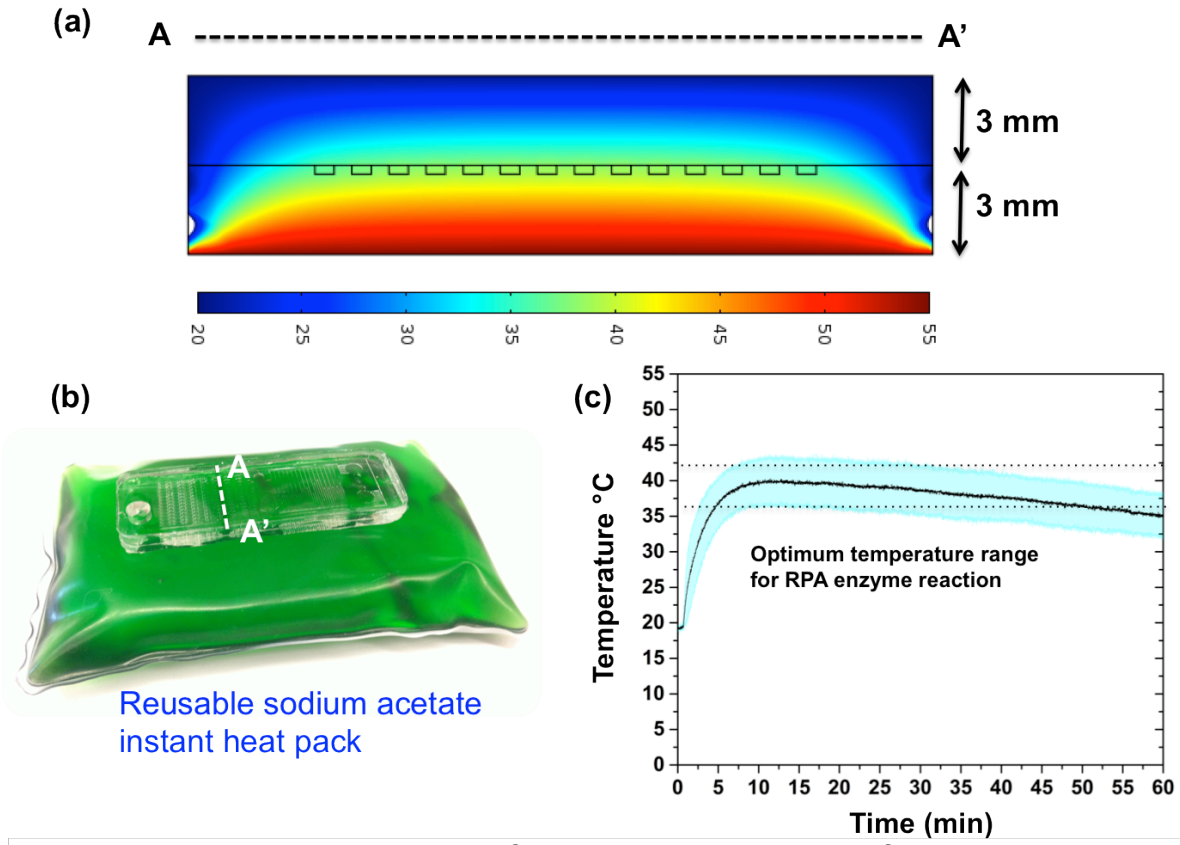

Figure 15 Isothermal heating profile inside the iMDx chip from reusable instant head packs. The chip's thickness (3 mm on both top and bottom PDMS) was optimized to achieve ~40°C heating inside the wells for up to one hour at 25°C ambient temperature. **(a)** Shows the simulated temperature profile inside the chip's cross section. **(b)** A commercial reusable instant heat pack (Hotsnapz, ~$5 each) was used. The sodium acetate heat pack can be reused after soaking in boiling water for ~10 mins. Heating is caused by the exothermic phase change crystallization of super saturated sodium acetate. The digital amplification reactions were run by simply putting the chips onto a heat pack for 20~60mins. **(c)** Temperature measured at the wells in the iMDx chip using a thermal couple. The heat pack was functional for ~1 hr. n=3, mean ± s.d.. At 40°C, this temperature range will also work with other isothermal amplification technologies such as NASBA, SMART, SDA, BAD AMP.

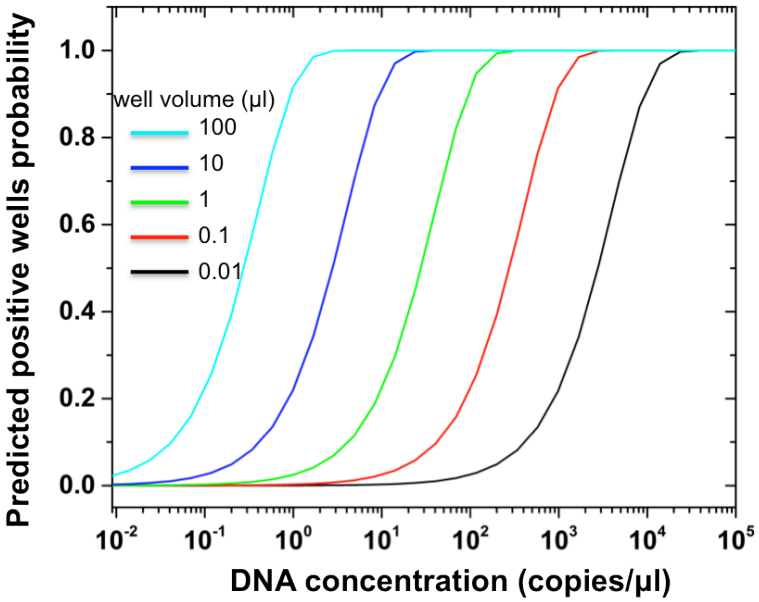

Figure 16 Simulation of the well volume's effect on digital amplification dynamic range. Poisson statistics were used to estimate the effects of well volume on sensitivity. A volume of 0.1 µl per well was chosen because it is able to detect in the range of physiological concentrations of common blood born pathogens (eg. HIV, MRSA). In these calculations, 2.5 µl of samples were assumedly added to a total volume 100 µl reaction mix.

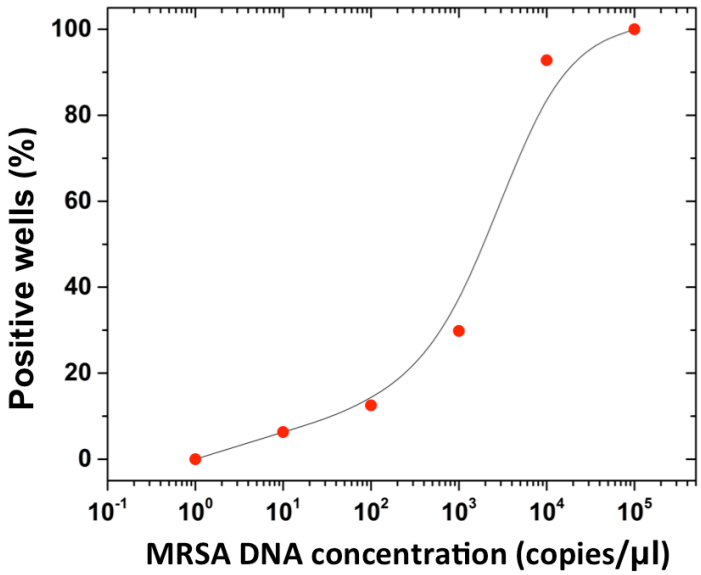

Figure 17 Experimental results of on-chip digital quantitative detection of Methicillin-Resistant Staphylococcus Aureus (MRSA) DNA spiked in water. The same procedures of testing in **Fig. 6c** were followed, except that the matrix was in water rather than human blood. The sensitivity was slightly higher as there was less interference of the plasma components. This shows that the device has potential to be used as a replacement of real-time PCR machines for general quantification of DNA concentration or water quality monitoring applications.

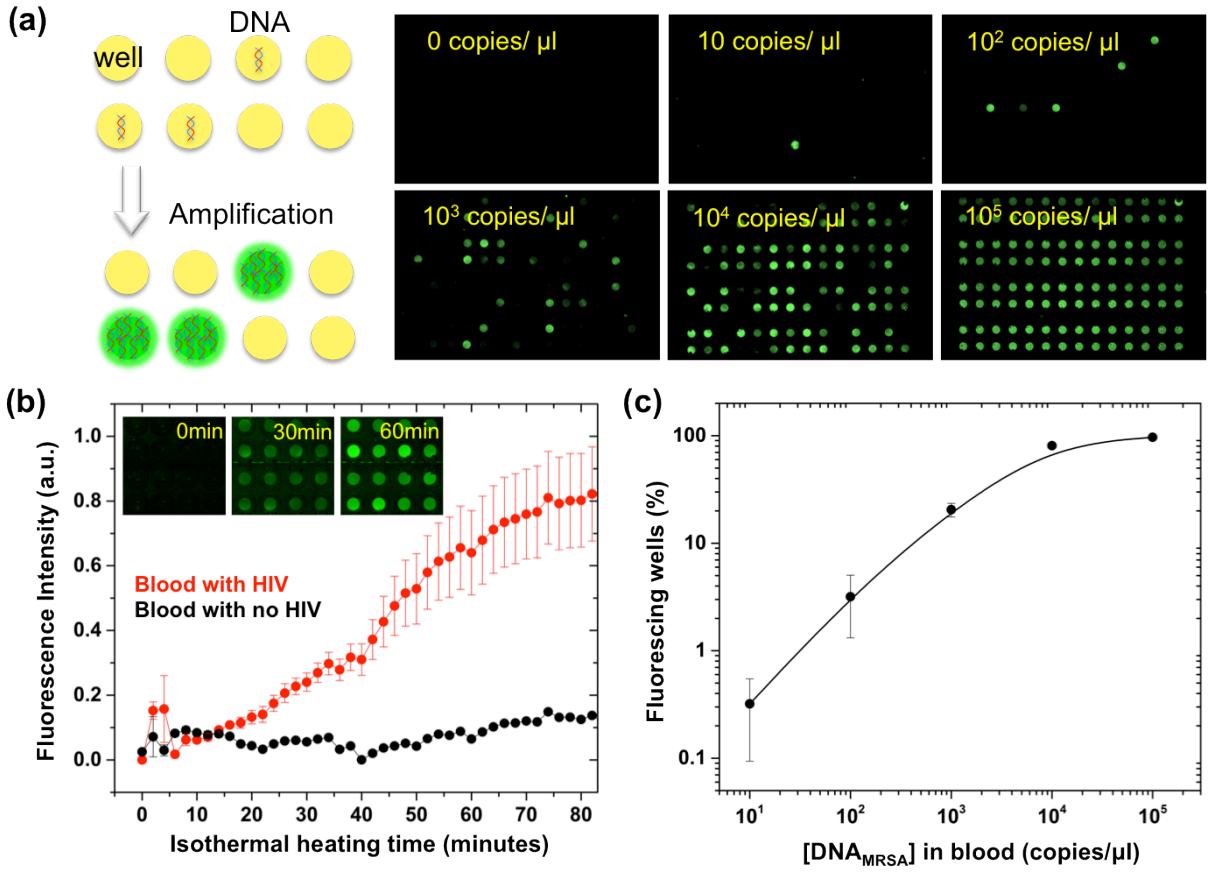

Figure 18 Quantitative digital amplification of nucleic acid directly from human blood. **(a)** Left side shows the concept of digital amplification. Wells that have at least one or more target templates are amplified, while others remain unamplified. One can determine the original template concentration by counting the number of amplified wells. Isothermal nucleic acid amplification was done with recombinase polymerase amplification. Isothermal heating was done via reusable sodium acetate heat packs. Right side shows end-point fluorescent images of reactions with different starting concentration of Methicillin-Resistant Staphylococcus Aureus (MRSA) DNA spiked in human whole blood. **(b)** The average intensity of positive spots increases to a detectable level within 18 minutes (mean ± s.d., $p<0.05$, power= 0.999, two tailed t-test, n=5). In this test HIV-1 RNA spiked in human whole blood. **(c)** Shows the quantification range of the iMDx chip. MRSA DNA was spiked into human whole blood for these tests (mean ± s.d., solid line fitted with B-spline. n=3).

Discussion

The goal was to design a microfluidic chip capable of functioning in low resource settings such as rural villages in third world countries. The assumption was that there would be minimal infrastructure, such as lack of centralized labs, electricity, medical personnel, and funds for costly equipment. Therefore, the design rule was to create a portable diagnostic device that can be operated in one-step, while maintaining complex function and minimum cost. A key goal was to bring forth next generation technology that can substitute real-time PCR for on-site rapid nucleic acid quantification while maintaining the advantages of lateral flows assays such as affordability and portability. The aim was to solve three bottlenecks of nucleic acid amplification assays in one chip, namely problem (1): lack of integrated sample preparation mechanisms, problem (2): lack of low cost quantification methods, and problem (3): lack of robust portable pumping systems that can allow complex microfluidic actuation without external equipment/power sources.

The solution presented here is the iMDx chip, which has the following key merits compared with existing technologies- simplicity and affordability, integrated sample preparation, portable next generation pumping, and fast quantitative nucleic acid readout. Simplicity and affordability: the iMDx chip is designed for one-step operation and no specialized technicians are needed. The disposable chip has a simple two-layer construction, the materials and reagents cost is less than $10, and can be further reduced when mass fabricated. Integrated sample preparation: with the digital plasma separation platform, for the first time the possibility of simultaneously performing automatic plasma separation (>95% blood cell removal, without hemolysis or clogging) and microwell compartmentalization was shown. Portable next generation pumping: the vacuum battery system demonstrates equipment/power-source free complex microfluidic pumping. Robust and tunable loading is possible for up to 2 hrs. Pumping is fully integrated into the small chip (6mm*25mm*75mm), and the chip can be stored in vacuum seals, making the chip highly portable. Also, since this chip is based on highly transparent material (silicone), optical readout is superior compared to fibrous lateral flow assays. Fast quantitative nucleic acid readout: It was possible to detect nucleic acids quantitatively (10~10^5 copies/μl) within 18 minutes in incubation using isothermal digital amplification (RPA), directly from human blood samples. Consequently, the total assay time can be done in ~30 minutes (plasma separation ~10 minutes). This is comparable to bench top PCR machine sensitivity, but at a significantly lower cost and faster readout. A summary of all merits can be found in **Fig. 19**.

For the next step, the goal is to conduct field trials with larger clinical sizes. Another aim is to incorporate microfluidic sample concentration modules to further increase the assay sensitivity. Currently used for imaging is a bench top macroscope. However, the future goal is to develop a simple low-cost portable imaging platform, which can be integrated with smart phones for mobile data acquisition and analysis, thereby making it possible for telemedicine applications.

Conclusion

The iMDx chip not only can provide a solution for low resource settings, but also has potential to be adopted in developed countries for point-of-care diagnostics as well. For example, this chip is aimed for monitoring HIV viral load both in the field and also at home, or it may be used for rapid detection of MRSA infection in hospitals. It is also possible to pattern different primers into the wells and perform multiplexed detection on pathogens that cause similar symptoms such as ebola, dengue, and malaria on the same chip. This chip provides much faster and lower cost on-site quantitative nucleic acid detection compared to bench-top real-time PCR machines. The versatility of this chip will be very beneficial for the development of future point-of-care medical diagnostics.

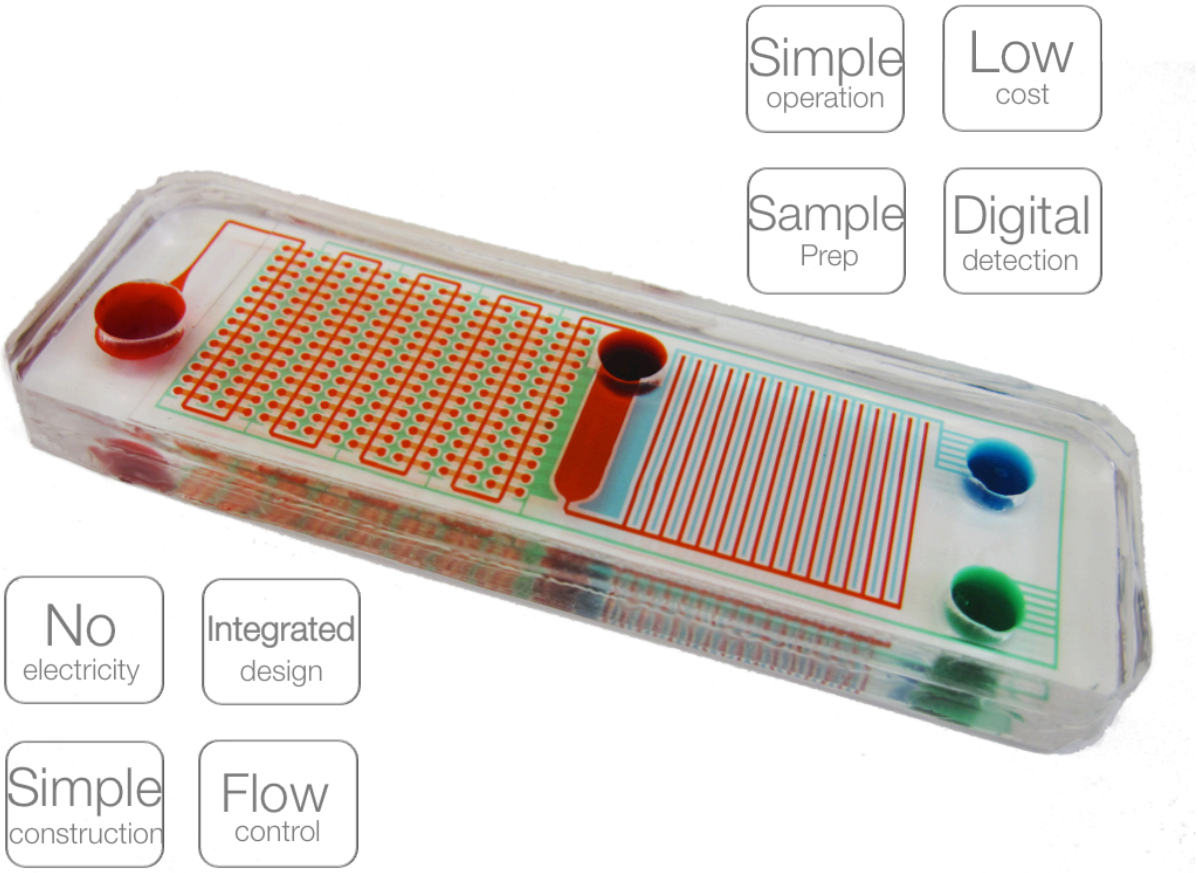

Figure 19 The iMDx chip is designed for low resource point-of-care scenarios. Actual device loaded with food dye to highlight microfluidic channels.

Notes and references

1. Niemz, A., Ferguson, T. M. & Boyle, D. S. Point-of-care nucleic acid testing for infectious diseases. *Trends in Biotechnology* **29,** 240–250 (2011).
2. Vogelstein, B. Digital PCR. *Proceedings of the National Academy of Sciences* **96,** 9236–9241 (1999).
3. Selck, D. A., Karymov, M. A., Sun, B. & Ismagilov, R. F. Increased Robustness of Single-Molecule Counting with Microfluidics, Digital Isothermal Amplification, and a Mobile Phone versus Real-Time Kinetic Measurements. *Analytical Chemistry* **85,** 11129–11136 (2013).
4. Day, E., Dear, P. H. & McCaughan, F. Digital PCR strategies in the development and analysis of molecular biomarkers for personalized medicine. *Methods* **59,** 101–107 (2013).
5. Shen, F. *et al.* Digital Isothermal Quantification of Nucleic Acids via Simultaneous Chemical Initiation of Recombinase Polymerase Amplification Reactions on SlipChip. *Analytical Chemistry* 110408160603036 (2011). doi:10.1021/ac200247e
6. Gansen, A., Herrick, A. M., Dimov, I. K., Lee, L. P. & Chiu, D. T. Digital LAMP in a sample self-digitization (SD) chip. *Lab on a Chip* **12,** 2247 (2012).
7. Zhu, Q. *et al.* Self-priming compartmentalization digital LAMP for point-of-care. *Lab on a Chip* (2012). doi:10.1039/c2lc40774d
8. Kersting, S., Rausch, V., Bier, F. & Von Nickisch-Rosenegk, M. Rapid detection of Plasmodium falciparum with isothermal recombinase polymerase amplification and lateral flow analysis. *Malaria Journal* **13,** 99 (2014).
9. Al-Soud, W. A. & Radstrom, P. Purification and Characterization of PCR-Inhibitory Components in Blood Cells. *Journal of Clinical Microbiology* **39,** 485–493 (2001).
10. Li, C., Liu, C., Xu, Z. & Li, J. A power-free deposited microbead plug-based microfluidic chip for whole-blood immunoassay. *Microfluidics and Nanofluidics* **12,** 829–834 (2011).
11. Kersaudy-Kerhoas, M. & Sollier, E. Micro-scale blood plasma separation: from acoustophoresis to egg-beaters. *Lab on a Chip* (2013). doi:10.1039/c3lc50432h
12. Fan, R. *et al.* Integrated barcode chips for rapid, multiplexed analysis of proteins in microliter quantities of blood. *Nature Biotechnology* **26,** 1373–1378 (2008).
13. Tachi, T., Kaji, N., Tokeshi, M. & Baba, Y. Simultaneous Separation, Metering, and Dilution of Plasma from Human Whole Blood in a Microfluidic System. *Analytical Chemistry* **81,** 3194–3198 (2009).
14. Sun, M., Khan, Z. S. & Vanapalli, S. A. Blood plasma separation in a long two-phase plug flowing through disposable tubing. *Lab on a Chip* **12,** 5225 (2012).
15. Zhang, X.-B. *et al.* Gravitational Sedimentation Induced Blood Delamination for Continuous Plasma Separation on a Microfluidics Chip. *Analytical Chemistry* **84,** 3780–3786 (2012).
16. Dimov, I. K. *et al.* Stand-alone self-powered integrated microfluidic blood analysis system (SIMBAS). *Lab Chip* **11,** 845–850 (2011).

17. Xia, Y. & Whitesides, G. M. SOFT LITHOGRAPHY. *Annual Review of Materials Science* **28,** 153–184 (1998).
18. Piepenburg, O., Williams, C. H., Stemple, D. L. & Armes, N. A. DNA Detection Using Recombination Proteins. *PLoS Biology* **4,** e204 (2006).
19. Batchelor, G. K. *An introduction to fluid dynamics*. (Cambridge University Press, 1999). at <http://search.ebscohost.com/login.aspx?direct=true&scope=site&db=nlebk&db=nlabk&AN=511005>
20. Kirby, B. *Micro- and nanoscale fluid mechanics: transport in microfluidic devices*. (2013).
21. Kreutz, J. E. *et al.* Theoretical Design and Analysis of Multivolume Digital Assays with Wide Dynamic Range Validated Experimentally with Microfluidic Digital PCR. *Analytical Chemistry* **83,** 8158–8168 (2011).

Chapter 5. Conclusions and Future Direction

Proposed future research direction

Existing technologies for molecular diagnostics, including those associated with lateral flow assays, real time PCR, and ELISA are impractical for use in remote and low-resource settings. These assays are prohibitively expensive, slow, and difficult to perform, while providing inadequate singelplex results. The proposal is for the development of the Integrated Molecular Diagnostics System 2.0 (iMDx 2.0), a next generation platform capable of performing multiplexed nucleic acid quantification, protein detection, and $CD4^+$ T cell counting. The plan is to build a portable, low-cost system based on the expertise in microfluidics, biomolecular analysis, and optics. This system will provide a cornerstone example of integration of upstream sample collection and downstream quantitative analysis with a manufacturable sample preparation module. The vision for a simplified user workflow is shown in **(Fig. 1**). This system provides a number of key advances over competing technologies (**Table.1**). The hope is to work towards demonstrating an integrated system that can provide end-to-end blood based diagnostics from sample collection to signal readout. Focus the initial efforts on diseases such as malaria, HIV, or dengue, the system was designed according to the Gates Foundation's target product profile specifications. It is envisioned that this system

Table 1 Technology Comparison

	Lateral flow assay	Real time PCR (Genexpert)	ELISA	RPA on Paper*	Future iMDx 2.0 (Berkeley)
Time per assay	10~20min	1~2hr	3~6hr	15 min	10~20min
CLIA waived	yes	yes	no	no	yes
Cost	$5-30/test	~$10/test, $17k/machine	$40-70/test, $300-1000/kit	$4.5/test	<$5/test, less than $200/reader
Quantitative nucleic acid detection	no	yes	no	no	yes
Quantitative protein detection	no	no	yes	no	yes
$CD4^+$T cell count	no	no	no	no	yes
Power requirement	no	electrical outlet with UPS	electrical outlet	no	battery
Portability	yes	no	no	yes	yes
Telemedicene	no	possible	no	no	yes

will accelerate a paradigm shift in the future of quantitative medicine in remote and low-resource settings.

***Reference:** Rohrman, B. A. & Richards-Kortum, R. R. A paper and plastic device for performing recombinase polymerase amplification of HIV DNA. *Lab on a Chip* **12,** 3082 (2012).

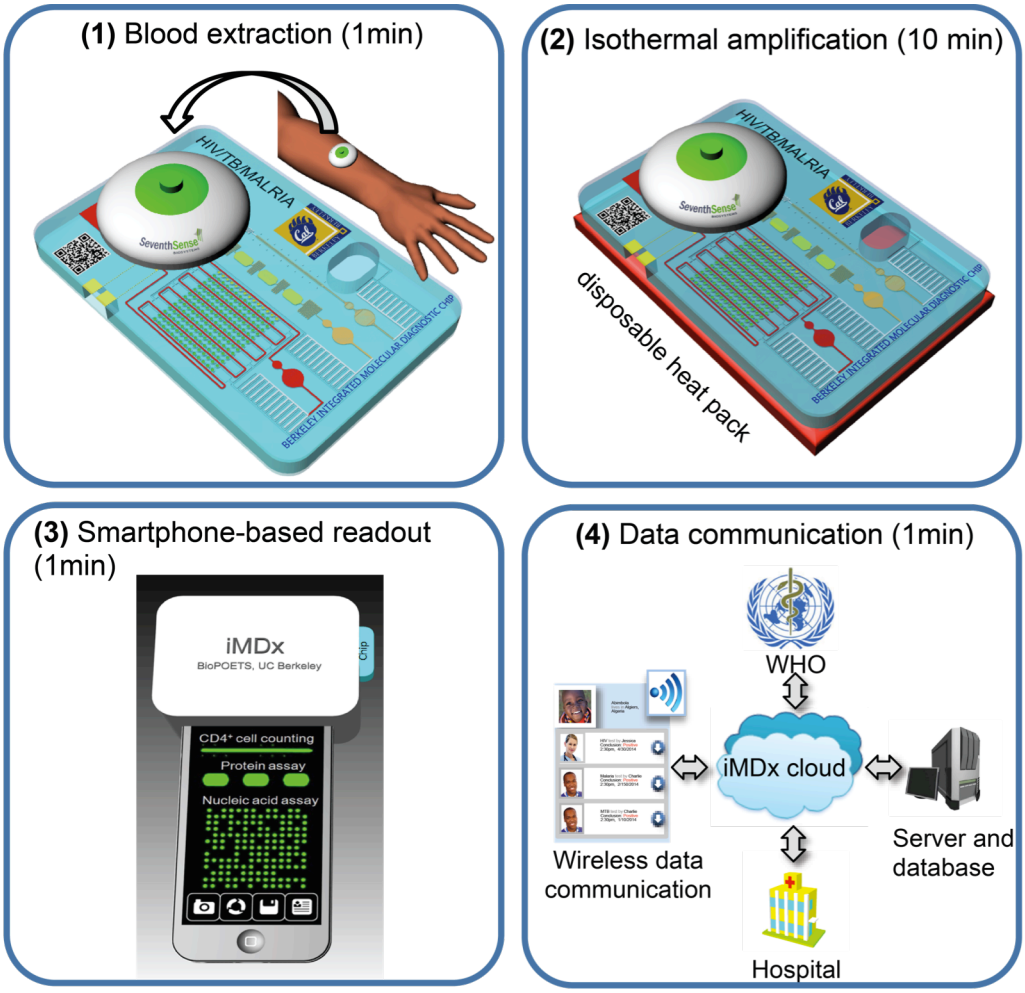

Figure. 1 Proposed Integrated Molecular Diagnostics (iMDx 2.0) System Work Flow. **(1)** The user collects blood with a seventh sense device and clicks it onto the iMDx 2.0 chip, then automatic sample preparation is initiated. **(2)** Isothermal amplification is used (e.g. RPA) to amplify nucleic acids at 40°C on disposable heat packs. Througput can be very high as incubation can be done in parallel. Protein assays and $CD4^{+}$T cell counts will be also be quantified. Chips for HIV and malaria will be developed using the same platform technology. It may also be adopted to other blood based diseases in the future. **(3)** A smartphone based optical reader will read the fluorescence signal and display the results on a app. **(4)** The app will send data to a cloud to be shared with relevant clinicians.

Future direction 1: Integrate sample preparation module with upstream collection and downstream analysis components

A number of technologies for rapid and selective sample preparation were developed during this PhD. The plan is to introduce a number of advanced technologies to test and complement the sample preparation module. Both upstream sample collection and downstream analytical components will be incorporated into a complete diagnostic prototype (**Fig. 2**). The hope is to partner with Seventh Sense Biosystems for simple and pain-free phlebotomy as a front-end sample introduction module. Further developed assays for nucleic acid and protein analysis that meet the strict target product profile required by the Gates Foundation is necessary. The plan is to develop an integrated platform that leverages upstream and downstream technologies for sample diagnostic applications such as HIV and malaria.

Activity 1.1: Sample collection integration

The expectation is to work together with Seventh Sense Biosystems to standardize the inlet/outlet format, so that Seventh Sense's TAP 100 technology can be integrated seamlessly with these sample preparation technologies. TAP 100 technology is capable of painlessly collecting 100 microliters of whole blood in one step. The blood volume is in the range of iMDx2.0's requirements. The technologies presented here are an ideal strategic match: while Seventh Sense specializes in sample collection, this team specializes in microfluidic-based whole blood sample preparation for nucleic acid and protein-based assays downstream. Integrating this contained sample collection method will allow users to bypass dangerous and painful needle based extraction methods and simplify the blood collection process.

Activity 1.2: Develop HIV viral load quantification module

The wish is to continue these efforts in integrating a HIV viral load chip with the previously reported digital plasma separation platform (**Fig. 3**). The main focus is to test clinical HIV samples with this chip and compare that to benchmark technology such as real-time PCR. On-chip reagent storage and sample lyophilization will have to be addressed to achieve full functionality. The main advantage of this system is the possibility to bypass costly real time thermal cyclers since only an endpoint result is needed. Speed and ease of use is also greatly reduced due to the integration of sample preparation (plasma separation+sample digitization) with digital RPA readout. Previous chapters have shown detection of HIV-RNA in whole blood within 30 minutes. Optimizing these advantages and integrating this module with upstream sample collection and downstream readout modules will be continued.

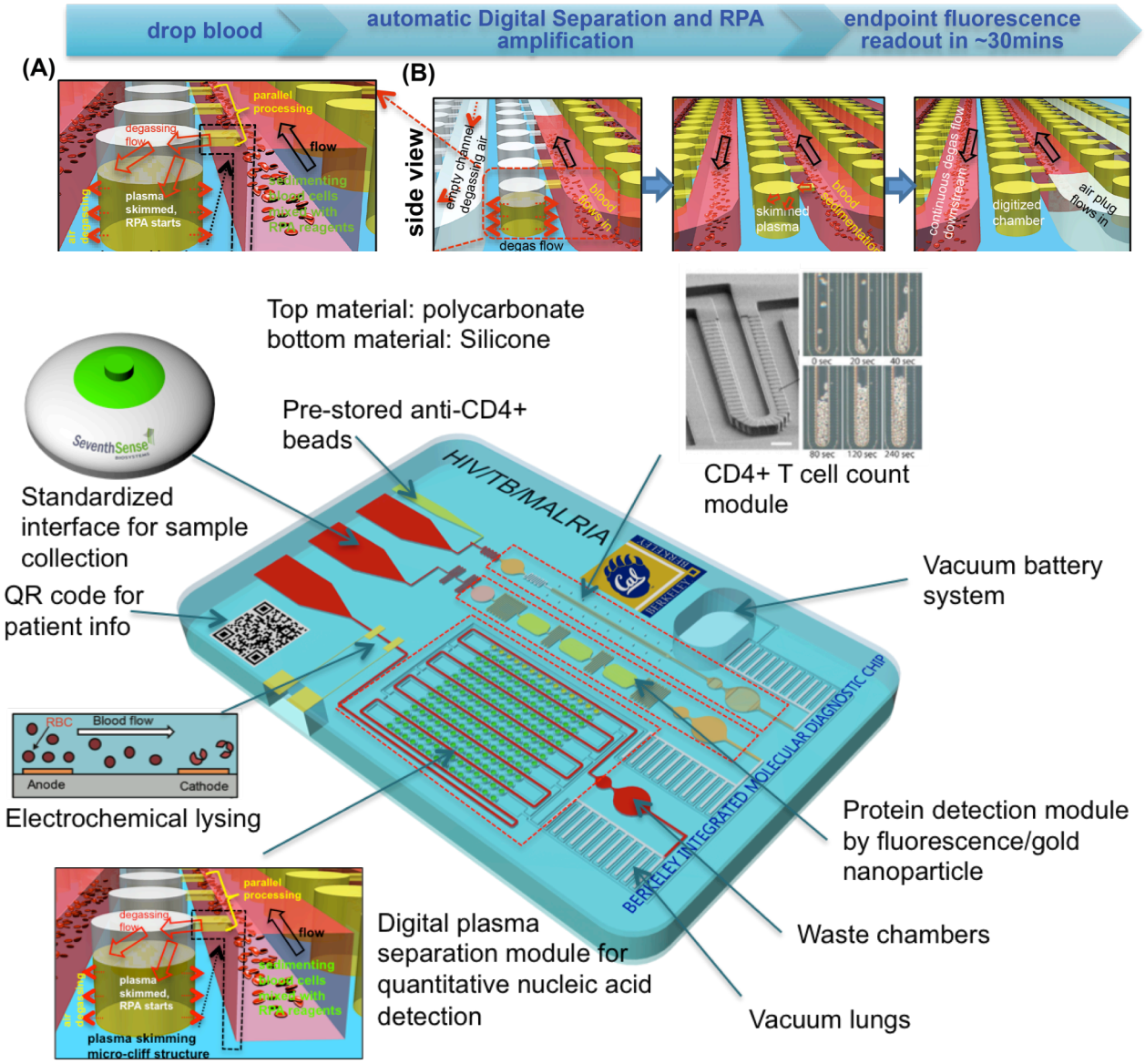

Figure 2 Design of the iMDx 2.0 chip. This chip will be capable of performing quantitative nucleic acid and quantitative protien detection, $CD4^{+}$T cell counting modules will also be included. Fluid flow is actuated by the vacuum battery system. Additional upgrades in function can be integrated easily since the components are designed to be modularized.

Activity 1.3: Develop *$CD4^+$T cell count module*

Another wish is developing a one-step $CD4^+$T cell counting module based on $CD4^+$antibody coated polystyrene bead tagging and cell stacking (**Fig. 4**). The main advance compared to other current methods is that this is designed to perform $CD4^+$T cell counting with minimal manual steps and use minimal optical equipment for quantification. Currently the standard method for $CD4^+$T cell counting is using flow cytometry systems, however, these systems are costly (>$10k), and require bulky equipment. Newer manual hemocytometry techniques (e.g. Beckman Coulter Manual Count kit), use polystyrene bead labeling, which can greatly reduces the cost; however they still require multiple manual steps, a microscope, and extra time for counting cells manually. Taking advantange of the already validated off-chip kits, the process will be automated with microfluidics. Commercial kits such at the Beckman Coulter $CD4^+$T cell count kit will be used to first block $CD11^{+/}CD4^+$ monocytes with 0.5μm anti-$CD11^+$ beads. The 0.5μm beads cannot be resolved under a microscope, but blocks the subsequent anti-$CD4^+$ 2μm bead attachment. After attaching $CD4^+$2μm beads, RBCs will be lysed by acetic acid and the tagged $CD4^+$T cells will be stacked with a mechanical filter structure. $CD4^+$T cells will be stacked due to a ~4μm increase of diameter from the result of bead tagging. A naked eye or simple fluorescence readout can be performed with the proposed reader, eliminating the need of a microscope objective. A single reading of the stacked length will also be much faster than counting all the beads. This lab has already developed similar cell stacking technologies for building artificial livers in other projects. (**Fig. 4, B-D**), a spin out company from this lab, Cellasic, has been created and successfully sold to Millipore based on this technology. It is anticipated that this technology will be adapted smoothly for $CD4^+$T cell counting purposes in the future.

Reference: Lee, P. J., Hung, P. J. & Lee, L. P. An artificial liver sinusoid with a microfluidic endothelial-like barrier for primary hepatocyte culture. *Biotechnology and Bioengineering* **97,** 1340–1346 (2007).

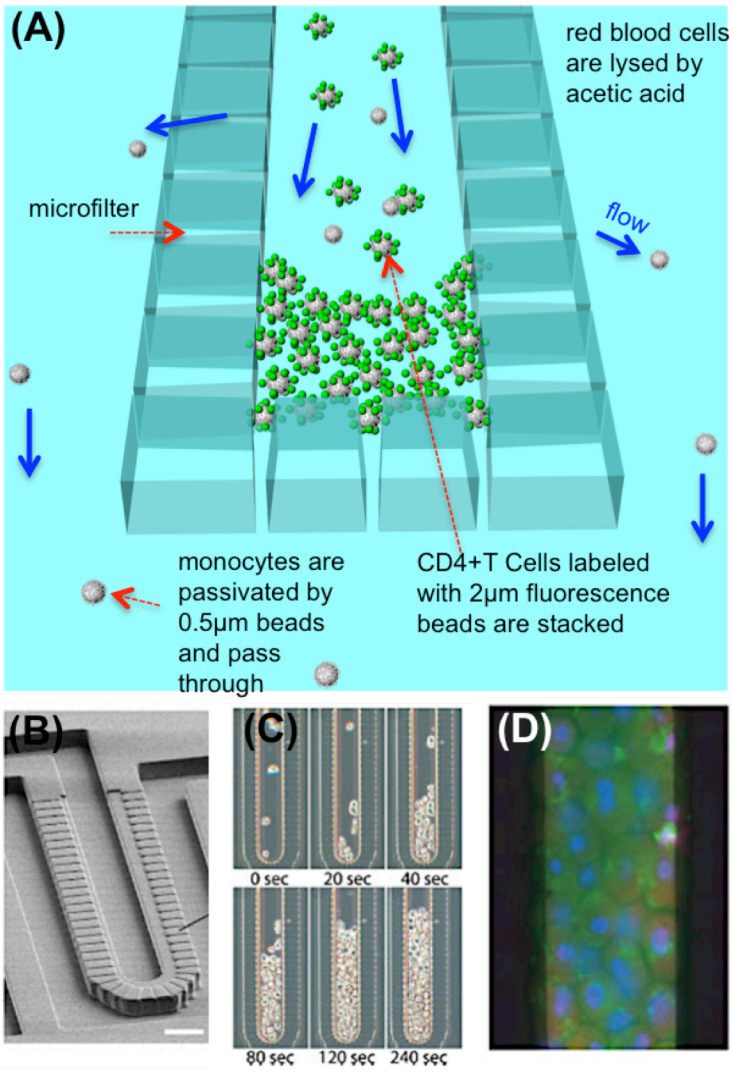

Figure. 4 Proposed $CD4^+T$ cell counting module design. **(A)** The plan is to build a cell counting assay based on stacking polystyrene bead tagged $CD4^+T$ cells. The tagged $CD4^+T$ cells will be enlarged by ~4μm in diatmeter and start stacking in a microfluidic filter. **(B-D)**, this lab has developed similar technolgies for stacking cells to create artificial livers on chip.

Activity 1.4: Develop a quantitative protein detection module

Protein detection is highly desirable to be done in parallel with nucleic acid detection. This is because protein and viral load peaks at different phases of infection. A dual detection scheme will ensure a short window of detection and minimize false negatives. The plan is to develop a next generation quantitative protein assay module by using gold nanoparticle scattering. It is possible to achieve single biomolecular (protein) detection using gold nanoparticles (GNPs) as labels for the detection of target molecules. Due to the resonant Rayleigh scattering of GNP, which has is equivalent to that of 10^6 fluorophores; GNPs allow efficient and bright optical detection. Single

biomolecular binding events can be imaged in dark-field measurement using total internal reflection based GNP scattering excited by wave-guided light. Therefore, highly sensitive assays can be developed using this technique. This method can be used for protein detection including interferon gamma for TB, p24 for HIV, pLDH and pGluDH for malaria.

Activity 1.5: Optimize System Materials and Design for Scalable Manufacturing

Material selection and optimization for scalable manufacture

Considering the cost effectiveness and yield, the injection molding technique is well suited for the production of diagnostic fluidics. In order to take advantage the vacuum battery system, the substrate needs to be porous and thus there is a need to optimize injection-molding compatible air permeable materials. The integrated devices for manufacturing will be sent out to test their compatibility for mass production.

Scalable reagent patterning and lyophilization

Proteins such as antibody, polymerase are formulated in aqueous solutions to allow ease of use, but several degradation processes may be facilitated by the aqueous environment. To obtain the desired stability during storage in point-of-care (POC) devices, proteins should be dried to reduce the rate of chemical and physical degradation. For this, sugars such as sucrose and trehalose can be used during lyophilization and storage in a dried solid. The mechanism of stabilization by these sugars during drying has been proposed to occur by producing a glassy matrix to restrict mobility and/or acting as a water substitute. This freeze-drying technique will be used with sugar molecules to prevent the lyophilization-induced protein unfolding, aggregation, and degradation during dehydration. Lyophilized reagents will be pre-stored on the device for one-step detection.

Module integration for scalable manufacturing

In this part, the plain is to integrate all the optimized individual modules into one chip as shown in **Figure 1**. The design will be sent to a manufacturing company for making large-scale fabrication of the iMDx2.0 chip. The system design will be iterated and optimized with the feedback from field-testing. Chip cost is expected to be controlled under $5 at scale.

Investigate manufacturing of optical reader system

The plan is to make a portable iMDx 2.0 optical reader device (See future direction 2). After the optimization design for mass production is finalized with 3D printing in the Lab, the design will be sent to one suitable company for large-scale production of the iMDx 2.0 reader. The cost of the iMDx 2.0 reader device will be controlled within $200.

Future direction 2: Develop smartphone optical reader and integrate wireless data communication for telemedicine

Activity 2.1: Develop Mobile phone optical chip reader and data communication app

The wish is to develop a simple, portable and inexpensive optical module using a smartphone, which is designed to enable wide distribution in low resource settings. The only equipment users would need is the optical box, assuming they have a smart phone already. Fabrication costs of this optical reader is to be contrained within $200 USD. The optical module is designed to rapidly record fluorescence and dark-field images. The information regarding number of copies of target nucleic acid and HIV $CD4^+$T cell count will be based on fluorescence images. On the other hand, to determine the resulting GNP-based protein assay, the optical system will take dark-field images as well. An App, coined iMDx 2.0, will facilitate images recording, image processing, generating the diagnosis report and data communicating with cloud system via Health Level Seven (HL7) standards.

Fluorescence images will be recorded and processed by the iMDx App. For observation of GNPs, the sideway illumination was made by an array of white LEDs equipped on the wall of the chip camber. The LED arrays will excite the microfluidic chip with well-defined angle to generate total internal reflection (TIR) illumination, which enables high signal-to-noise ratio of dark-field imaging. The strong scattering from the particles will share the same optical path with fluorescence channel and be guided into camera as well. After image reordering and processing, the diagnosis results will be transferred into the report system (see details in **Activity 2.2**).

Activity 2.2: Develop App software for wireless data communication

The iMDx App will also be designed to report the results of point-of-care diagnosis of HIV, TB or Malaria patients. First, operators (such as nurses) will create the patients' profiles along with personal information. After scanning the QRcode and loading a chip, the iMDx reader will identify test type, based on the barcode, and followed by image acquisition. After processing both fluorescence and dark-field images, a program algorithm will be able to analyze the results and generate a report. For instance, for a HIV test, a report will include infection status (e.g. positive or negative), HIV subtype, viral load, number of $CD4^+$T cells and the concentration of p24 antigen. Finally, the data will be shared with computer severs in hospitals or organizations (such as the World Health Organization, WHO) via Health Level Seven (HL7) standards by a cloud system. According to the information, doctors in hospitals will be able to suggest treatments and organizations will be able to track specific dieses in certain area.

Future direction 3: Conduct Field Tests with iMDx 2.0

A sample preparation module has been designed to specifically meet the constraints imposed both by the expected sample matrix (human blood) and by the expected testing environment (remote and low-resource setting). Initial laboratory experiments with spiked and simulated samples were conducted to confirm sample preparation performance. In this objective, the aim is to conduct clinical tests using diagnostic devices integrating the sample preparation module with downstream readout components developed both internally and through external collaborations. The plan is to work with local and international clinical partners to characterize device performance in realistic expected environments. The most significant challenge in this objective will be obtaining reproducible results using a range of samples that may vary drastically in terms of clinical origin. Furthermore, the wish is to conduct initial tests with minimally trained users, quantifying user-to-user variation.

Activity 3.1: *Evaluation of integrated device with human samples*

Sample materials from the Gates Foundation that simulate clinical samples for tuberculosis, HIV, and malaria have already been obtained. Initial tests with these samples has begun, and will be continued. The plan is to identify any modifications that may need to be made in order to achieve sensitive, specific, and repeatable results using these simulated samples.

Activity 3.2: *Evaluation of integrated device with samples from UCSF and international collaborators*

The plan is to test the developed assay with clinical samples obtained from partners at UCSF and international sites (e.g. Africa). Further device tests will be conducted with minimally trained operators in order to measure assay simplicity and reproducibility.

Conclusion

This dissertation describes several components that are useful for point-of-care diagnostics. The digital micro-patterning method was developed—unique in the sense that it can produce highly concentrated micropatterns of reagents with common lab equipment. No special equipment such as inkjet printers, dispensers, or contact pin robots are needed. Unlike inkjet printing, no special solvents are necessary. As a proof of concept, the possibility of patterning amplification initiation reagents into microwells and enabling isothermal amplification within these wells was demonstrated. This simple patterning method may be easily adopted for low-resource lab settings.

Another innovation is a new microfluidic pumping method, termed the vacuum battery system. This system allows pumping without any external equipment or power sources for up to two hours. It is completely portable and integrated with the microfluidic device, requiring no additional cost. Compared to previous degas pumping, the vacuum battery system is significantly advanced in terms of robustness, speed, and stability. It is also possible to load dead-end channels. The silicone material used has excellent optical transparency, therfor ideal for optical readout. This is a major advantage compared to opaque fibrous capillary systems. Although very simple in design, the vacuum battery system has potential to become a transformative technology for portable point-of-care devices and compete with conventional capillary pumping in the near future.

A microfluidic sample preparation module was also demonstrated—the digital plasma separation platform—capable of processing whole blood for downstream biomolecular detection assays. Integrating the above three mentioned inventions, it was possible to perform one-step nucleic acid (NA) detection from whole blood within 30 minutes on the Integrated Molecular Diagnostics (iMDx) chip.

For future research, the proposal is to expand goals towards system integration. A recommendation is to demonstrate the seamless integration of these sample preparation modules with common downstream molecular detection such as protein assays and cell-counting assays. Another proposition is to investigate materials and processes for scalable manufacturing, iterating through this initial design to align with the requirements of a streamlined industrial product. A further plan is to develop a low-cost optical reader that leverages smartphone technology for rapid data analysis and transmission at the point of need. The ultimate aim is to conduct initial field tests with international collaborators in order to validate this device and assay design.